TU Delft

PERFORMANCE AND MECHANISTIC UNDERSTANDING OF

SODIUM GALACTARATE

AS A GREEN CORROSION INHIBITOR AND ADHESION PROMOTER FOR ALUMINIUM ALLOYS

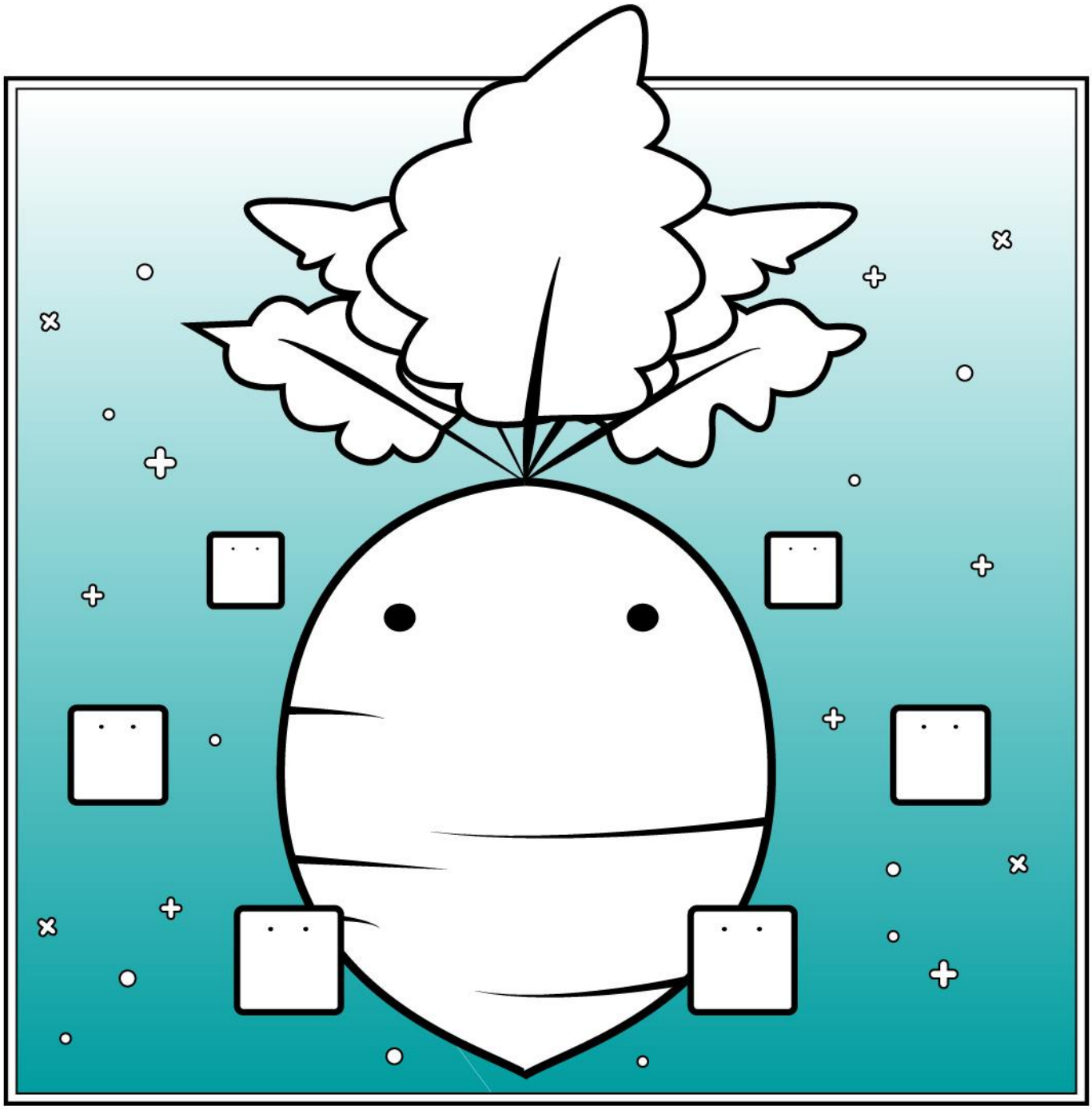

TASAMA POTANG

Performance and mechanistic understanding of sodium galactarate as a green corrosion inhibitor and adhesion promoter for aluminium alloys

By

Tasama Potang

in partial fulfilment of the requirements for the degree of

Master of Science

in Material science and engineering

at the Delft University of Technology,

to be defended publicly on Thursday 12th May 2022 at 10:00 AM.

Supervisor:	Prof.dr.ir. J.M.C. Mol	
Thesis committee:	Dr. Peyman Taheri,	TU Delft
	Agnieszka Kooijman, MSc,	TU Delft

TU Delft

Contents

Abstract

Pretreatment has become a necessary process to enhance the surface chemistry and morphology of aluminium alloys before implementing subsequent corrosion protection measures, especially organic coating application. Traditionally, hexavalent-chromium-based pretreatment processes were frequently used in many industries, but hexavalent-chromium-based chemistries are now recognized as a potentially carcinogenic hazard and environmentally harmful. The development of alternative, non-toxic and eco-friendly corrosion inhibitor and pretreatment technologies has become of pivotal importance to industries as a basic license to operate and to reach a sustainable society as a whole.

In this work, sodium galactarate (NaGal) was investigated as a potential green corrosion inhibiting chemical for hexavalent-chromium-free pretreatment and to serve as a coating adhesion promoter on aluminium alloy AW3003. The pretreatment layer formation was examined at five different pHs; 3, 4, 7, 10, and 11. The surface analysis was performed by Fourier transform infrared – reflection absorption spectroscopy (FTIR-RAS), contact angle measurement and white light interferometry (WLI). Samples with pretreatment layers formed in acidic and alkaline environment showed an increase in polar energy and surface roughness, which are strongly related to the coating adhesion properties, in line with the failure stresses obtained from the pull-off adhesion tests. The corrosion resistance was evaluated through the electrochemical behavior that was measured by linear polarization resistance (LPR), potentiodynamic polarization (PP), electrochemical impedance spectroscopy (EIS) and open circuit potential (OCP) measurements. Immersion testing was performed to evaluate the pitting corrosion behavior. The pretreated sample exhibited less pitting than the reference sample, especially in an alkaline environment where aluminium alloys severely corrode due to limited protectiveness of the oxide layer. The pretreatment prevented the corrosion products from accumulating on the sample surface, limiting stain and smut layer redeposition, subsequently reducing the pitting corrosion.

Acknowledgements

It would be impossible for this thesis to reach its successful end without the assistance and collaboration of many people to whom I would like to express my sincere gratitude.

First of all, I would like to express my gratitude to Prof. Arjan Mol for a great opportunity to do research on such an interesting topic. The path to exploring the world of corrosion and tackling corrosion science and engineering issues is endless as new and different problems and solutions will always emerge. It was one of my finest times to be able to be part of this fascinating journey.

Secondly, I would like to thank Agnieszka Koojiman for her full support as a daily supervisor. Thank you for all the meetings and the fruitful discussions that we have shared. Doing a thesis is a difficult task, doing a thesis during the world epidemic was surely not a simple task. I am grateful for the time we have spent together in the lab. All the small talks that we had helped me through the isolated time that we had to face in the Corona time. It was very fortunate of me to have you as my supervisor.

I also would like to thank Uncle Charles Joyner and Na Addie Onsanit for proofreading many of my thesis drafts before they reached completion. Also, the advice on academic writing and numerous encouragements during my writing time.

I would like to thank the Dutch Ministry of Education, Culture and Science and Dutch research universities and universities of applied sciences for granting me a Holland scholarship, which has financially supported me in my master's study at TU Delft.

As an international student, doing a master's in the Netherlands could be called a once-in-a-lifetime experience. I am very happy that I have found and joined my BB group during my study. All the support and times that we spent together are precious to me as they helped me through many difficulties during my study. Thank you for pulling my hand along the dark road that we have walked together for these past years to the end line.

I give my special thanks to P'Pump, Siwarak Unsiwilai who has become like a brother to me after all this time since I started my journey in the Netherlands two years ago. Thank you for always listening and being there for me during my hard time, especially during my sick days when you have looked after me. I would have not reached the finish line in this study if you were not there. I would like to extend my thanks to the Thai community in Delft as well for their joys and kindness.

Lastly and most importantly, I would like to thank my friends and family back in my beloved home country who constantly fill me up with positive energy until I reached today's accomplishment.

Tasama Potang
Delft, April 2022

1 Introduction

1.1 Common corrosion inhibitors for aluminium alloys

Aluminium alloys are used in industries from aircraft to offshore equipment fabrication. This versatility is owing to their great combination of properties such as light weight (density of 2.7 g/cm3), high strength to weight, high conductivity and recyclability [1]. Due to the good formability of aluminium, there is a wide range of aluminium alloys series with diverse combinations of properties available for general or specific engineering applications. AW3003 is an aluminium-manganese alloy, which is used in various applications such as food packaging and combustion engines in an automobile [2],[3].

Aluminium alloys have high resistance toward corrosion in the atmosphere and many mild aggressive aqueous environments due to the ability to form a passive oxide layer. However, this oxide layer can be dissolved and destroyed in aggressive acid and alkaline environments [4]. Moreover, it is even more threatening in halide ion environments (such as saline water), since the ions can attack the film on the areas that have high chemical sensitivity, leading to localized corrosion such as pitting [5], [6]. They will slowly and continuously degrade the properties on a micro-scale deep underneath the surface, making it difficult to monitor or detect.

To counter this problem, many applications use multi-layer coating systems to protect the material. To achieve this system, metals are conducted with a series of treatments consisting of cleaning, pretreatments, primers, and organic coatings. However, aluminium alloys have a drawback in their surface quality, which tends to be heterogeneous due to the alloying elements' presence. The native oxide layer that covers the surface also demotes the coating adhesion due to high electrical resistance and hydrophobicity. Thus, the pretreatment becomes a crucial step to ensure strong bonding between the alloy and coating by removing not only the native oxide but also the organic contaminations and corrosion products that have accumulated on the surface. It also helps to create a uniform surface with fewer defects and intermetallic particles (IMP) at the very outer surface exposed to a corrosive environment. To further strengthen the corrosion resistance of the application, a corrosion inhibitor can be added to the pretreatment step. In the previous decades, the pretreatments that contained chromate, phosphate or other heavy metals were broadly accepted as the benchmark for corrosion inhibitors. Chromates in particular showed cost-effective protection and ubiquitous usage. However, it was later discovered that these compounds were extremely toxic and caused health hazards. Moreover, poor waste management from the industries caused pollution to the botany and wildlife in these areas [7]. Not long after that discovery, the World Health Organization (WHO) announced a warning causing the use of hexavalent chromium to be banned in many countries. This raised a demand to find an alternative corrosion inhibitor that provides sufficient corrosion resistance while being non-toxic and ecologically acceptable.

To support the environment and create a more sustainable product life cycle, most of the recent research is performed with the use of "green" corrosion inhibitors, which are non-toxic compounds often obtained from plant or animal products. Many researchers are now collaborating with agriculture-based industries to investigate and develop their by-products, not only to search for an alternative compound but also to add extra value to the industry. Sugar extract substances are now getting more attention and inquiry as a possible replacement for petroleum products. In Europe, the sugar beet pulp industries are substantial, especially in western Europe with the production of approximately 13 million tons per year according to the PULP2VALUE project. One of the by-products in sugar production – galactaric acid shows promising

corrosion resistance results on cold-rolled steel and various aluminium alloys. Patents on surface treatment and stain removing methods were filed by Royal Cosun as one of the PULP2VALUE partnerships [8]–[10].

1.2 Objective

Corrosion inhibitor's efficiency is constrained by many external factors such as temperatures, times and pHs. Since the initial stage of research had revealed that sodium galactarate had a promising result in neutral pH, the investigation of its effect on different pH continued in this work as aluminium alloys are practically used in applications that surround the environment of low pH (acid) or high pH (alkali). In this work, the effect of corrosion inhibitor was studied along with the effect of alkaline cleaning, which has been used in the industry for decades. There is vast information on how alkaline cleaning affected the surfaces of aluminium alloys in the pretreatment whereas the research on the effect of green corrosion inhibitors used in a pretreatment step is very little to none.

This study is carried out in two parts. In the first part, the effect of the use of potential corrosion inhibitor - Sodium Galactarate in a pretreatment step on the aluminium alloy surface is studied to determine if it improves coating adhesion. The second part investigates the changes in the electrochemical behaviour caused by this pretreatment and whether it improves the corrosion resistance of aluminium alloys. The research questions regarding the aim of this thesis are addressed below:

1.3 Research questions

1. Does the NaGal pretreatment improve the organic coating adhesion? If so, how?
2. What is the influence of NaGal on the corrosion behavior of AW3003? Does it show an inhibitive effect?

Additionally, to answer the main questions thoroughly, the following sub-questions are formulated:

1.1 What is the NaGal adsorption mechanism on aluminium alloys in different environments (acidic, neutral, and alkaline)?
1.2 Does pH have an effect on NaGal pretreatment with regard to improvement in coating adhesion?

1.4 Scope of study

The corrosion protection system in this thesis will be considered as a multi-layer coating system with respect to the pretreatment steps that are applied on aluminium alloys as shown in Figure 1.1.

Evaluating the corrosion resistance is a difficult and time-consuming task. Hence, this study focuses on observing the corrosion resistance of the freshly prepared sample in the corrosive environment up to 24 hours to have an insight on the effect in both short (2-4 hr.) and long (10-24 hr.) periods since time is also one crucial factor that affects the corrosion inhibitor's efficiency. In addition, the corrosion resistance of the sample is mainly evaluated based on the uniform corrosion and pitting corrosion before applying the coating. Filiform corrosion is not being considered in this work.

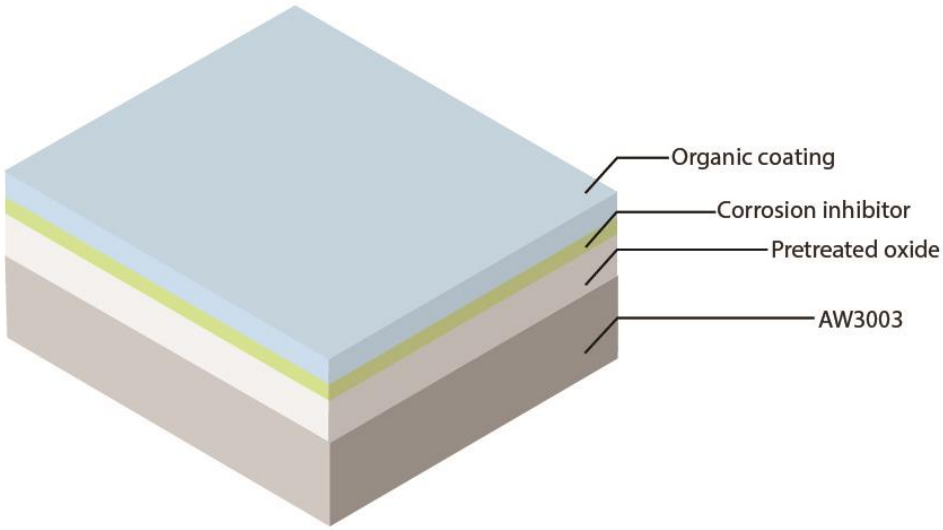

Figure 1.1 A schematic of the sample's layers

1.5 Thesis outline

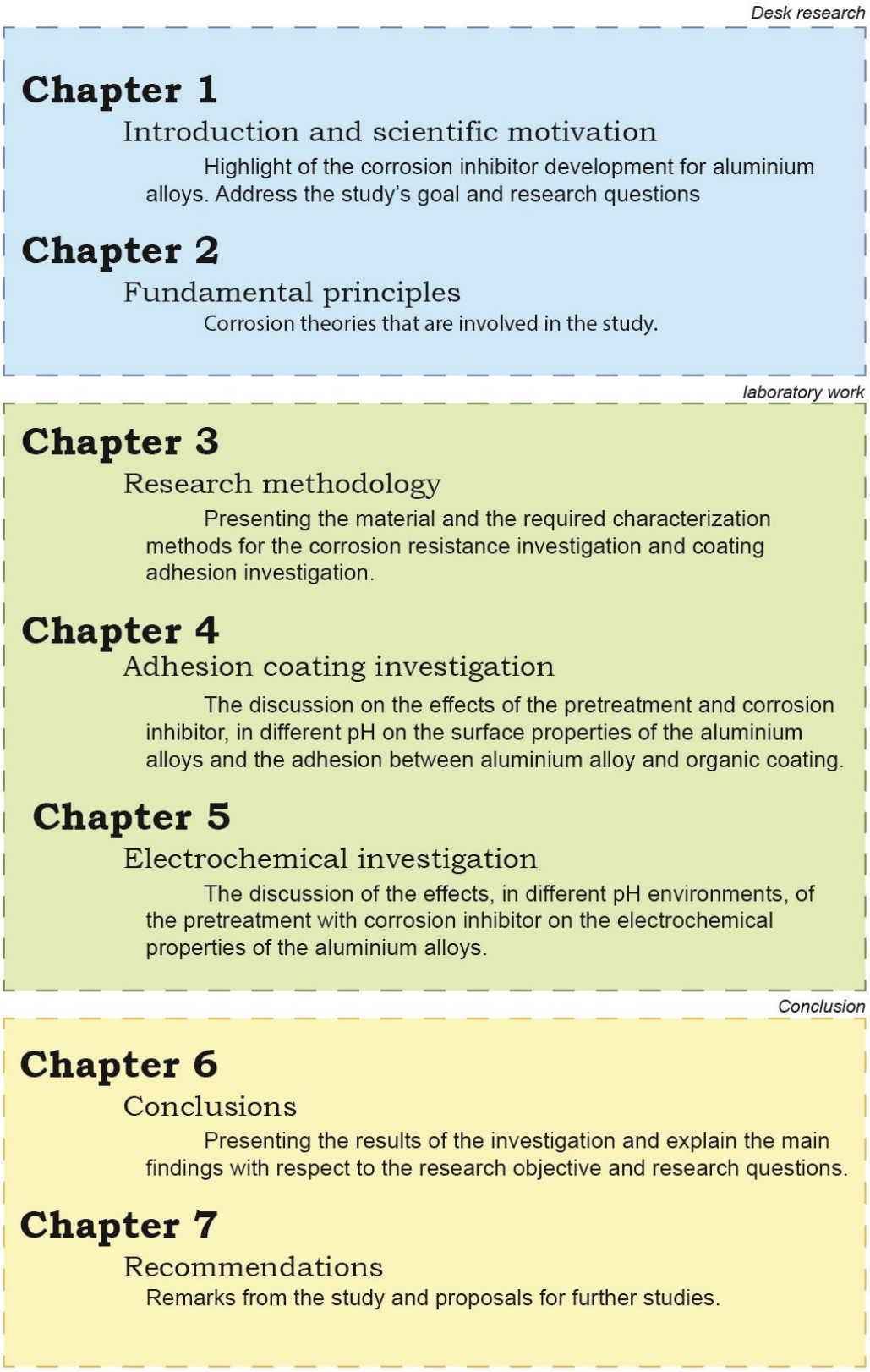

2 Fundamental principles

2.1 Corrosion of aluminium

Aluminium alloys offer high corrosion resistance in many settings such as atmospheric, marine, industrial and urban environments, making them attractive for applications that aim to have a long service life. This resistance is due to passivity, which is the ability that allows metals to generate their oxide to cover the surface when subjected to an aggressive environment. The oxide layer becomes a barrier and prevents further corrosion as it is more inert to the environment than the metal itself. Commonly, when determining the passive range of the metal, the Pourbaix diagram is used. Pourbaix diagram plots potential vs pH showing possible thermodynamically stable phases of the studied electrochemical system. Pourbaix diagram for Aluminium is shown in Figure 2.1, according to it, aluminium forms a passive film in a pH range from pH 5 to 8. However, it was reported that Aluminium also showed passivity in some types of acid in pH4 as well [11].

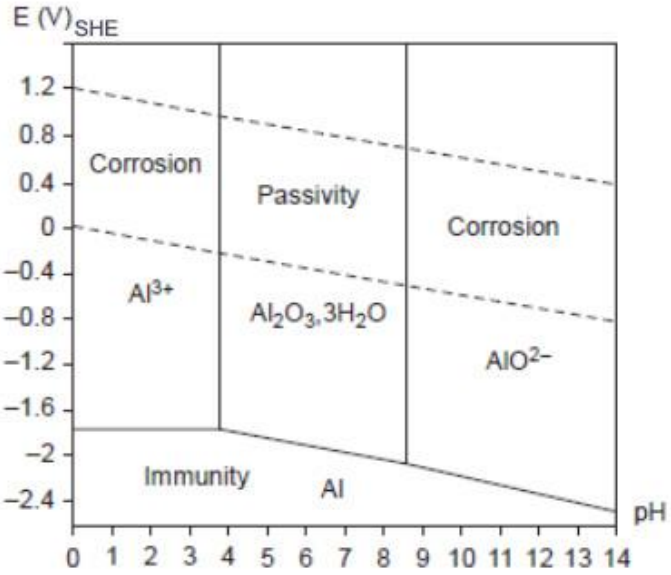

Figure 2.1 Potential-pH equilibrium diagram for the system aluminium-water at 25°C [12].

2.1.1 Neutral environment

As denoted by the Pourbaix diagram in Figure 2.1, Aluminium forms passive film in the neutral media. Because alumina (Al_2O_3), which is the most stable oxide form of aluminium can exist stably and cover the majority part of the surface areas.

Alumina is formed through the reaction of the aluminium and oxygen:

$$2Al + \frac{3}{2}O_2 \rightarrow Al_2O_3 \qquad \text{Equation 2.1}$$

2.1.2 Acidic environment

In highly acidic media, aluminium has no longer passivity. As the oxide film is dissolved,corrosion occurs in aluminium.

The partial anodic reaction is the dissolution of aluminium:

$$Al \rightarrow Al^{3+} + 3e^- \qquad \text{Equation 2.2}$$

The partial cathodic reaction can be considered as two different reactions:

1. The reduction reaction of oxygen:

$$O_2 + 4H^+ + 4e^- \rightarrow 2H_2O \qquad \text{Equation 2.3}$$

2. The reduction of the protons:

$$2H^+ + 2e^- \rightarrow H_2 \qquad \text{Equation 2.4}$$

In general, the cathodic reaction from the Equation 2.4 is more favourable in an acidic environment. The combination of the partial anodic and cathodic reactions leads to the dissolution of aluminium as shown in the following Equation 2.5 and Equation 2.6 [13].

$$Al + H_2O \rightarrow AlOH + H^+ + e^- \qquad \text{Equation 2.5}$$
$$AlOH + 5H_2O \rightarrow Al^{3+} + H^+ + 6H_2O + 2e^- \qquad \text{Equation 2.6}$$

The product in Equation 2.6 shows that the major thermodynamic state of aluminium in acid is aluminium in ionic form (Al^{3+}), this is also exhibited in the Pourbaix diagram.

Nevertheless, Al^{3+} can react with the water again to form $[AlOH]^{2+}$, which may react with the chloride ions (if present) and cause the following reaction (Equation 2.8).

$$Al^{3+} + H_2O \rightarrow [AlOH]^{2+} + H^+ \qquad \text{Equation 2.7}$$
$$[AlOH]^{2+} + Cl^- \rightarrow [AlOHCl]^+ \qquad \text{Equation 2.8}$$

The final soluble complex ion in Equation 2.8 escalates the dissolution rate of the metal and decreases the pH solution to more acidic, resulting in an incredibly increased corrosion rate in the system [14].

2.1.3 Alkaline environment

It can be seen in the Pourbaix diagram (Figure 2.1) that at high pH values, corrosion is the most thermodynamically favourable state for aluminium in almost the whole potential range. This is due to the oxide film becoming more vulnerable when exposed to alkali. Unfortunately, many industrial applications involve processes in this pH range such as aerospace, offshore and advanced nuclear reactors [15]. Furthermore, the usage of alkaline cleaning solutions for equipment is also common in many industries despite it being highly corrosive to aluminium and its alloys. Hence, many research studies have been conducted in this area to find suitable protection.

The OH^- ions in the alkaline solution, which are attracted to the oxide film surface, can form soluble aluminate ions (Equation 2.9) with Al^{3+} ions from the Aluminium dissolution (Equation 2.2) [16].

$$Al^{3+} + 4OH^- \rightarrow Al(OH)_4^- + 3e^- \qquad \text{Equation 2.9}$$

Similar to the acidic media, there are two possible partial cathodic reduction reactions. The partial cathodic reactions in alkali are water reduction (Equation 2.10) and oxygen reduction (Equation 2.11). Many scientific papers have reported that the water reduction is more favorable as the gas has been detected to evolve during the corrosion [17].

$$3H_2O + 3e^- = \frac{3}{2}H_2 + 3OH^- \qquad \text{Equation 2.10}$$

$$\frac{2}{4}O_2 + \frac{3}{2}H_2O + 3e^- = 3OH^- \qquad \text{Equation 2.11}$$

By combining both partial anodic and cathodic reactions, the direct dissolution reaction is defined as:

$$Al + 3H_2O + OH^- \rightarrow \frac{3}{2}H_2 + Al(OH)_4^- \qquad \text{Equation 2.12}$$

From Equation 2.12, It can be concluded that the dissolution rate of aluminium depends on the hydroxide ions concentration and the transport of the aluminate ions ($Al(OH)^{-4}$) between the interface (solid/liquid). Although $Al(OH)^{-4}$ is the most stable form of aluminium in an alkali, the aluminium ions (Al^{3+}) can still create an oxide film through hydroxide diffusion. However, aluminium ions, which transport through the oxide film, also contribute indirectly to the metal dissolution. Scientific studies reported that the oxide film, which was pre-composed from alumina, attracts the hydroxide ions and consequently promotes film dissolution (Equation 2.13) [18].

$$Al(OH)_3 + OH^- \rightarrow Al(OH)_4^- \qquad \text{Equation 2.13}$$

In comparison, the process of forming aluminate ions in Equation 2.14 is much slower than oxygen reduction in Equation 2.11. Therefore, the oxide film composition will eventually turn into a hydroxide layer if enough hydroxide ions diffuse into the oxygen vacancies as demonstrated in Equation 2.15. This causes the dissolution of alumina proportional to the concentration of the hydroxide and aluminate ions in the interface between the oxide film and the alkaline media.

$$Al_2O_3 + 2OH^- + 3H_2O \rightarrow 2Al(OH)_4^-$$ Equation 2.14

$$Al_{Al} + \frac{3}{2}V_O^{2+} + 3OH^- \rightarrow Al(OH)_3$$ Equation 2.15

In both acidic and alkaline environments, aluminium only exits in the form of Al^{3+}, $Al(OH)^{-4}$, $AlOH_2^+$, $Al(OH)^+_2$, $Al(OH)_3$ [17]. Nevertheless, that is only the case for pure aluminium, where the corrosion rate can be solely determined by the anodic reaction.

2.1.4 Chloride environment

It is well known that halide ions are aggressive toward metals that can form passive layers. Not only do they destroy the passive films, but also competitively absorb into the metal surface hindering the film growth. This section solely focuses on chloride ions since they are the most common halide ions in applications where aluminium is used.

The chloride ions induce the pitting corrosion by attacking the weakest parts of the oxide film, leading to film dissolution and a decrease in localized pH (Equation 2.16). Moreover, when aluminium chloride ($AlCl_3$) is present in the solution, the water reduction (partial cathodic reaction), which is shown in Equation 2.17, can also rapidly increase the acidity of the solution.

$$Al^{3+} + 3H_2O \rightarrow Al(OH)_3 + 3H^+$$ Equation 2.16

$$AlCl_3 + 3H_2O \rightarrow Al(OH)_3 + 3HCl$$ Equation 2.17

Furthermore, the aluminium dissolution rate can be increased with an increased concentration of the hydroxide ion from the oxygen reduction (partial cathodic reaction) as demonstrated in Equation 2.18 - Equation 2.19.

$$\frac{1}{2}O_2 + H_2O + e^- \rightarrow OH + OH^-$$ Equation 2.18

$$OH + e^- = OH^-$$ Equation 2.19

Regardless of the chloride ions concentration, it always poses a threat to aluminium. In low concentration electrolytes, chloride ions have high mobility and attach themselves to the aluminium surface, preventing passivity. While the high concentration of chloride ions leads to an increase in aluminium dissolution rate and chloride complex, which can rapture the oxide film (Equation 2.20).

$$Al + 4Cl^- = AlCl_4^- + 3e^-$$ Equation 2.20

In addition, the presence of the hydroxide ions shown in Equation 2.18 and Equation 2.19 may cause the chain reaction and create the oxychloride compound:

$$Al^{3+} + 2Cl^- + 2OH^- = Al(OH)_2Cl_2^-$$ Equation 2.21

Both products in Equation 2.20 and Equation 2.21 ($AlCl^{4-}$ and $Al(OH)_2Cl^{-2}$) are promoting the dissolution of aluminium, hence increasing both uniform corrosion (corrosion rate) and localized corrosion.

In summary, the corrosion mechanism in aluminium differs depending on the media. Since the passive film can exist stably only in the neutral pH, aluminium incurs significant corrosion in acid and alkaline electrolytes. Even though the passive film is the main source of the high corrosion resistance, it is weak against the halide ions as they can induce localized corrosion.

2.2 Corrosion of aluminium alloys

The application or use of pure aluminium is very limited due to its softness and extremely low standard electrode potential, which is about -1.66 V (SHE), leading to the high reactivity with oxygen. Hence, the corrosion is also in the favor of aluminium as it is a spontaneous reaction from having a minus value for Gibb's free energy. Moreover, the process is rapid due to the high kinetic rate. Therefore, aluminium alloys are more frequently used for commercial applications.

Although only small amounts of the alloying elements are added to make aluminium alloys, they have a great influence on the aluminium alloy properties and a significant impact on localized corrosion. From a microstructure perspective, the intermetallic particles (IMPs) can precipitate during the cooling state of the alloys. The particles' sizes can vary from nano- up to micro-scale. The presence of the IMPs affects the corrosion resistance properties of the alloys because each IMP has its own oxide form, which contrasts with the matrix. This causes some areas to have different chemical compositions leading to a heterogeneous surface. Depending on the density of the IMPs, in some alloys, the passive layer protecting the alloys themselves is not formed by the matrix, but rather by the alloying elements. Moreover, many alloys are reported to have a mixed oxide film and certain elements in the alloys themselves can modify the film properties [19]. For instance, copper atoms filling the vacancies in the oxide film can lead to a dielectric constant reduction. Another example is magnesium, which has higher diffusion coefficient than aluminium, it can create an extra external layer of the passive film made of MgO, this layer is a mixed composition between $MgO{\cdot}Al_2O_3$ and/or Al_2MgO_4 [20], [21]. Thus, to consider the corrosion of aluminium alloys to be near perfect, the corrosion originating from the alloying element needs to be considered as they can induce localized corrosion or strengthen the passivity.

2.2.1 Corrosion forms in aluminium alloy

The aluminium alloys can be divided into two groups: heat treatable and non-heat treatable. The non-heat treatable series are 1xxx, 3xxx, 4xxx and 5xxx, which have more corrosion resistance toward general corrosion. Nevertheless, all aluminium alloys are commonly reported to have undergone general, galvanic, localized, stress-corrosion cracking or intergranular corrosion [2].

Uniform corrosion

When uniform corrosion occurs, the metal surface homogeneously corrodes and decreases. It is also known as 'general corrosion' because it is the most commonly found corrosion in metals. During the time that metal is exposed to water or an oxygen-rich environment, the corrosion damages the metal surface uniformly at a slow rate. Thus, it is deemed to not be dangerous because the progress can be observed and predicted in order to make a prior protection [22]. However, the corrosion rate is dynamic and can change if the potential changes [23]. Although general corrosion is commonly found in metal, localized corrosion is more concerning. The presence of the second phases particles promotes pitting corrosion, which may lead to mechanical

failure. On the other side, general corrosion is a slow and homogeneous destructive process that most aluminium alloys oxide films can withstand and retard the damage due to its self-healing passivity [24].

Localized corrosion

In contrast to general corrosion, localized corrosion only attacks specific sites on the metal surface which are more chemically active. The composition of the alloy is not homogeneous, which means that there are a lot of differences in the potential over the surface. Aluminium alloys are likely to undergo localized corrosion because the passivity causes them to have a high ratio of the cathode and anode areas [25]. Localized corrosion is considered to be more dangerous than uniform corrosion because it occurs deep, underneath the surface causing it difficult to detect before the material reaches the failure state.

Pitting

Pitting is common in aluminium alloys because of their intrinsic passive film. The reaction between the metal and electrolyte causes the breakdown of the anode region by generating many small pits. These pits penetrate the passive film from the surface deep into the alloy structure vertically assisted by the gravity force. Pitting corrosion only lasts shortly before the re-passivation starts again. Nevertheless, the active pit can still be active in high positive potential conditions due to the ion exchange between the solution and alloys to preserve electroneutrality, resulting in the trapped solution (at the bottom of the pit) getting higher concentration and acidity. The schematic in

Figure *2.2* exhibits pitting corrosion in chloride solution. Generally, the pitting corrosion in aluminium alloy occurs on the weak spot of the oxide layer, which is the area near the IMP that causes the layer to be imperfect. The localized pH of the pit is low, but the nearby pit that also has IMP will have high pH due to the redox reaction. The figure also demonstrates that the IMP (in this case; Fe) can redeposit on the oxide layer and become a new cathodic site (redeposited Fe ions) because the alloying elements are normally nobler than aluminium.

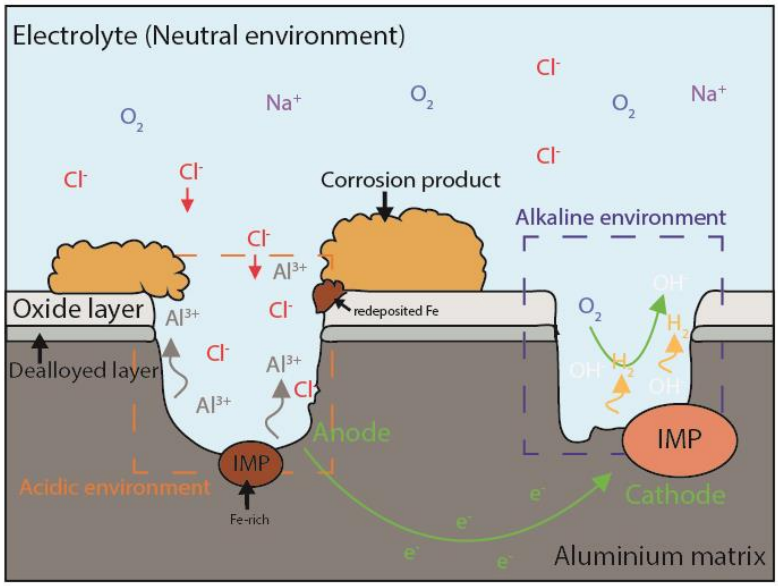

Figure 2.2 Schematic of pitting corrosion on aluminium alloy

Despite a small loss of metal due to pitting, it can cause mechanical failure [26]. In a chloride-containing environment, alloys that consist of more alloying elements are easily subjected to pitting corrosion. The corrosion resistance to pitting decreases in order of 1xxxx> 5xxx> 3xxx> 6xxxx> 7xxx >2xxx [21].

Galvanic /Micro galvanic corrosion

A galvanic reaction occurs when two different metals are in contact with each other in a corrosive electrolyte. The contact becomes a path for ion transportation because of the difference in electrochemical potential in each metal. As previously mentioned, aluminium has low standard electrode potential hence easily corroding when in contact with another metal since it will act as an anode. It is extremely important to take the area ratio between the anode (aluminium) and cathode (other metal) as a concerning point when designing applications [23]. Especially in the halide solution since the halide ions can greatly polarize the metal potential to reach the pitting potential, which makes metals corrode easier [27]. Micro galvanic corrosion has the same mechanism as galvanic corrosion but takes place in the microstructure. It is often caused by the IMPs. In short, galvanic corrosion has a higher chance to occur in aluminium than in other metals.

Intermetallic corrosion

Because of the difference in the chemical composition of the alloys, the IMPs that are precipitated in the aluminium alloys' matrix can serve as the cathodic or anodic sites, which is very detrimental in the presence of the chloride ions as it greatly induces the pitting corrosion. In the alkaline solution, the cathodic IMPs can generate localized corrosion and the matrix areas near them will be reduced. They also increase the partial cathodic reaction and oxygen reduction, leading to the increase of the hydroxide ions concentration, which consequently increases the passive film dissolution rate and local pH [28]. Nevertheless, the oxide film generated by IMPs can also serve as a physical barrier preventing the alloys from further corrosion. It is noted the dissolved metal ions tend to redeposit near the IMPs as corrosion products. The corrosion products that accumulate on the surface make the alloys lose their shiny surface and induce pitting corrosion to the nearby matrix. This layer is well-known as metal stain, the development of the stain layer is shown in Figure 2.3.

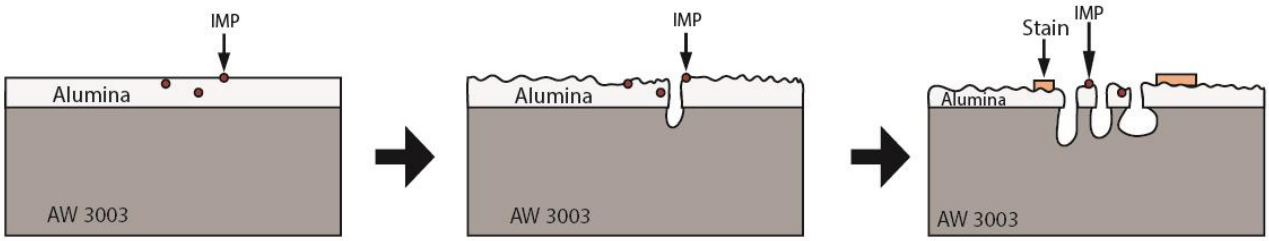

Figure 2.3 Development of the stain layer caused by IMPs on the alloys' surface

2.3 Corrosion protection

In this work, corrosion protection was approached with the concept of a multi-layer protection system. This section focuses on each layer that the system consisted of.

2.3.1 Pretreatment

Aluminium alloys have a drawback in the surface quality, which tends to be heterogeneous due to the presence of the alloying elements and contamination with lubricant oil and dust. In addition, their oxide layer demotes the adhesion between the coating layer and metal surface. Hence, surface modification such as pretreatment becomes a crucial step in aluminium alloys for preparing and ensuring surface quality.

The pretreatment consists of various steps that can be optimized to the cost and time restriction. It generally has cleaning, conversion coating and organic coating orderly. The cleaning process, which intends for removing the oxide layer, usually involves degreasing, sanding and grinding to improve surface roughness by several mechanical methods. Another outstanding cleaning method is alkaline etching or so-called alkaline cleaning, which is a chemical method. Alkaline cleaning is a safe method because it does not need to operate at high temperatures during chemical use or toxic chemicals. Alkaline etching also has advantages in ease of control, low cost, and high yield [29].

Generally, the first step is removing the local lubricant by sonicating in degreasing solvents such as acetone or alcohol. In addition, mechanical preparation is possible to achieve smoother surfaces and remove any contaminations before etching. The alkaline etching process is similar to the aluminium alloys' corrosion in an alkaline medium, which is shown in Equation 2.12 [30]. During the etching process, the etching products are formed and cover the entire surface. This layer composes of various oxide/hydroxide compounds of Al, O and the intermetallic phases of the alloys and it is often described as the 'smut' layer. The schematic illustration during the etching process is shown in Figure 2.4. The smut layer is attached loosely to the surface and can be easily removed by rinsing or sonicating. This undesired layer is later thoroughly removed in the next step by acid, called 'desmutting'. By immersing the sample in the acid, the smut layer is removed and most of the IMPs are inactive owning to their passivity. However, it was reported by Jin's group that HNO_3 can still react with the IMPs, and since they are commonly found to be cathodic, this promotes corrosion at the beginning of the desmutting process until the alumina film is covered [31]. Moreover, some IMPs such as iron/iron oxide, are soluble in acid, hence after the desmutting, the porosity of the matrix also increases.

The main disadvantage of alkaline cleaning is that the desmutted surface tends to have higher IMPs density than the original because IMPs have dissolution rates slower than the aluminium matrix. Not only the particles on the surface may remain, but the particles beneath the surface will also gradually emerge. Thus, the optimal time needs to be determined otherwise the specimens' surface will have a higher composition ratio of the intermetallic phase [32]. Furthermore, the IMPs have different potential than the matrix, they can serve as galvanic corrosion sites (localized corrosion) and corrode the matrix during the etching process by promoting the aluminium dissolution, resulting to surface quality downgrading instead.

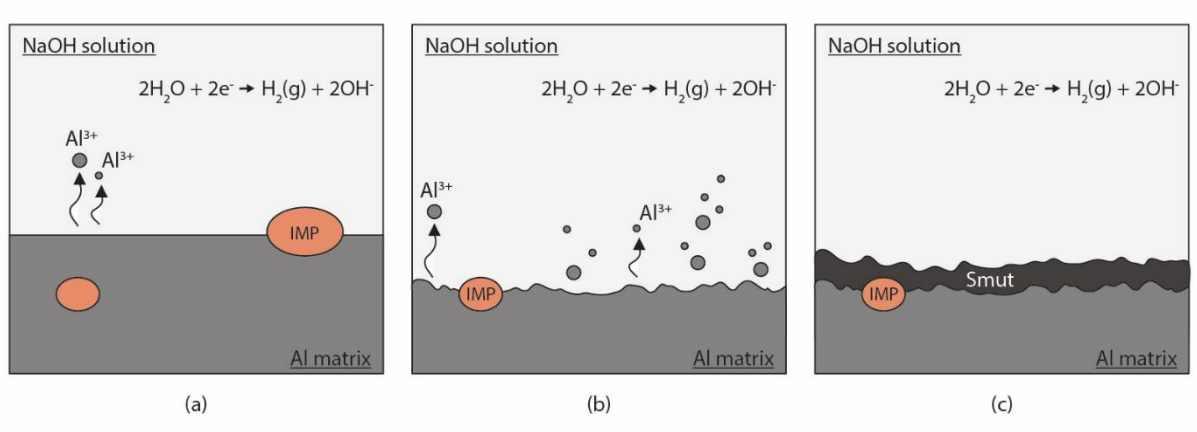

Figure 2.4 Smut layer forming process during alkaline etching (a) at the beginning, (b) IMP dissolves into the solution when the threshold is reached and underneath IMP emerges, and (c) smut forming.

In conclusion, alkaline cleaning is a common surface modification method that has been used in industries due to its many benefits. However, the increase of IMPs on the metal surface can be detrimental since aluminium is highly electrochemically active, and most of the IMPs serve as cathodic sites leading to an increase in localized corrosion.

Conventionally, the conversion coating with a selected corrosion inhibitor is done as the following step to promote both corrosion resistance and the coating adhesion for the organic coating. Previously, phosphate-based and chromate-based pretreatments were used in the industries, but now they are deemed to be complicated, high energy consumption and toxic to health and the environment [33]. Hence, other alternatives are being used. Currently, Zr-based conversion pretreatment is considered to be a great alternative for chromate-free pretreatment as the result of the surface, which is comparable to phosphate- and chromate-based, but it consumes less energy while operating and is less harmful to humans and the environment. Another advantage is that the additives can be added to increase the final performance of the product such as self-healing and better durability [34]. However, since there are many series of aluminium alloys that have different compositions, the final results are varied, and some properties could weaken in some series. For instance, Santa Coloma's group reported that in AA2024 and AA7075 the electrochemical results showed great performance, but the result from salt spray was inferior to chromate-based pretreatment [35]. Since the best method has not been found yet, the search continues and now the trend lies in green corrosion inhibitor as the corrosion inhibitor's efficiency needs to compromise with the eco-system.

2.3.2 Organic coating

The organic coating is often applied in the last process of the application. It shields the metal from the environment by providing protection against humidity, UV radiation, and mechanical damages. Not only does it serve for passive corrosion protection purposes, but also aesthetic appearance for decorative purposes. In addition to the conversion coating, the organic coating has higher resistance against external stress that may cause mechanical failure such as cracking. Some research has combined composite principles, nanotechnologies and corrosion inhibitors into the organic coating, advancing it to functional coating with active protection, for instance, self-healing and damage-detectable ability [36], [37]. Most commercial coatings contain additives that enhance corrosion resistance such as pigments, which give color and opacity, and fillers, which reduce water and oxygen concentration in the coating. It is a complicated task to successfully cooperate additives into the organic coating because many factors could easily alter the coating properties such as pigment size, shape and dispersion state [38].

Coating adhesion strength

Even though the coating has been used for a long time for corrosion protection, the optimal condition to apply a uniform coating layer on the metallic substrate, such as aluminium alloy, is due to the difference in the surface properties. Adhesion strength is strongly related to the interfacial reaction; hence the surface quality of the aluminium alloy plays an important part to obtain a strong interfacial reaction. According to the literature [39]–[41], the adhesion strength can be quantified base on:

- Hydrophilicity (polarity)
- Surface free energy
- Surface roughness
- Porosity

The adhesion strength can be determined in terms of force (stress, work or energy) required to break the interfacial bond. The pull-off adhesion test used in this work is evaluated by the tensile force.

2.3.3 Corrosion inhibitors

Corrosion inhibitors are commonly used in the industry as one of the corrosion protection methods. There are various application methods of corrosion inhibitors, i.e. the inhibitor can be added to the coating, it can also be used to control the environment by adding a low concentration of the inhibitor into the electrolyte. This method is very attractive due to its effectiveness and low maintenance cost.

In past decades, inorganic corrosion inhibitors such as chromium (VI) and phosphate compounds were ubiquitous and in demand. However, they are harmful to humans and the environment. Together with the need to find a replacement and the desire for sustainable business, the focus is shifted to organic corrosion inhibitors.

The increasing emphasis on the ‘green chemistry’ concept based on the principle of being environmentally friendly, sustainable, and safe influences scientists and engineers to create and develop ‘green’ corrosion inhibitors. Green corrosion inhibitor is a term for a chemical substance that has an inhibitive effect on metal and possesses these properties [42] :

- Biodegradable
- Non-toxic
- Ecologically acceptable

These are often chemical substances extracted from plants because they are biodegradable, renewable and abundant [39]. They contain organic substances such as natural polymers and organic acids. Usually one heteroatom (N, S, O and P), heterocyclic or π-electrons serves as adsorption centre [43]–[45].

Although many papers have recognized their effectiveness as they have shown high potential for development, it is still a long path to reach the hexavalent chromium benchmark standard.

Inhibitor mechanism type

Because the main source of the green corrosion inhibitors is nature, the organic chemical compositions can be more complex and contain various elements. For instance, long chain polymer, in comparison with inorganic substances. Their corrosion inhibition mechanisms are often not fully understood, and many

theories have been developed to explain the phenomena. Two types of mechanisms that have been widely accepted are:

- Film forming type

This mechanism is commonly found in the inorganic inhibitor type because the inhibitors are directly involved with the formation of the oxide film of the metal by promoting the growth of the oxide film or creating the oxide film by themselves on the alloys surface through precipitation [46].

- Adsorption type

By electron exchanging or sharing between two surfaces, the metal and the inhibitor can form a strong bond. This is called 'chemisorption'. The inhibitor can act as a barrier to prevent further electrochemical reactions to the metal surface. It also involves the physisorption such as van der Waals force as well, but the bond from the chemisorption is much stronger, more permanent and irreversible. Nevertheless, we tend to mention only chemisorption since its effect is much greater. Most of the organic inhibitors are adsorption type because of the presence of the multiple bonds and the polar functional groups, which consist of heteroatoms, especially H, N, O and S atoms, such as $–NH_2$, –OH, $-NO_2$, $–OCH_3$, –COO, C_2H_5, -CN, $-CONH_2$, –COOH [47]. The inhibition effect is reversed with the electronegativity of the atoms because that causes them to easily form the bond on the surface due to being an electron donor as shown in the figure below.

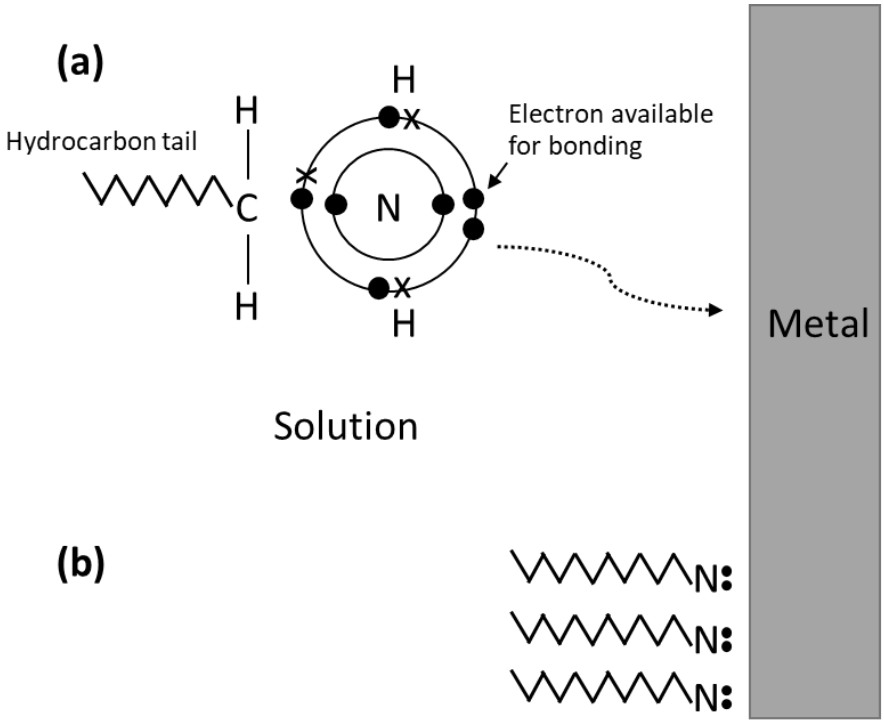

Figure 2.5 A schematic of the adsorption inhibitor with
(a) the electron donor to the metal surface and
(b) the hydrophilic head group attaching to the metal surface and the hydrophobic tails preventing the corrosion

The inhibition increases along with the inhibitor concentration and decreases the corrosion rate as the inhibitor molecules are covering the metal surface. According to the isotherm of the adsorption, the corrosion

rate will reach its minimum when the inhibitors have created their monolayer on the metal surface. After this point, the inhibition effect will no longer depend on the inhibitor concentration (Figure 2.6).

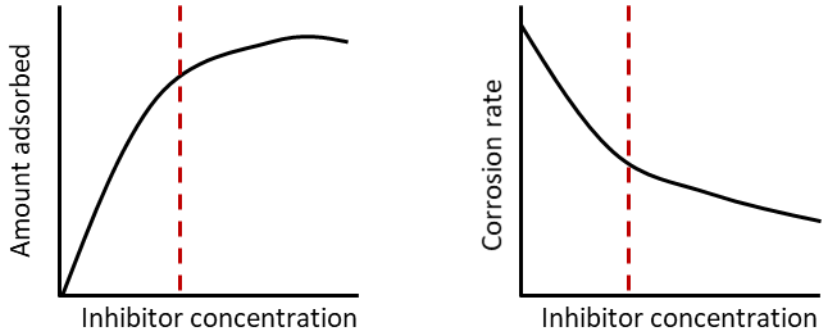

Figure 2.6 A schematic diagram of the relationship between the inhibitor concentration and (left) adsorption isotherm and (right) corrosion rate

There are several chemical factors that affect chemisorption and are strongly related to the efficiency of corrosion inhibition:

1. Electron donating ability of the inhibitors.
2. Chemical structure for example molecular size, bonding type and aromatic bonding, conjugated bonding of the C-chains.
3. Type of the electrolyte or environment.

The capability of adsorption of the metal surface depends on the bonding, which can be either pi-bonding or sigma-bonding, depending on the number of atoms and their types. To reach the maximum effect of the corrosion inhibitors, the bonding between the matrix (metal surface) and the inhibitors needs to be in excellent condition. Hence, it has become a difficult condition when designing the system.

2.3.4 Galactaric acid

Beet pulp is biomass leftover from sugar beet production. It often sells out as low-price cattle feed or raw material for the biogas process without further refinement. In order to increase the value of the beet pulp, biorefinery is introduced into the sugar beet pulp process. It was discovered that various sugar acids can be obtained from the refined beet pulp with chemical conversion techniques. This has captured many researchers' interests as they are searching for green products that could be a replacement for the chemical that relies on petroleum production. Galactaric acid is an oxidation product from the gulacturonic acid, which is the primary biorefinery product from the beet pulp. It has benefits in many fields such as cosmetics, biopolymers and corrosion inhibitors.

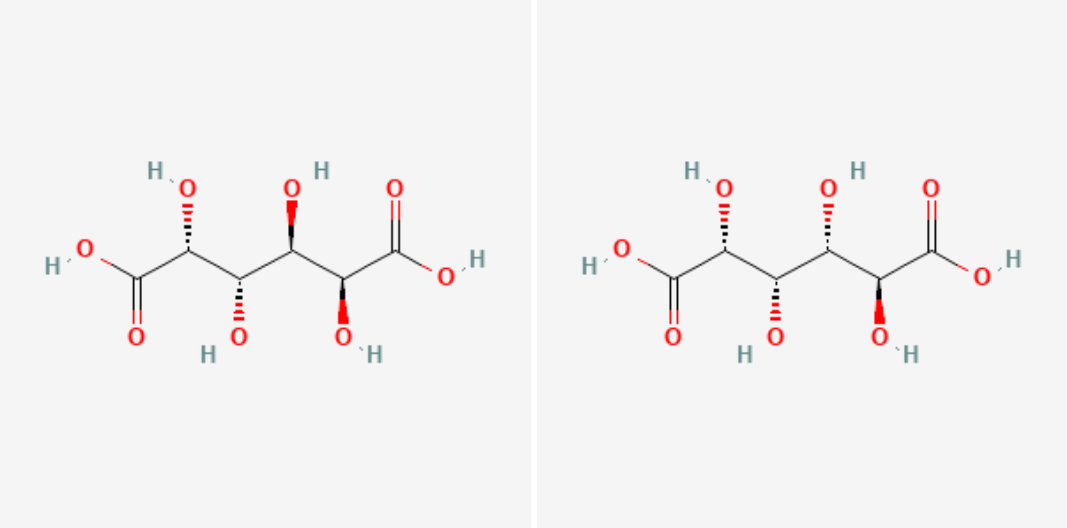

Figure 2.7 Galactaric acid (left)and Glucaric acid (right) chemical structures [48], [49].

Theoretically, galactaric acid has the potential to become a corrosion inhibitor due to its functional groups: hydroxyl and carboxylic groups. Currently, many papers have reported successful corrosion inhibition in organic substances that contain carboxylic acid [50]. The high polar force allows it to form a film on the alloy surface. This organic film will further prevent the alloy from direct contact with the environment. In addition, galactaric acid has similar properties to glucaric acid, which is another type of sugar acid that has already been used commercially as a corrosion inhibitor. Although they only have a slight difference in the chiral position, there is a huge difference in physical and chemical properties due to the hydrogen bonds. The recent research performed by the Cosun group has shown that galactaric acid performance as a corrosion inhibitor on carbon steel surpasses glucaric acid. Hence, further investigation is being conducted to find the optimal condition that allows galactaric acid to perform stably for commercial applications and use. Unlike glucaric acid, galactaric acid is not soluble in water. The salt form of the galactaric acid, sodium galactarate has higher solubility and is being used instead.

3 Research methodology

3.1 Material

In this research, aluminium alloy AW 3003 which had manganese as the major alloying element as shown in Table 3.1 was used. The Aluminium alloy plates were provided by Cosun. The plates were cut into square pieces of 2.5 x 2.5 cm. Each piece was ultrasonically cleaned in isopropanol for 10 minutes and blown dry with compressed air before starting further pretreatments.

Element	**Mn**	**Zn**	**Fe**	**Si**	**Cu**	**Others**	**Al**
composition	1.0–1.6	1.1	0.7	0.6	0.05–0.21	0.0–0.16	Balanced

Table 3.1 Chemical composition of aluminium alloy EN AW-3003 [51]

3.2 Sample preparation

In this thesis, the samples were categorized into 3 types according to Table 3.2. The Blank sample was simply degreased, and the Baseline sample was only pretreated with alkaline cleaning. Both samples were used as a standard for comparison purposes. The Reference samples were immersed in deionized (DI) water with adjusted pH values pH to be used compared with Inhibitor samples. The Inhibitor samples were immersed in NaGal solution in particular pH to observe the properties changes. The sample preparation is described in the following sections and shown in Figure 3.1.

Type	pH	Name
Standard	-	Blank
Standard	-	Baseline
Reference	3	Reference_pH3
Reference	4	Reference_pH4
Reference	7	Reference_pH7
Reference	10	Reference_pH10
Reference	11	Reference_pH11
Inhibitor	3	NaGal_pH3
Inhibitor	4	NaGal_pH4
Inhibitor	7	NaGal_pH7
Inhibitor	10	NaGal_pH10
Inhibitor	11	NaGal_pH11

Table 3.2 Sample categories

3.2.1 Alkaline Cleaning

Alkaline cleaning is one of the common pretreatments used for removing the oxide layer from aluminium prior to other pretreatments and coating. The advantage of alkaline cleaning is that it does not require mechanical pretreatment. The alkaline cleaning removes not only the oxide layer of the aluminium alloy but also the lubricant oil from the manufacturing process and small debris on the metal surface. It also does not involve toxic chemicals or rare-earth compounds [30]. Hence, the solution preparation is simple and cost-effective.

The alkaline cleaning method in this research consisted of 2 steps: The alkaline etching step followed by the desmutting by acid. The sample was etched in 30 g/L NaOH solution for 15 minutes, then it was rinsed with DI water, and blown dry with compressed air. For the following desmutting step, the sample was immersed in a 200 g/L HNO_3 solution for 2 minutes to remove the smut layer. After that, it was again rinsed and blown dry. The samples were kept in dry condition.

3.2.2 Corrosion Inhibitor immersion (NaGal)

The NaGal was weighed and dissolved in DI water to make a 0.5% wt concentration. The solution was stirred for at least 30 minutes until all the powder was fully dissolved and the solution became transparent. The solution was then divided into 5 batches, each containing 80 ml of solution. The pH of 5 batches was adjusted to pH 3, 4, 7, 10 and 11 by adding diluted NaOH or HNO_3. The samples were immersed in each inhibitor solution for 1 hour with a closed lid then blown dry with compression air. For reference purposes, separate samples were immersed in the demi water solutions with adjusted pH values without adding inhibitor for 1 hour.

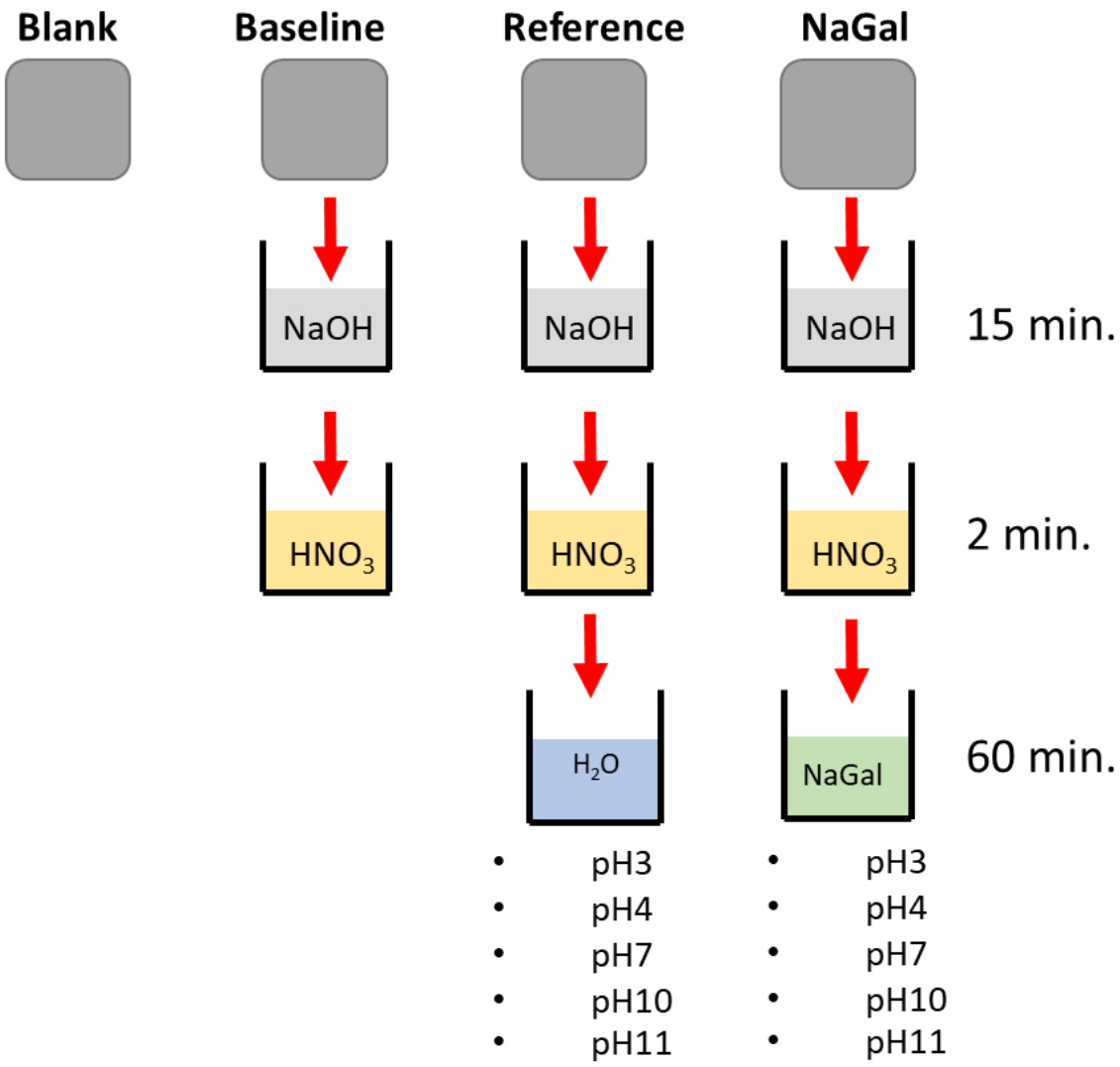

Figure 3.1 Schematic of sample preparation

3.3 Characterization methods

3.3.1 Contact angle and surface free energy

Contact angle or wetting angle measurement (θ) is a quantitative technique for determining the wettability of a solid surface. The obtained data can be further analyzed to determine, surface free energy, adsorption, and adhesion properties [52]. The material surface is often characterized by simply observing the behavior of the liquid droplet. The contact angle is defined as the angle where the 3-phases boundary (solid, liquid and air) interact as demonstrated in Figure 3.2.

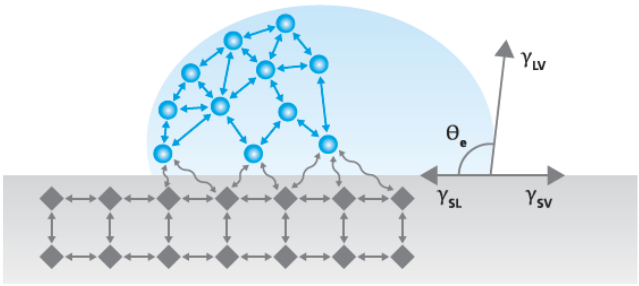

Figure 3.2 Contact angle measurement from the liquid droplet [52].

The Young-Laplace equation, which was developed by Thomas Young and Simon Pierre de Laplace is used to explain the balance of three phases holding the shape of the droplet:

$$\gamma_{sv} = \gamma_{sl} + \gamma_{lv} Cos\theta_y \qquad \text{Equation 3.1}$$

The θ_Y is often referred to as Young's contact angle or simply contact angle.

The dome-like shape of the droplet is a result of surface tension (liquid-liquid) and interfacial tension (solid-liquid). Relying on this observation, the surface free energy (or surface energy, as 'free' is often omitted in practical terms) can be derived and calculated. Even though it cannot be measured directly from the samples, it is still an important parameter and is frequently used in industries to determine the surface quality of the product. There are many models available for surface energy calculation. This work considered using Owens-Wendt-Rabel & Kaelble or OWRK, which has calculated the interfacial force based on polar and dispersion force theories. Contact angle measurement has advantages in simplicity and only a small amount of the liquid is needed to acquire chemical and physical properties on the sample surface. On the contrary, the small amount of liquid being used is increasing the risk of impurity [53].

The OWRK theory was selected to use in this work. It states that the free surface energy consists of a polar component and a dispersive component. Therefore, the method requires a minimum of two different types of liquid of known surface tension, one should be a non-polar liquid (high dispersive force) and another a polar liquid (high polar force). In this thesis, three different liquids are used. The polar liquids are ultrapure water (milli-Q) and ethylene glycol (Sigma-Aldrich). The non-polar liquid is di-iodomethane (Sigma-Aldrich). The experiment was carried on by the optical tensiometer (Biolin Scientific) in sessile drop mode.

In practice, the drop of liquid (volume 2.0 µl) was placed on the sample surface by a micro-syringe and the images of the droplet were recorded for approximately 10 seconds. The angle was analysed

automatically from the static images by OneAttension software. The measurement was done in triplicate. The results were averaged and compared. The surface energy was later calculated from the contact angle values with the same software using the OWRK model.

3.3.2 Fourier transform infrared-reflection absorption spectroscopy (FTIR – RAS)

FTIR relies on polychromatic radiation that measures the vibration from the excitation of molecular bonds. The vibration and rotation are caused by the energy transition inside the molecule, which can be defined as stretching, bending, rocking and wagging. Because each molecule has a unique response to infrared (IR) frequencies, FTIR can be used to identify the mixture composition. Moreover, the height of the spectra peak represents the amount of the material, which can also be used for quantification purposes. FTIR-RAS is known as infrared reflection absorption spectroscopy (IRRAS). This technique is very suitable for thin film analysis (approximate thickness 0.5-20 μm), especially for the monolayer films on the metal surface that follow the Langmuir adsorption model. The technique can be used to identify thin film composition and observe the molecular orientation in corrosion inhibitor's film [54], [55]. After sample preparation, the measurements were performed on a Thermo Scientific Nicolet 6700 with a Smart SAGA Accessory. The infrared spectra were set to 64 cycles and the wavenumber region was scanned from 4000 to 650 cm^{-1}. The measurement is performed directly after the pretreatment of the samples. The baseline spectrum was used as a background for all samples. OMNIC software was used for baseline correction and peak identification.

3.3.3 White light interferometry (WLI)

WLI is an established technique that can precisely measure the 3D shape of the object. It has been adopted to measure the roughness of the surface. The technique relies on the optic path which enables non-contact measurement of the samples. The Bruker ContourX-100 Optical Profilometer was used to perform roughness measurements. The green light was selected as an illumination parameter with the fringe scan speed 1x. The interferometer averaged three scans per measurement. Five different areas on the sample were measured, the selected areas were demonstrated as the red circles in Figure 3.3. The Root mean square roughness (Rq) was chosen as a comparison parameter because it is more sensitive to height differences than the average roughness (Ra). The data correction and parameter calculation were done in Gwyddion 2.60 software.

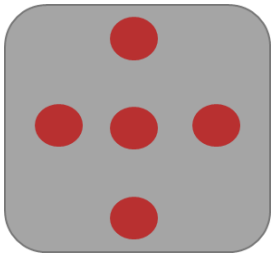

Figure 3.3 The areas that were selected to perform the roughness measurement per sample

3.3.4 Pull-off adhesion test

To evaluate the coating adhesion the adhesion test according to the ASTM D4541 – 17 standard was done [56]. The test was performed by attaching a dolly to the sample surface (coating layer) with adhesive and then using a pull-off adhesion gauge to measure the force (stress) that causes the coating to fail. The pull-off adhesion test is based mainly on the tensile force, the shear force can be neglected. The force that caused the failure is recorded and used as a factor to determine the adhesion quality. In practical terms, two types of failure can occur, which are an adhesive failure and cohesive failure as illustrated in Figure 3.4. The adhesive failure is a failure caused by the coating and sample interface while the cohesive failure is caused within the coating interface, which could mean that the interface between the sample and coating is stronger, or the coating was not applied evenly.

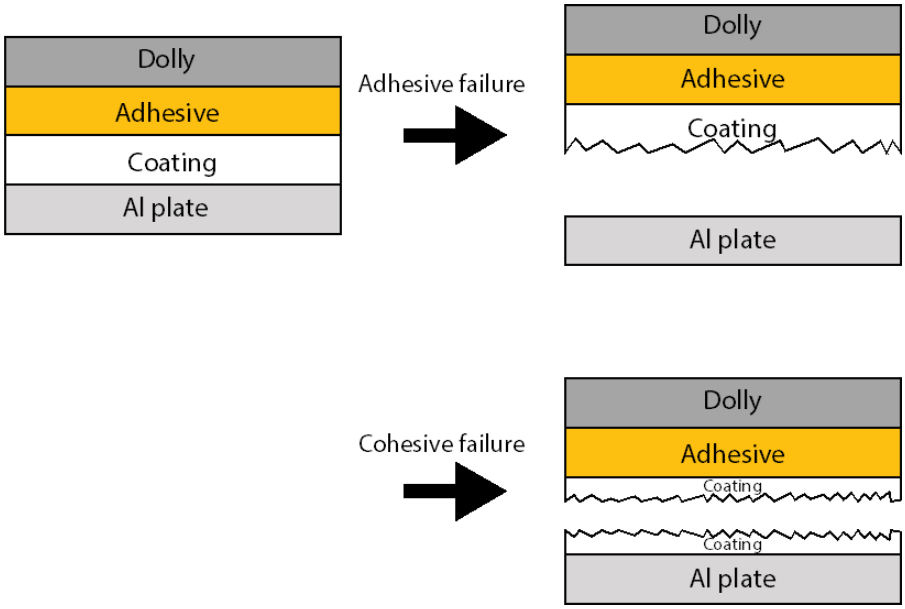

Figure 3.4 Schematic of adhesion failure types

Before the test, the aluminium plates were cut into a square shape (5 x 5 cm^2) for ease of sample preparation and to ensure enough surface for dollies placing. An Epoxy Primer 37076 coating was prepared by mixing the primer with Hardener 92133 and Thinner 98064 by the ratio of 2 :1: 1 in a beaker, supplied by AkzoNobel. After the pretreatment, the coating was applied to the sample by a bar coater of 30 µm, hence the thickness of the organic coating was assumed to be 30 µm. The paint was left for 48 hours to dry. After that, the coated aluminium plates were gently sanded with sandpaper and rinsed with isopropanol to increase surface roughness for better attachment of the dollies. The 20 mm-diameter dollies were then prepared by sanding with sandpaper, rinsing with isopropanol and drying. Next, each dolly was glued with Araldite 2000+ glue (Huntsman) and glass beads (Sigma-Aldrich) to the sample surface. The excess glue was cleaned from the sample surface and the samples were left for another 24 hours for the glue to dry. The test was carried out by the Elcometer 510 automatic pull-off adhesion gauge with the pulling force of 20 Mpa on the dolly. The force that caused the adhesion failure was then recorded and reported along with their failure type for comparison on each sample.

3.3.5 Electrochemical techniques

The electrochemical analysis is a group of powerful techniques that can be used to evaluate the effectiveness of corrosion inhibitors and determine their adsorption mechanism. A broad range of analyses is used to measure the corrosion rate and inhibition efficiency of the films formed by corrosion inhibitors. By applying an external potential or current to the electrode, the electrode becomes polarized and various observations can be taken to evaluate the electrochemical properties. The techniques are well suited for both qualitative and quantitative measurement analysis.

One of the advantages of the electrochemical techniques is that most of the time the conventional three-electrodes set-up (Figure 3.5) is used so one can carefully design the order of the experiment to utilize the most out of one sample. The setting of the experiment used in this thesis is shown in Figure 3.6.

The electrochemical system consisted of three electrodes:

1. Working electrode: the electrode or sample of interest

2. Reference electrode: The electrode used to measure the potential of the working electrode. The Ag/AgCl double junction electrode was selected for this work.

3. Auxiliary electrode or counter electrode: this electrode provides a closed circuit. The platinum mesh was used in the work.

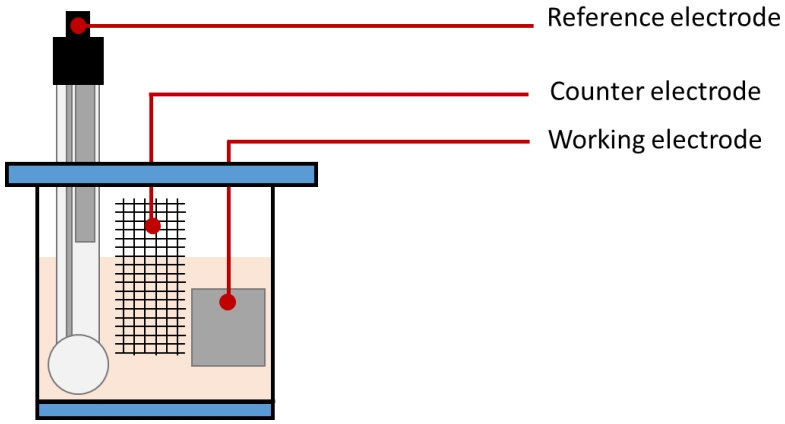

Figure 3.5 An illustration of the conventional electrochemical experiment setup

The sample was loaded into a cell with an exposed area in a circular shape of 1.8 cm^2. All electrodes were submerged in 80 ml of 0.05 M NaCl electrolyte which has created a mild aggressive environment with the presence of Cl^- ions and then connected to a BioLoGic VSP-300 electrochemical workstation, a multiple-channel potentiostat. The measurements are set in the sequence starting with open-circuit potential (OCP) mode for 30 minutes. The following measurements, linear polarization resistance (LPR) and Electrochemical Impedance Spectroscopy (EIS), took place after the OCP was stabilized. The system was set for OCP monitoring while the LPR and EIS measurements were taking place approximately every 2 hours. The time difference in each measurement is due to the time that the LPR and measurement took in each loop. After 24 hours passed, the potentiodynamic polarization was performed. In each condition, the electrochemical measurements were performed on three different samples, a representative curve was chosen to portray with standard deviation. The diagram of the experimental sequence is shown in the following schematic.

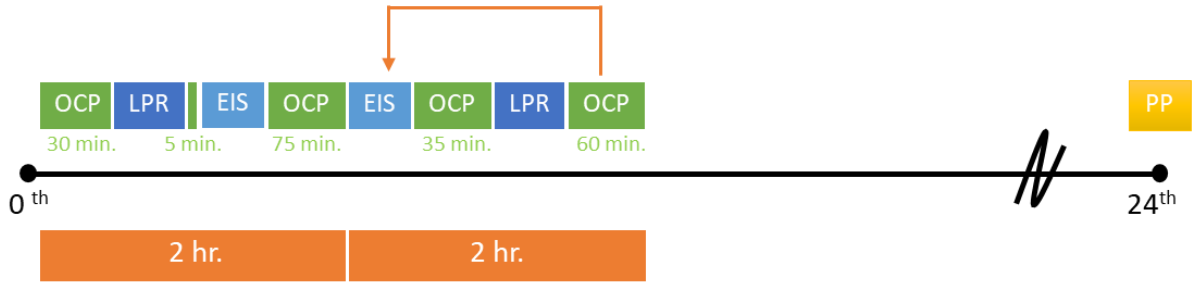

Figure 3.6 The electrochemical measurement sequence

Open-circuit potential

The open-circuit potential, which is often shortened to OCP, is a common technique, often used as an initial technique to stabilize the system and find optimal time before continuing to other electrochemical analyses. The analysis was carried out by measuring the potential between the working electrode (sample) and a reference electrode without applying any external potential. In the corrosion inhibitors study, this technique is often used as a quick identification of the corrosion inhibition behavior by observing the change in potential. A decrease of potential (toward negative) indicates the dissolution of the passive film. On the contrary, an increase of the potential (toward positive) can be an indicator of forming of the inhibitor's film [57]. However, further analysis is still needed to confirm the identification. In addition, OCP can be used for monitoring the stability of the passive film formed by the inhibitors since it is used to observe the thermodynamic properties of the working electrode.

Linear polarization resistance

By applying the potential around the corrosion potential (E_{corr}) of the metal, the current response (icorr) is being monitored. E_{corr} is the potential value when the anodic and cathodic reaction rates are equal, and the sample is stabilized with the electrolyte. The Polarization resistance (R_p) is calculated from the slope of the current density vs potential plot. In this thesis, the R_p was obtained by using the EC-lab software.

In the corrosion inhibitor study, this technique is suitable for determination of the corrosion protection properties of the inhibitor layer. An index of the inhibition efficiency of a corrosion inhibitor on the working electrode surface can be calculated via Equation 3.2.

$$\text{Inhibition efficiency } [\%] = \frac{R_p^i - R_p}{R_p^i} \times 100 \qquad \text{Equation 3.2}$$

R^i_p Polarization resistance of the sample with inhibitor (NaGal sample)
R_p Polarization resistance of the sample without inhibitor (Reference sample)

The disadvantage of the LPR is the shortage of the result since the information it provides is like a snapshot of the time period (simple, fast, instantaneous data collection). Hence, the corrosion rate cannot be calculated from LPR data and only R_p (Polarization resistance) is retrieved in the end [58]. Moreover, complications during the measurement can arise from potential scan rate, non-linear and non-stationary behavior of the system, which could easily cause data loss in a long-observed experiment. Nevertheless, LPR is still a useful, non-destructive technique that can be repeated many times on the same sample without its degradation [59]. In addition, LPR can also be used in the time-dependent experiment to monitor the

corrosion of the sample, which is often used for screening inhibitors since it gives the real-time evaluation over the exposure time without the need to apply a wide window of the potential [60], [61].

Electrochemical Impedance Spectroscopy

Electrochemical Impedance Spectroscopy (EIS) is a common tool for studying the electrode surface (or the metal surface). The unique feature of the EIS, that sets it apart from other techniques, is that instead of the DC voltage, it applies the low amplitude of the sinusoidal voltage (AC) perturbation to the electrode and measures the current response, providing the frequency-resolved information. In the corrosion field, this technique is used to evaluate the characteristic of the passive film via the Bode plot and Nyquist plot. EIS is often used as a follow-up measurement to support other analyses because it is a non-destructive technique and can use the same conventional electrochemical setup.

The electrochemical Impedance (Z) is defined between the applied potential and the observed current. The impedance can be expressed as a function of the magnitude (Z_0) and the phase shift (ϕ) as shown in Equation 3.3 [62].

$$\mathrm{Z} = \frac{E(t)}{I(t)} = \frac{V \cdot \cos(\omega t)}{I \cdot \cos(\omega t - \varphi)} = Z_0(cos\varphi + jsin\varphi) \qquad \text{Equation 3.3}$$

Where j is an expression represents the imaginary number (j = $\sqrt{}$ -1)

The Bode plot shows the impedance (|Z|) vs frequency (f). The inhibition mechanism can be observed at the low frequency because it is related to the protective layer that is formed by the corrosion inhibitor. By comparing the magnitude of the impedance at the frequency of 0.01 Hz over a time period, it can be used as evidence of inhibitor film and the corrosion resistance can be estimated [63]. Generally, |Z| is used to determine the corrosion resistance of the inhibitor. The increase of this value implies the increase of the corrosion resistance, while the decrease suggests the corrosion acceleration. Additional information can be determined by the phase angle which is also obtained in the Bode plot. The increase of an angle in the sinusoidal voltage perturbation can indicate the existence of the inhibition [64].

Equation 3.3 can be further calculated and expressed the impedance data by plotting in terms of real and imaginary components by $Z_{real} = Z_0 cos\phi$ and $Z_{imag} = Z_0 jsin\phi$. Both are represented in the Nyquist plot (Z_{real} on the x-axis and Z_{imag} on the y axis) as exhibited in Figure 3.7.

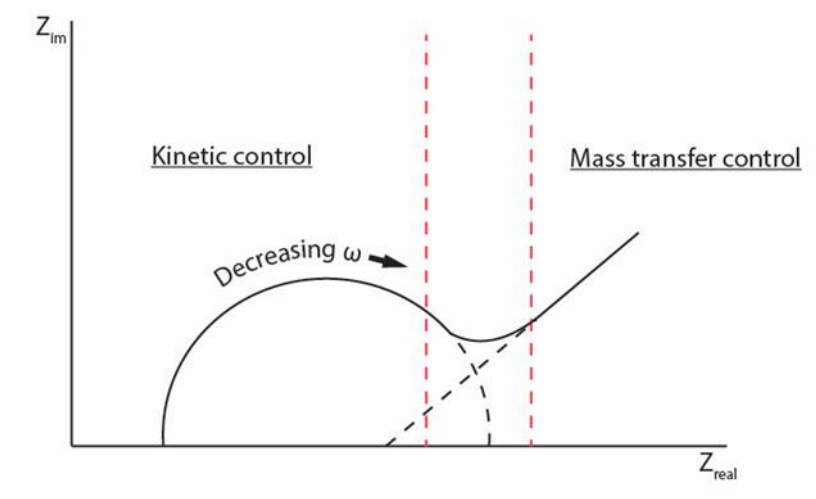

Figure 3.7 A diagram of the Nyquist plot

The Nyquist plot in Figure 3.7 shows that at high frequency, the kinetic of the system is rapid as it is controlled by the charge transfer. As the frequency decreases, the diffusion process becomes more important and takes control of the kinetic. However, the diffusion process is much slower and the plot changes to linear. This region is called mass control, the impedance calculated from this region is called Warburg impedance. For corrosion investigation, the electrical equivalent circuit is selected to fit the Nyquist plot for analysis. Despite many complex models that have been proposed, the result interpretation is still complicated and time-consuming due to non-stationarities and non-linearities [65].

The charge transfer resistances of the samples were calculated by the EC-lab software with respect to the proposed equivalent circuit. The charge transfer is used as a determining factor for corrosion resistance, the sample with high charge transfer resistance has better corrosion resistance due to fewer metal ions dissolved. Furthermore, the corrosion inhibitor efficiency can be calculated by the following equation.

$$Inhibitior\ efficiency\ (\%)\ \frac{R_p^{inhibitor} - R_p^{reference}}{R_p^{inhibitor}} \times 100 \qquad \text{Equation 3.4}$$

Potentiodynamic polarization (PP)

PP is often performed after the OCP measurement which ensures that the working electrode is thermodynamically stable. The technique is widely used in corrosion studies to observe the kinetics of the corrosion system. Unfortunately, PP is a destructive method because it forces an oxidation reaction on the specimen, hence, the consistency of the data might be difficult to obtain in a large polarization range. The measurement starts with the potentiostat applyingpotential sweep to the electrode and collecting the current response data, which are used in the polarization curve plotting. The polarization curve (Figure 3.8) is a powerful tool that shows the relationship between the potential (E) and current or current density (i), consisting of two partial reactions: cathodic reaction (reduction) and anodic reaction (oxidation).

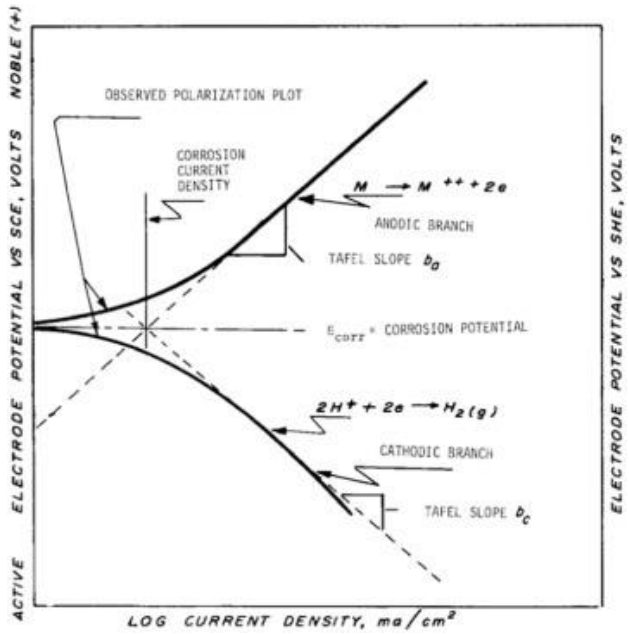

Figure 3.8 A schematic of the polarization curve or Tafel plot [66].

Considerably useful information about the electrochemical reactions on the working electrode surface can be obtained from the polarization curve. Corrosion potential (E_{corr}) and corrosion current/current density (I_{corr} /i_{corr}) can be estimated from the Tafel slopes at the intersect point between the extrapolated linear part of cathodic and anodic branches (where both cathodic and anodic rates are equal). Furthermore, Icorr can be further used to calculate the corrosion rate with Faraday's law to determine the corrosion resistance ability of the inhibitor film. For localized corrosion, E_{pit} can be determined from the anodic branch at the end of the linear part, at the inflection point of the potential. In the samples where localized corrosion dominated uniform corrosion, comparing corrosion rates might be misleading. In this case, ∆E is used to represent the potential range that the samples have resistance or undergo passivation, which can be calculated based on Equation 3.5.

$$\Delta E = E_{corr} - E_{pit} \qquad \text{Equation 3.5}$$

Similar to LPR and EIS, icorr from the polarization curve can also be used to estimate the inhibition efficiency of the corrosion inhibitor by the following equation where icorr and $icorr_{(inh)}$ are the corrosion current density without the inhibitor and with the inhibitor, respectively [67], [68].

$$inhibition\ efficency\ (\%) = \frac{i_{corr} - i_{corr\,(inh)}}{i_{corr}} \times 100 \qquad \text{Equation 3.6}$$

In this thesis, the inhibition efficiency calculated from LPR and PP were compared. The polarization curve can also be used to observe the behavior of the passive film during the corrosion process (Figure 3.9). In aluminium alloys, the corrosion process can be divided into three stages. Firstly, when the metal is in an aggressive environment, corrosion is prone to happen. This 'active state increases the corrosion rate rapidly until the second step is reached. The second step, 'passive state' starts when the oxide film is generated to cover the metal surface, changing the corrosion rate to plateau. Nevertheless, the corrosion process is still ongoing during this step, but in form of competitive processes between the dissolution of the aluminium from the direct contact with the corrosion environment and the formation of the oxide film (passivation). The

dissolution of aluminium leads to an increased corrosion rate, while the formation of the oxide film slows down the rate as the film blocks the species' transportation. Lastly, when the first process kinetically exceeds the second process by the increasing potential or the medium becoming more aggressive, the third state, 'transpassive state', occurs. This state is described as the oxide film getting thinner or dissolute due to the change in the oxidation state and the increase of oxygen condensation (oxygen evolution) at the interface between alloy and its film [69]. Despite the common usage of passive alloys, only a few theories for transpassivity have been studied.

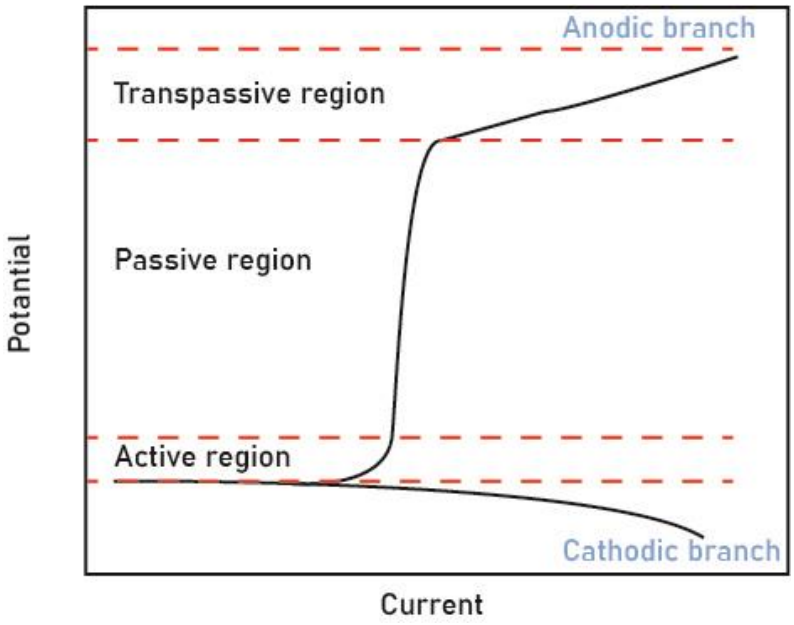

Figure 3.9 Schematic of polarization curve showing passivity region in metal.

To conclude, the alloys can endure corrosion by the passive film for a long time if there are no aggressive changes in the environment. Otherwise, the film will be ruptured, and the alloys are prone to corrode in the transpassive stage till the new passive films are formed.

3.3.6 Immersion test

The immersion test is carried out in order to observe the pitting corrosion on the sample surface after 24 hours of immersion. According to the immersion test and pitting corrosion examination standard G46 – 21 [70], the procedures consist of complicated setup and time-consuming observation, which is not feasible for this thesis. The test was simplified by immersing the sample in a closed-lid beaker for 24 hours. A solution of 0.05 M NaCl was used. At the end of the immersion, the samples were cleaned in isopropanol by ultrasonic cleaner for 10 minutes to remove loose corrosion products and small pollutants. The surface of the sample is then examined with VHX-5000 Keyence digital microscope with 50x magnification. The images were captured using the VHX-5000_900F communication software. For pitting evaluation, the middle area of the sample was examined within a 5 mm radius (80 mm^2). The pitting was assumed to have a circular shape for the ease of conducting the measurement. Measurement of the diameter of the pit and pit density were done manually by ImageJ software with Fiji plug-in. The pit was neglected if the diameter is smaller than 1 µm or not clearly visible.

4 Coating adhesion investigation

This chapter describes the research observations and key findings in surface analysis. The properties that may have effects on the coating adhesion were investigated. The result from Fourier-transform infrared-reflection absorption spectroscopy (FTIR-RAS), surface energy and surface roughness are presented. The pull-off adhesion test result is presented at the end.

4.1 Fourier transform infrared-reflection absorption spectroscopy results

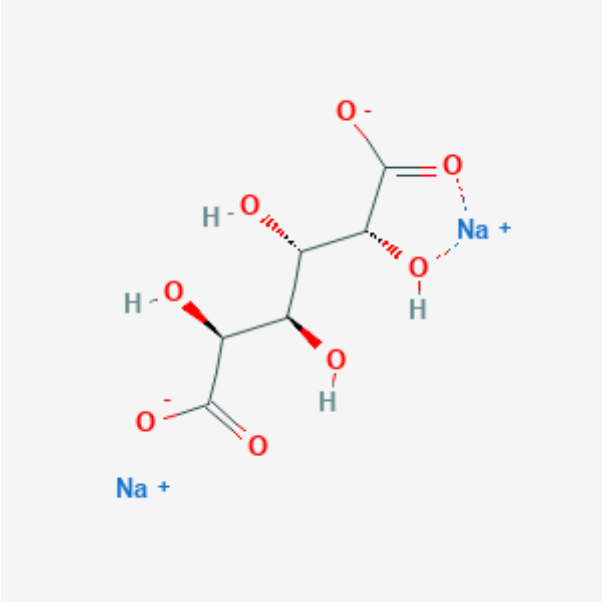

Figure 4.1 Sodium galactarate (NaGal) molecular structure [71].

According to the NaGal chemical structure, shown in Figure 4.1. The compound contains two functional groups: hydroxyl and carbonyl (part of carboxylate ion). The peaks that were detected in NaGal powder absorbance spectra in Figure 4.2 are shown in Table 4.1.

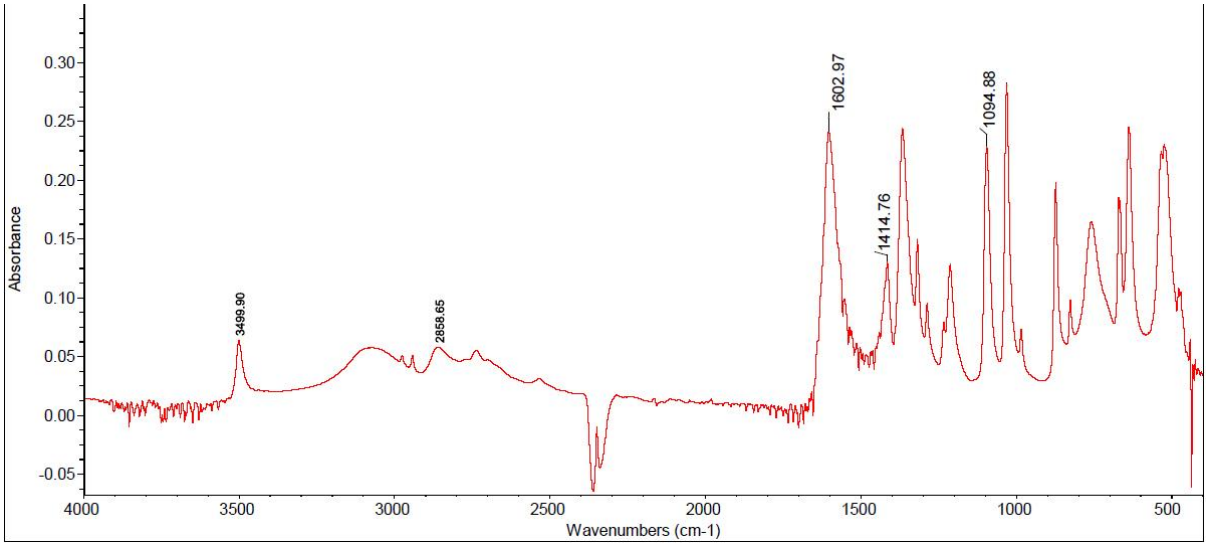

Figure 4.2 Absorbance spectrum of NaGal powder

Wave No.	Molecular reaction
3499	O-H stretching
2858	O-H stretching
1602	Asymmetric C-O stretching (partial bond)
1414	Symmetric C-O stretching (partial bond)
1094	C-O stretching

Table 4.1 Detected peaks in NaGal powder absorbance spectrum [72].

Figure 4.3 showed several peaks corresponding to the peaks of NaGal in a powder form. The largest peaks appeared around 1650-1510 and 1400-1280 cm^{-1} wavenumbers and were identified as carboxylates. Carboxylate ion served as an adsorption centre, therefore the detected peaks indicated that NaGal was able to adsorb on the aluminium alloy surface by bonding through carboxylates [73]. It is to be noted that the spectra of the NaGal samples showed an increase in the intensity of the hydroxyl peak (3469 m^{-1}). This was possibly due to the presence of the NaGal since its molecule contains six hydroxyl groups.

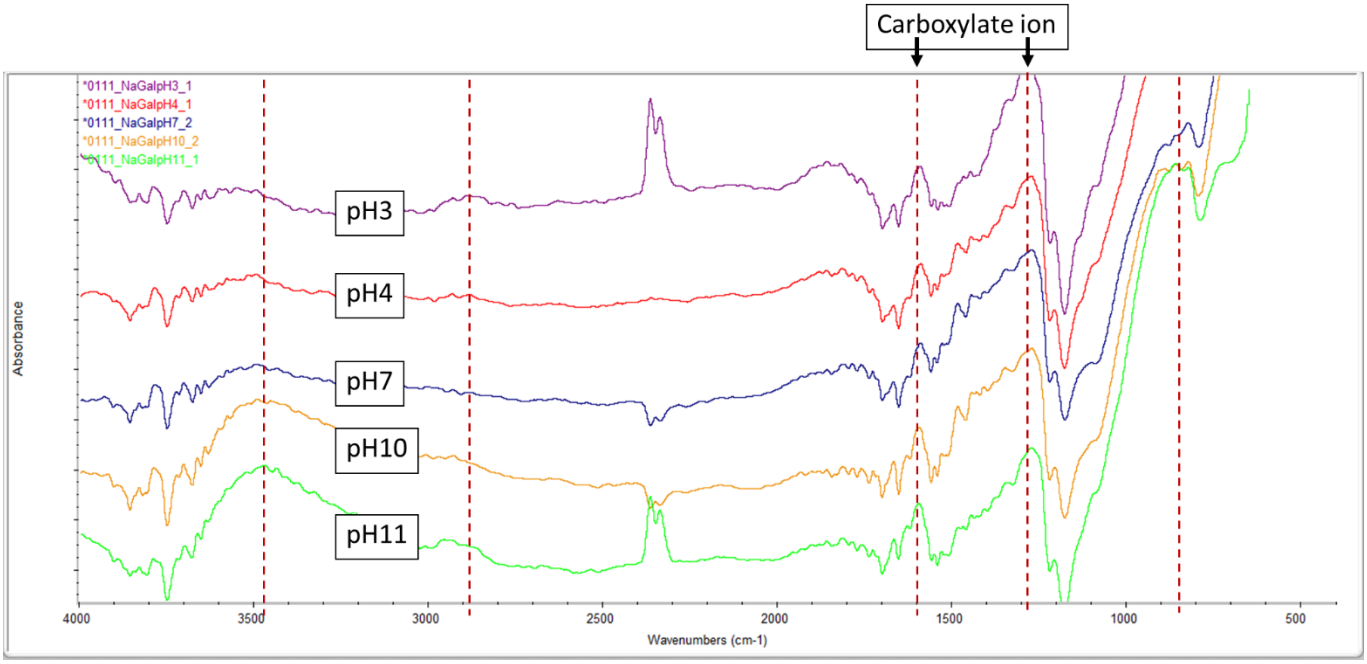

Figure 4.3 NaGal samples' relative absorbance spectra

WaveNo.	Molecular reaction
3469	O-H stretching
2867	O-H stretching
1650-1510	Antisymmetric C=O stretching
1590	O-H Bending
1400-1280	Symmetric C=O stretching
847	Alumina Al_2O_3

Table 4.2 Detected peaks in NaGal samples spectra [74]

While all the mentioned peaks were absent in the reference samples spectrum, the aluminium oxide peak was present in both Reference and NaGal samples as shown in Table 4.2 and Table 4.3. The absorbance spectra of NaGal_pH11 and Ref_pH11 were demonstrated in Figure 4.4 as a comparison.

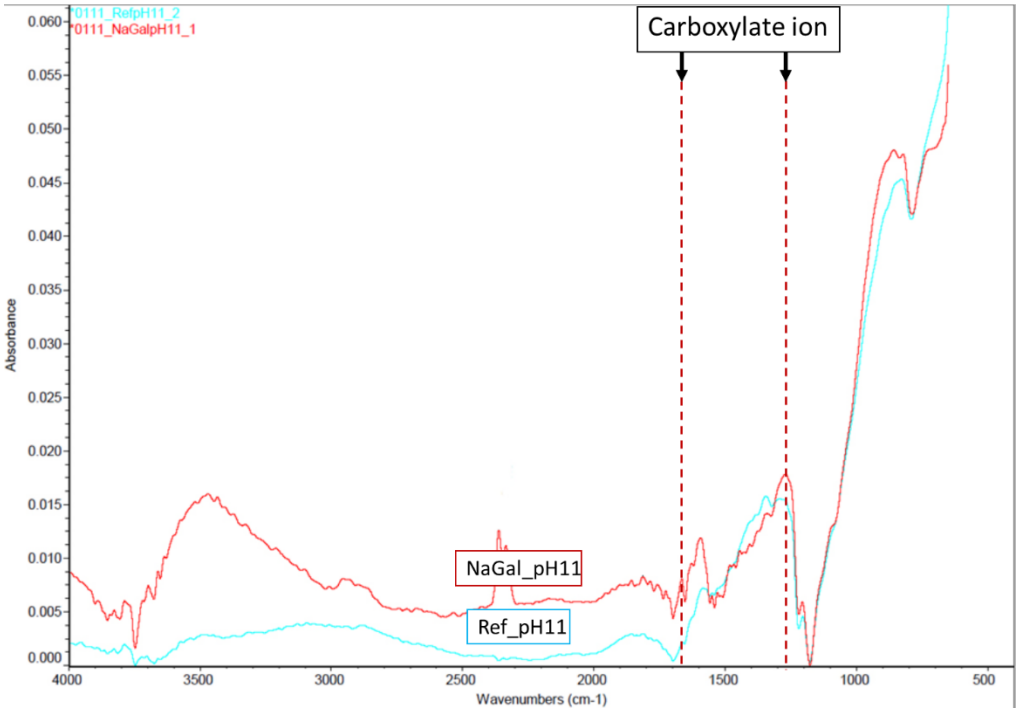

Figure 4.4 NaGal and reference samples (pH11) absorbance spectra

Wave No.	**Molecular reaction**
1814	O-H Bending
835	Alumina (Al_2O_3)

Table 4.3 Detected peaks in Reference samples spectra

Therefore, it can be concluded that NaGal adsorbed on the sample surface in pH 3, 4, 7, 10 and 11.

4.2 Surface energy

The OWRK model was used to calculate the surface energy from the contact angle measurements. The results are shown in Figure 4.5. Detailed results are provided in Appendix A.

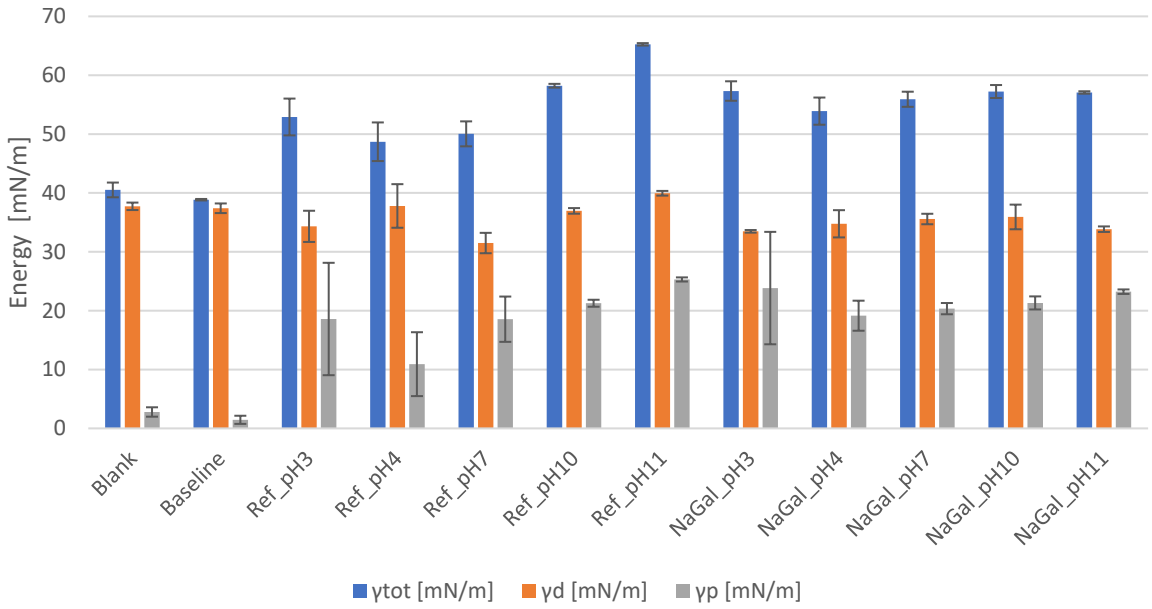

Figure 4.5 Averaged values of surface energy; γ_{tot}, γ_d and γ_p represent total surface energy, dispersive force and polar force orderly. The error bars show the S.D. of the measurements done in triplicate.

It is exhibited in Figure 4.5 that alkaline cleaning did not increase the surface energy of the aluminium alloy. The baseline sample had a drop in surface energy relative to the Blank due to the decrease of polar force. This meant that the alkaline cleaning likely caused the surface to become more hydrophobic or alternatively the pretreated oxide layer had different properties. When compared with the Blank, all samples that were immersed in NaGal solution showed an increase in surface energy, mainly from the polar force part. The face values suggested that the increase of the polar force was due to the change of the pH either more acidic (pH extremely low) or basic (pH extremely high). This was related to the concentration of the polar molecules, such as (H^+ and OH^-), in the solution. These increments exceed their references; hence the effect was mostly caused by the NaGal layer. This was likely because NaGal had many functional groups (as shown in Table 4.2.) and was considered to have high polarity.

The film-forming mechanism of the inhibitors can be classified as physisorption or chemisorption. Physisorption is fundamental for all absorption, it is generally regarded as weak molecular interaction, such as London dispersive and Van de Waal force, which is a primary molecular interaction. It can easily reverse by desorption of the adsorbate species [75], [76]. While chemisorption requires a stronger molecular reaction from the polar force, such as dipole-dipole interaction and chemical bonds, and cannot be fully reversed since it requires high energy to break the bond [76]. Despite the increase of the polar force in the surface energy, the adsorption of the NaGal was likely physisorption as the results in electrochemical analysis later showed possible desorption of NaGal, this topic will be discussed later in chapter 5. However, further investigations would be needed for confirmation.

In contrast to alkaline cleaning, the total surface energy of the samples which had been immersed in the NaGal solution has increased. Even though the effect of this increment was caused by both dispersive and polar force, the polar force has more impact on the coating adhesion property because the molecular interaction force was simply stronger as described in the chemisorption. Therefore, the comparison between the pH was made in Figure 4.6. The averaged values with S.D. were given. It showed that NaGal was very effective in increasing the polar force in low pH, but this effect is less as the pH increased. In pH11, the NaGal sample had a lower polar force than the reference. However, it is worth mentioning that Ref_pH11 was covered by corrosion products, which had a hydrophilic surface since NaGal prevented corrosion products to redeposit, NaGal_pH11 had a lower polar force.

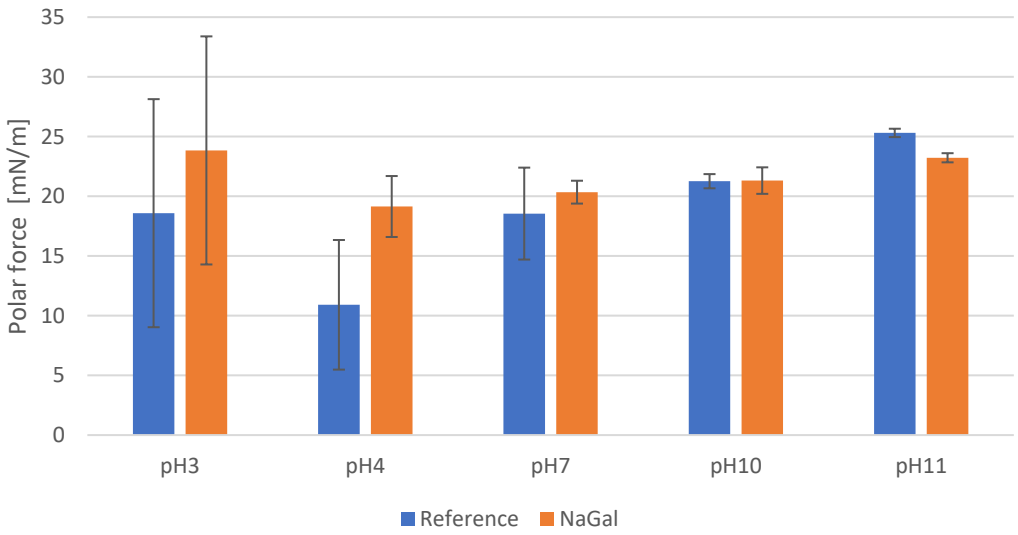

Figure 4.6 Comparison of NaGal effect on polar force

These results were well-supported by the electrochemical results that showed the increase of corrosion rate in the NaGal sample, which would be discussed in the following chapter. The hydrophobic surface would improve the corrosion resistance property of the alloy because it was difficult for the H_2O molecules to adsorb on the surface of the alloys due to the water affiliation. Contrastingly, the increase of the polar force was beneficial to the coating adhesion. It was reported that the increase of the polar force has a strong relation to adhesion strength [77].

In short, the increase of the total surface energy by the NaGal pretreatment led to an improvement of the coating adhesion, but this could also promote corrosion since the surface supported ion transportation.

4.3 Pull-off adhesion test

Continuing from the contact angle results, the pull-off adhesion test was carried out at three different pHs (3, 7, and 11) to observe the change of coating adhesion in acidic, neutral, and alkaline environments. As NaGal pretreated samples had increased polar force, NaGal showed a potential to be a coating adhesion promoter for the alloy. A Zr-based pretreatment sample (labelled 'Zr') was immersed in a 0.01 M H_2ZrF_6 solution that was adjusted to pH 4 for 40 seconds. The sample was then rinsed and blown dry with compressed air. The pull-off adhesion test was done in duplicate and the results from the pull-off test were summarized with a S.D. as error bars in Figure 4.7.

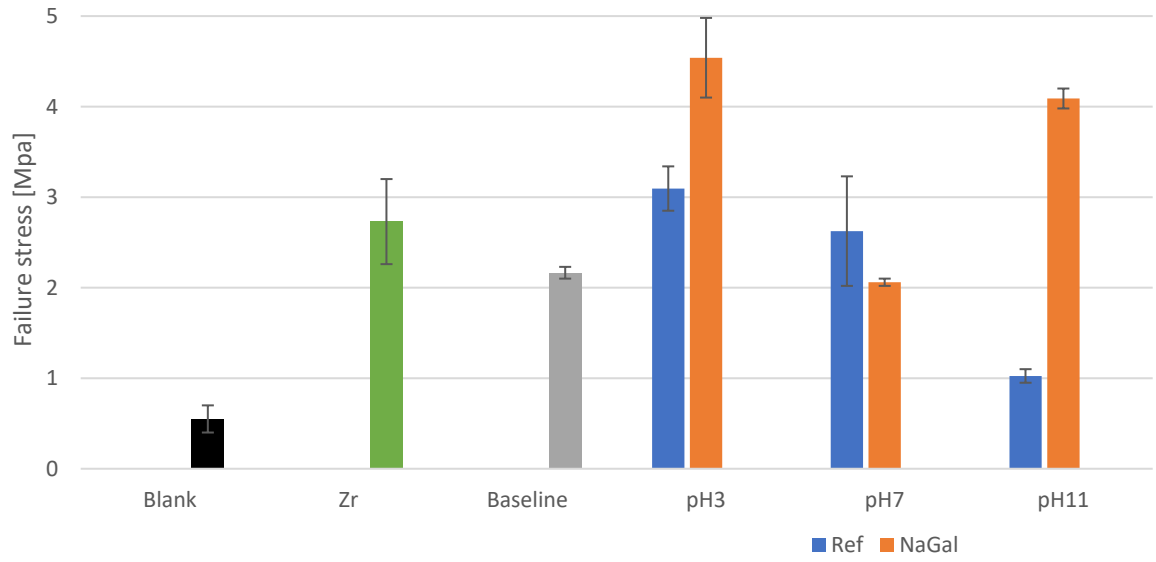

Figure 4.7 Average failure stress from pull-off adhesion test

It can be seen from face value that Zr-based pretreatment that was used as a benchmark had improved the coating adhesion as the failure stress increased to double from the Blank. The Baseline, which was alkaline cleaned, also showed an improvement relative to the Blank. This was in agreement with the literature's findings that the native oxide of aluminium alloys has characteristics (such as hydrophobic) that downgrade the surface quality for coating adhesion. However, the perfect pull-off could not achieve in the test, which was likely caused by the uneven coating or coating layer being too thick. The types of failure were also observed and reported in Table 4.4 for a more accurate conclusion. The adhesive failure means the pull-off test was done successfully, but cohesive failure could mean that the failure did not occur on the interface between the organic coating layer and metal substrate, but rather in the coating layer. Hence, the failure of the coating did not give accurate information about the coating adhesion property.

	1st	2nd
Zr (Benchmark)	Cohesive failure 25%	Adhesive failure 75%
Blank	Adhesive failure 25%	Adhesive failure 50%
Baseline	Adhesive failure	Adhesive failure
Ref_3	Adhesive failure 50%	Adhesive failure
Ref_7	Cohesive failure	Adhesive failure 75%
Ref_11	Cohesive failure 30%	Adhesive failure
NaGal_3	Adhesive failure	Adhesive failure
NaGal_7	Adhesive failure	Adhesive failure
NaGal_11	Cohesive failure 25%	Cohesive failure 10%

Table 4.4 Failure types of the pull-off test samples performed in duplicate [area %]

Even though the face value in Figure 4.7 suggested that NaGal pretreated samples had higher stress failure than Zr-based pretreated sample, it cannot be concluded that NaGal pretreatment improved the coating adhesion exceeding the Zr-based pretreatment. This is because Zr had a cohesive failure, the actual failure stress should have been higher if the coating had not reached its failure before. Nevertheless, NaGal samples, except NaGal_pH7, had their failure stress higher than their reference samples. Especially in pH11, the required force to pull the coating off was nearly double in comparison with the reference.

From the chemical bonding perspective, the hydroxyl groups from NaGal and acidic/alkaline environments treatments might have also contributed in creating a strong chemical bond between the coating and alloy surface. As previously described in Surface energy (4.2), NaGal pretreatment significantly promoted polar force. Figure 4.8 exhibits the relationship between polar force and failure stress, providing evidence supporting the relation. The error bars were omitted in this plot to clearly demonstrate the relationship as the S.D. of both results had presented in previous graphs. NaGal samples that have the highest stress failure also possessed the highest polar force. Interestingly, Ref_pH 11 sample had a very low coating adhesion despite having high polar force. However, the high polarity was likely caused by the loosely attached corrosion products to the surface of the sample. These corrosion products possibly created a smut layer, which could be easily removed, and made the surface heterogeneous. This led to the overall poor bonding of the coating. As shown in Figure 4.6, there was only a minor effect from the NaGal pretreatment in pH7 in terms of polar force. Hence the stress failure between the Reference and NaGal samples also showed little difference.

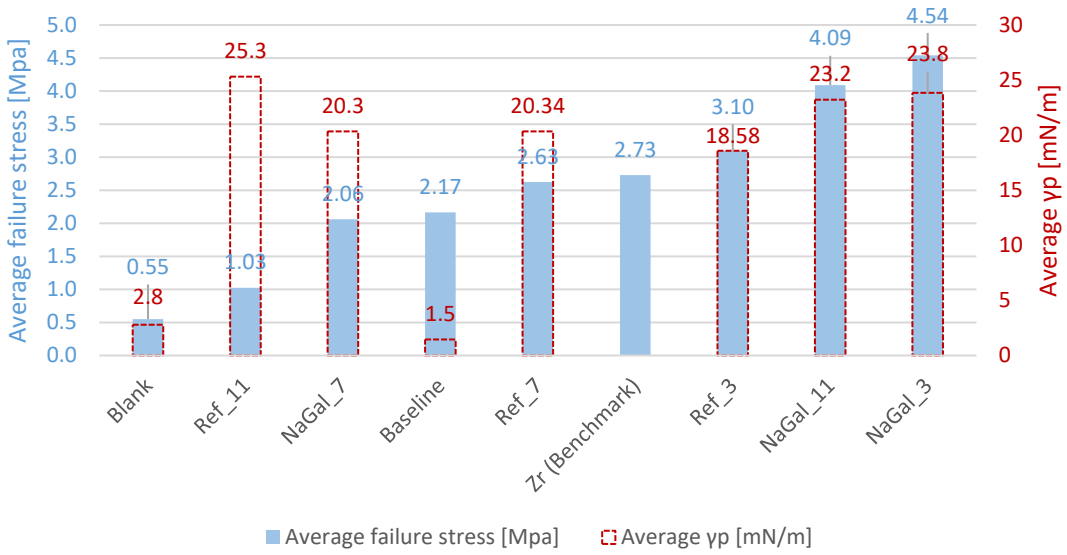

Figure 4.8 Relation between polar force and failure stress.

In summary, the increase of the failure stress indicated strong interfacial bonding between the surface of the samples and the effectiveness of the pretreatment. The increasing trend had a strong relation to the increase of the polar force, which was well supported theoretically.

4.4 Surface roughness test

Regardless of their surface energy in the Blank and Baseline, there was a significant improvement in coating adhesion as shown in Figure 4.8 despite having lower polar force. An explanation of improved adhesion due to surface roughness was suggested as there was also a strong relation between the coating adhesion and the surface profile. It was reported that the increasing of surface roughness favored the adhesion between the coating and the metal [78]. Figure 4.9 showed the averaged values of the root mean square roughness and the error bars represented the S.D. values. The results in Figure 4.9 complied with this argument as alkaline cleaning improved the coating adhesion by increasing the surface roughness.

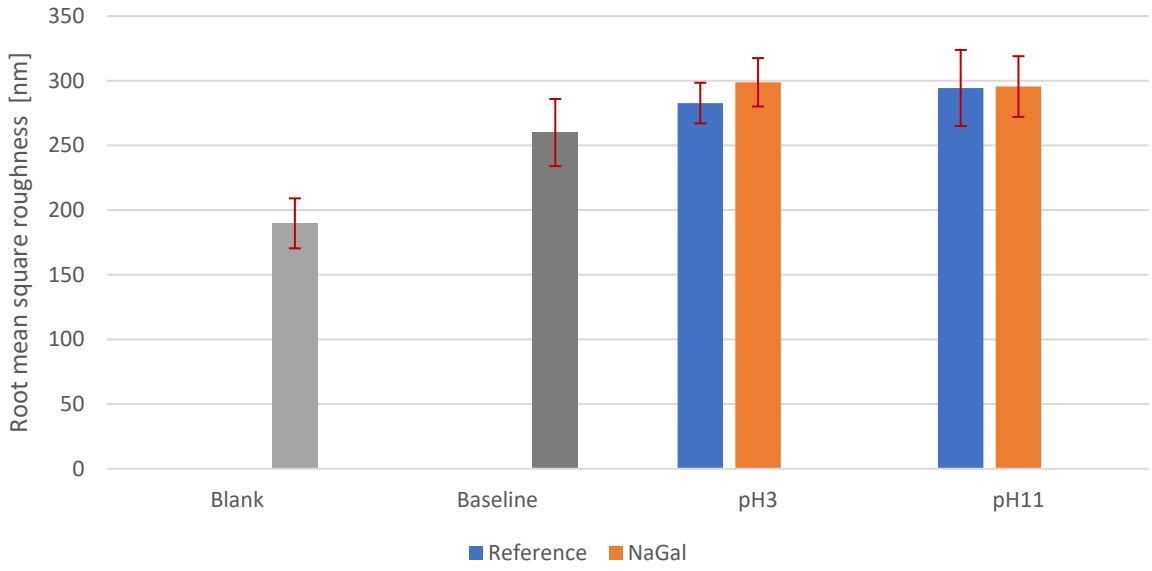

Figure 4.9 The pretreatment effect on samples' surface roughness.

The adsorption and mechanical interlock are the most accepted dominant mechanism that affect the adhesion strength of the organic coating. As the adsorption mechanism was briefly discussed in Surface energy section, The mechanical interlock is described in the surface roughness section because of their relation. Mechanical locking is a mechanism when the organic coating flows into the pores on the metal's surface. These interlocking also acts as an obstacle to cracking propagation [79], [80]. Due to this reason, the researchers presume that some specific surface topographies may have more influence on the adhesion strength than others. The schematic shows an example of an interlocking mechanism in the interface between the organic coating and metal substrate as shown in Figure 4.10.

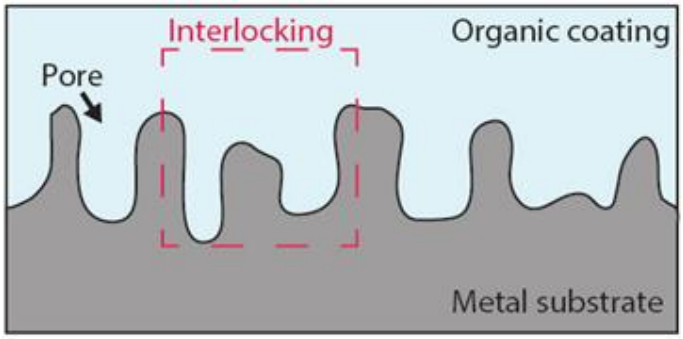

Figure 4.10 Interlocking mechanism

Although NaGal pretreated sample had a minor effect on the roughness, the samples still showed an improvement in coating adhesion. This could mean that both adsorption mechanism and interlocking had an influence on the adhesion strength, but if the adsorption mechanism passed the threshold, it could dominate the influence on the adhesion strength.

5 Electrochemical investigation

This chapter presents the results related to the electrochemical behaviors of the samples. The results are categorized according to their immersion environment.

5.1 Neutral environment immersion

5.1.1 Blank

Without any pretreatment, the Aluminium alloy had its native oxide layer on the surface (Figure 5.1) which consisted of mixed oxide created by alloying elements (mainly Fe, Mn and Si) and Al itself. At the beginning of NaCl immersion, the oxide/hydroxide layer grew as evidenced by increase in electrochemical parameters. Then they became to decline with an extension of time indicating the pitting from chloride ions adsorbed on the surface.

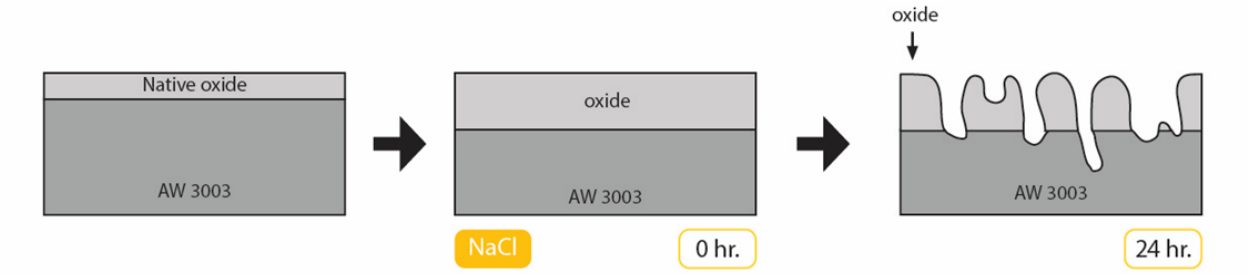

Figure 5.1 Blank sample behavior during NaCl immersion

2.3.1. Baseline

The surface modification, alkaline cleaning, was done on the baseline sample. During the alkaline cleaning, the layer called ‘smut’ was formed on top of the surface as illustrated in Figure 5.2. This layer consists mainly of the re-deposited products from the dissolved second phase particles and Al. This smut layer was later removed by submerging the sample into acid and the oxide layer, which was composed mainly of alumina was formed as the top layer during the process.

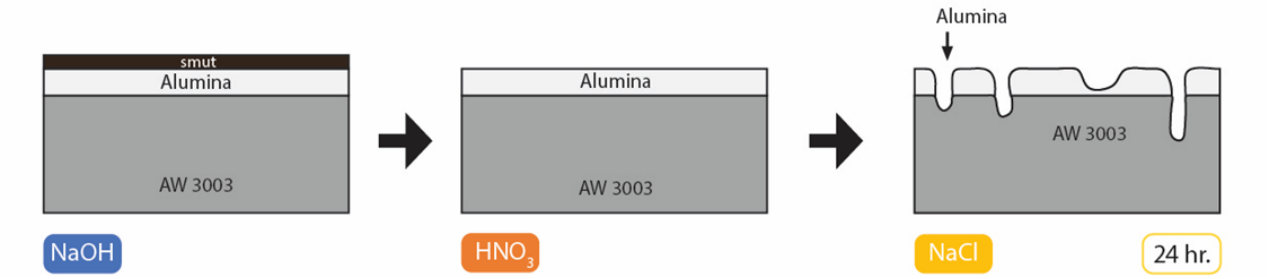

Figure 5.2 Baseline sample during alkaline cleaning and NaCl immersion

The electrochemical parameters in the baseline sample remained the same throughout the NaCl immersion time. Some results exhibited a decreasing trend near the end of immersion, which was probably caused by pitting.

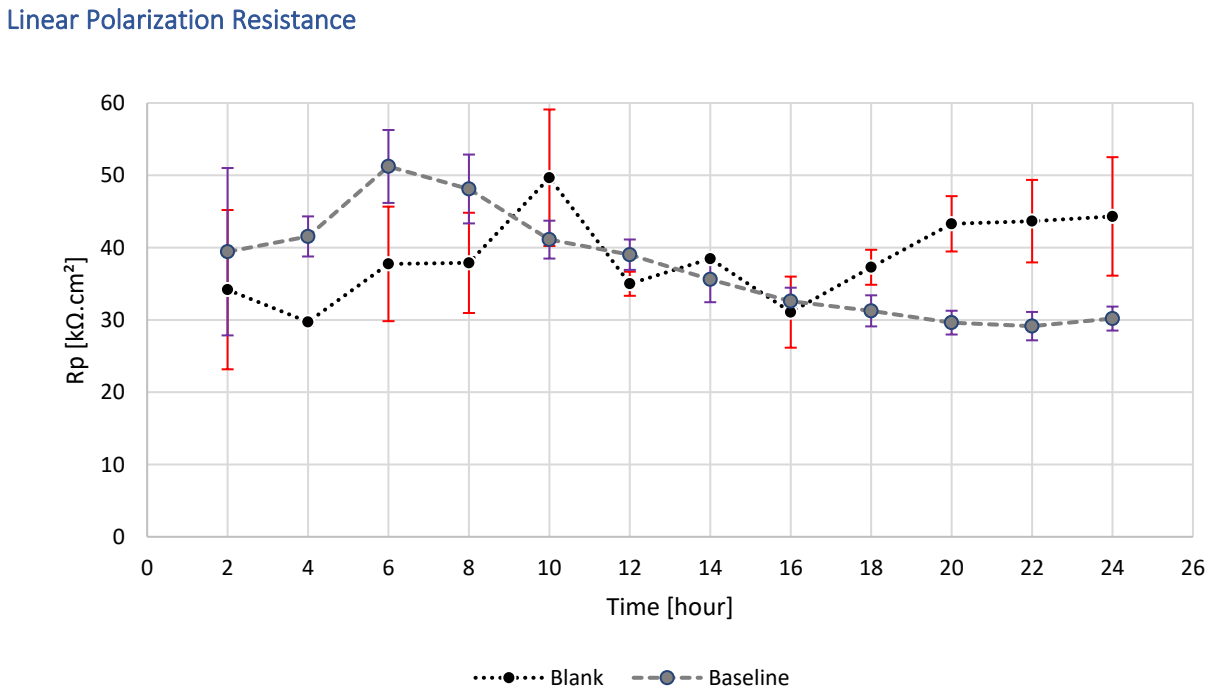

Figure 5.3 Polarization resistance of Blank and Baseline in 0.05 M NaCl with S.D. as error bar

At the beginning of the experiment, the Blank and Baseline were immersed in 0.05 M NaCl electrolyte, which had a neutral pH. This allowed the passivation of aluminium to grow as exhibited by the increase of polarization resistance in Figure 5.3. However, after the localized corrosion started, the Rp began to decline. This trend was more visible in the baseline sample. Although in the case of the blank sample, the oxide film could be reformed, which possibly increased the Rp again.

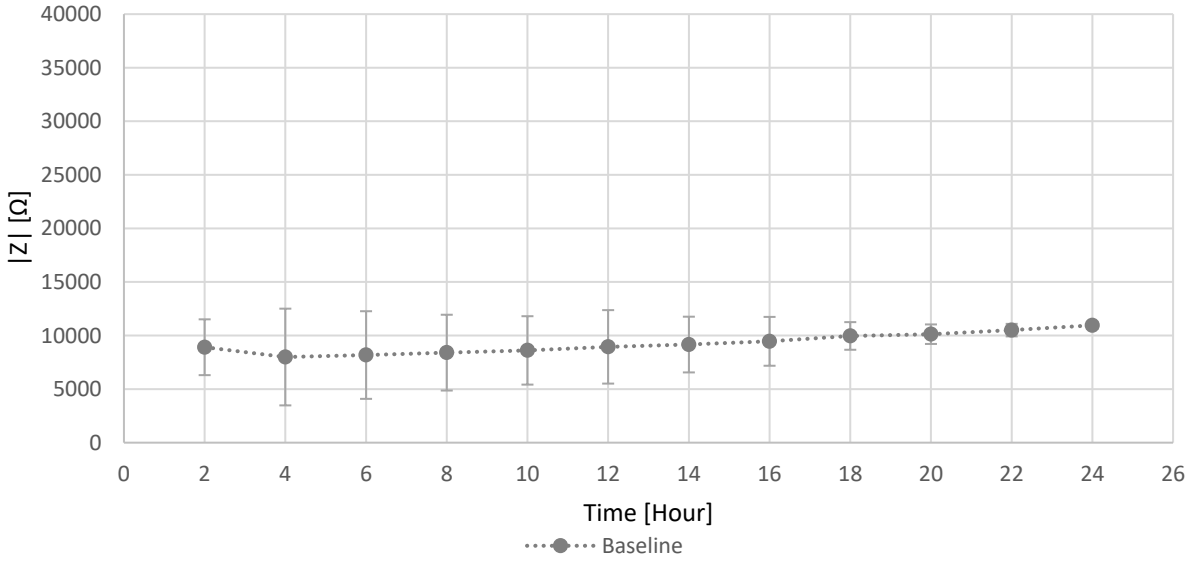

Figure 5.4 Impedance modulus at 0.01 Hz of Baseline sample during 24 hours immersion in 0.05 M NaCl, S.D. values are presented as error bars

The impedance modulus at the frequency 0.01 Hz was selected as a value represented the corrosion resistance property of the corrosion inhibitor [60].The Blank result was not shown here as it was unstable during EIS measurement despite several adjustment in the measurement setting. This was possibly due to the complexity and randomity of the native oxide composition since it was unknown which compounds were formed on the sample surface. This also made the surface appear to be heterogeneous. Nevertheless, the increase in the impedance was related to the growth of the oxide film. The Baseline was stable throughout the experiment likely because of the stability of the alumina on top of the baseline sample and less pitting corrosion on the sample surface. Unfortunately, both Blank and Baseline have high standard deviation (S.D.), hence it was not possible to make a comparison between these two samples.

The Nyquist plots of Blank and Baseline are provided in the following figures. For the Blank, the impedance at the low frequency (the left-side of the plot) gradually increased. Although it changed to decreasing trend near the end of the immersion time. The Baseline also showed an increasing trend of the impedance at low frequency from the beginning of the experiment. The impedance abruptly increased in the first few hours before continuously, slowly increasing over time.

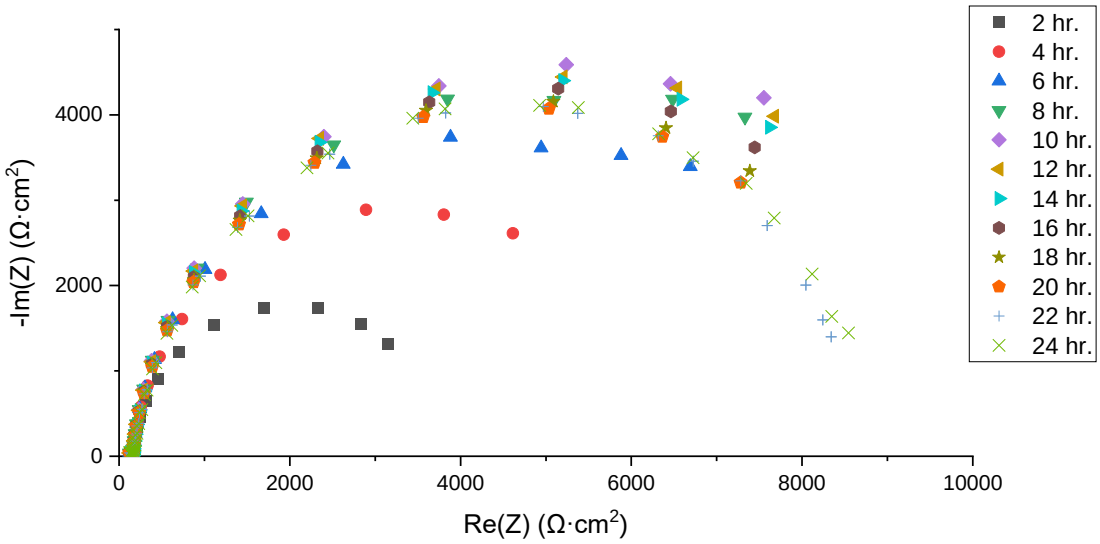

Figure 5.5 Nyquist plot of Blank in 0.05 M NaCl.

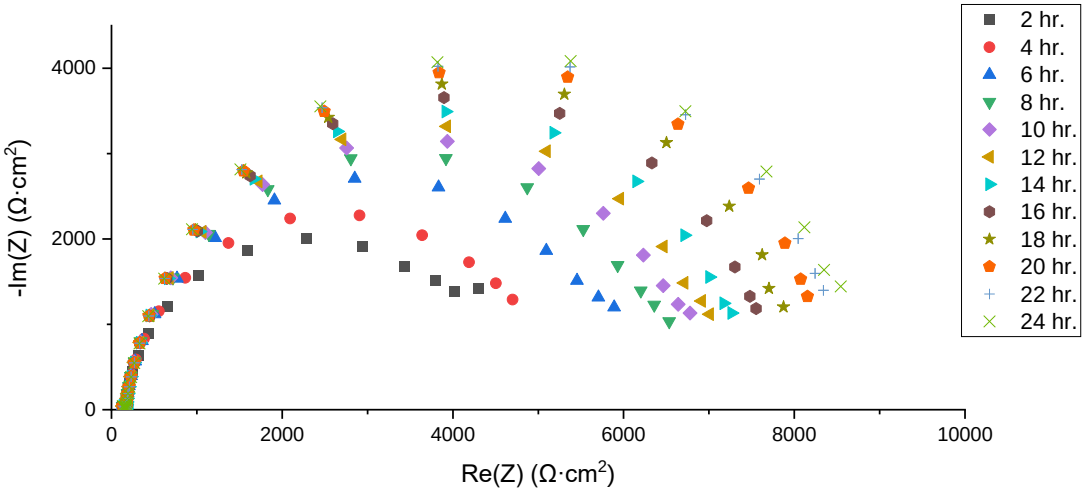

Figure 5.6 Nyquist plot of Baseline in 0.05 M NaCl.

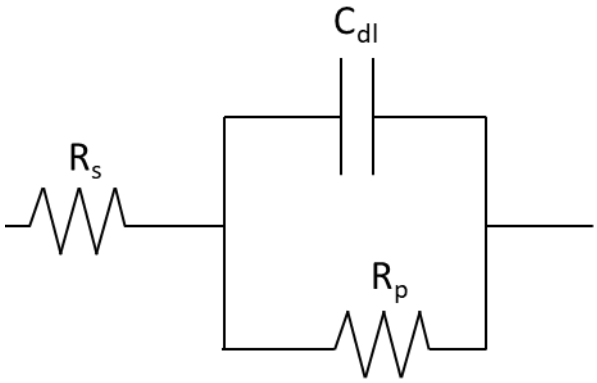

Figure 5.7 Simplified Randles cell equivalent circuit.

The Nyquist plots from the Blank and Baseline show a typical arc for the Simplified Randles cell. Hence, this equivalent circuit (Figure 5.7) was used for both samples to calculate the polarization resistance. The results shown in Table 5.1 Table 5.1were rounded up for ease of comparison, the exact values are shown in Appendix B: Rp calculated from equivalent circuits.

	Time [hour]	**2**	**4**	**6**	**8**	**10**	**12**	**14**	**16**	**18**	**20**	**22**	**24**
Blank	Rp [kΩ]	20	50	50	60	50	50	50	50	40	40	30	30
Baseline	Rp [kΩ]	5	5	6	7	7	7	7	8	8	8	9	9

Table 5.1 Polarization resistance of Blank and Baseline samples from Nyquist plot

The Blank had a comparable development in both the Rp obtained from EIS and LPR. Although Baseline's Rp remained the same with a subtle increase over time, its Rp was much lower than the Blank's. The increase and decrease of the Rp were likely related to the growth of the oxide film and the localized corrosion caused by the attack of the Cl^- ions. However, the baseline sample did not exhibit any of this behavior in any measurement, suggesting that only the original native oxide layer of the alloys has the self-healing ability during the immersion time. This was possibly due to the complex oxide/hydroxide in the layer or simply the layer was able to grow thick enough that the corrosion did not reach the original alloy material. Nevertheless, the native oxide was more attracted by the Cl^- ions, which consequently led to higher pitting corrosion. While the alkaline cleaned oxide layer did not grow during the immersion it had better resistance toward pitting.

For ease of comparison, other electrochemical results are presented with Ref_pH7 and NaGal_pH7 results in the following section.

5.1.2 Reference pH7 (Ref_pH7)

The Reference sample went through the same surface treatment as the Baseline sample. After removing smutting, the sample surface was assumed to be covered mainly by alumina (Al_2O_3). After that, the sample was immersed for one hour in DI water. Not only could this cause the Alumina layer to thicken, but some chemical reactions from the alloying elements and Al could form complex compounds and deposits on the sample surface. According to the Pouxbaix diagram in Figure 5.10, Fe, Mn and Si are passive in neutral pH, hence, the oxide layer on top of the Ref_pH7 had different composition and properties than Blank and Baseline.

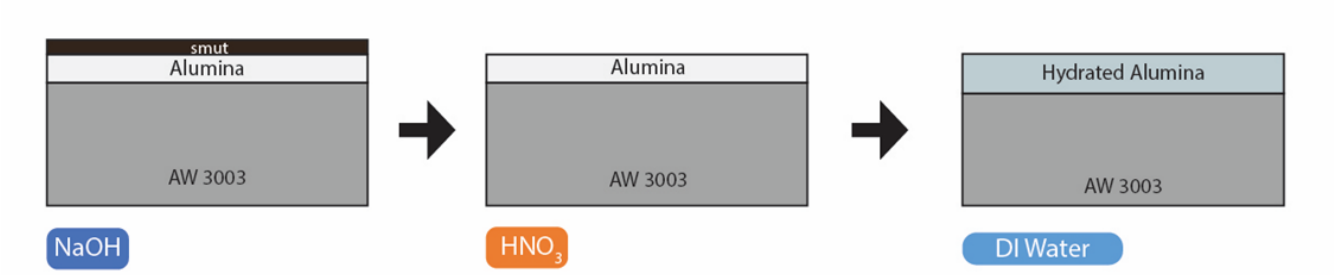

Figure 5.8 Ref_pH7 during the pretreatment

As illustrated in Figure 5.9, at the beginning of the experiment, the oxide layer grew as the polarization resistance (from EIS) increased. Eventually, the pitting started near the IMPs areas and the stain re-deposited near the pit. However, the stain layer acted as a physical barrier to the aggressive chloride environment.

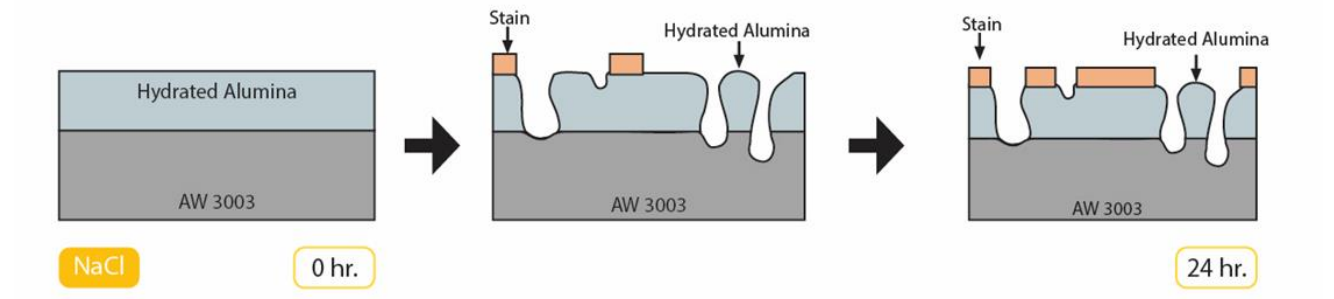

Figure 5.9 Ref_pH7 during NaCl immersion

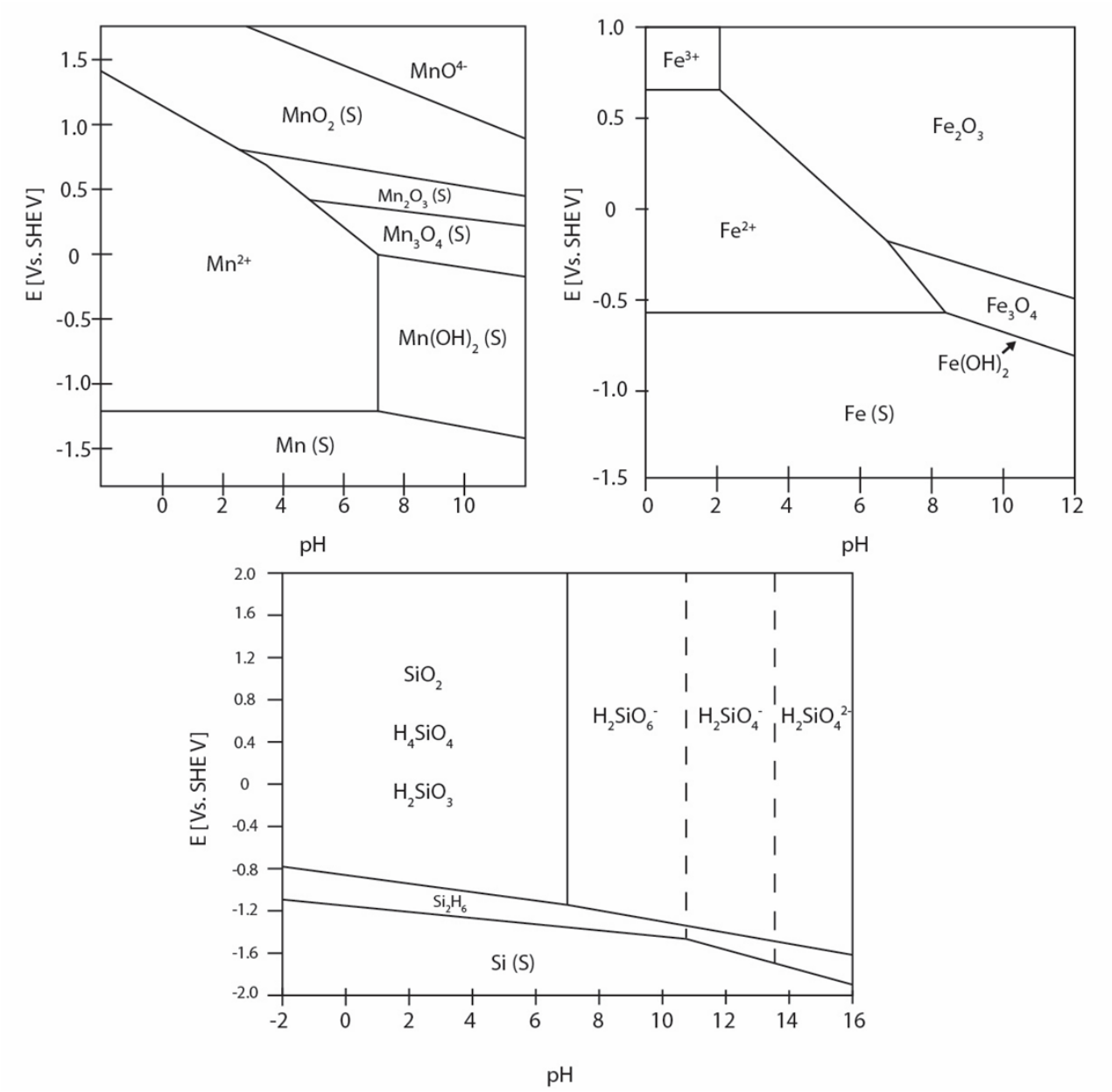

Figure 5.10 Pouxbaix diagram of the main alloying elements (Mn, Fe and Si)

2.3.2. NaGal_pH7

For NaGal_pH7 sample, the NaGal pretreatment was carried out after the alkaline cleaning. During the inhibitor immersion, NaGal was adsorbed on top of the oxide layer as evidenced and explained in section 4.1Fourier transform infrared-reflection absorption spectroscopy results. However, it was presumed that the NaGal layer did not perfectly cover all of the sample surface, some gaps or pores might appear in the layer.

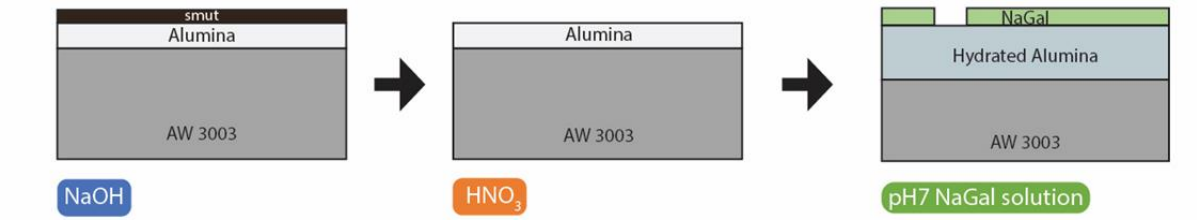

Figure 5.11 NaGal_pH7 during the NaGal pretreatment

Similar to the reference sample, the oxide layer became thicker at the beginning of the experiment as it was able to grow from being in contact with the solution as some of the NaGal was desorbed from the surface. Consequently, the areas were fully exposed to the electrolyte and started to corrode uniformly and locally. Although the sample suffered from localized corrosion less than the reference, the stains were also formed on some parts of the surface as the polarization resistance (from EIS) increased. The areas that were not covered with the stain underwent pitting as exhibited in Figure 5.12.

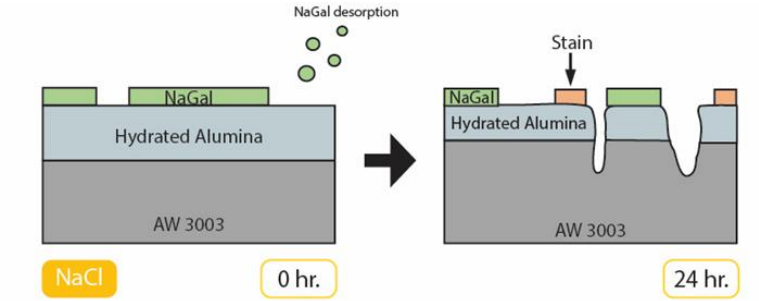

Figure 5.12 NaGal_pH7 during NaCl immersion.

Linear Polarization Resistance

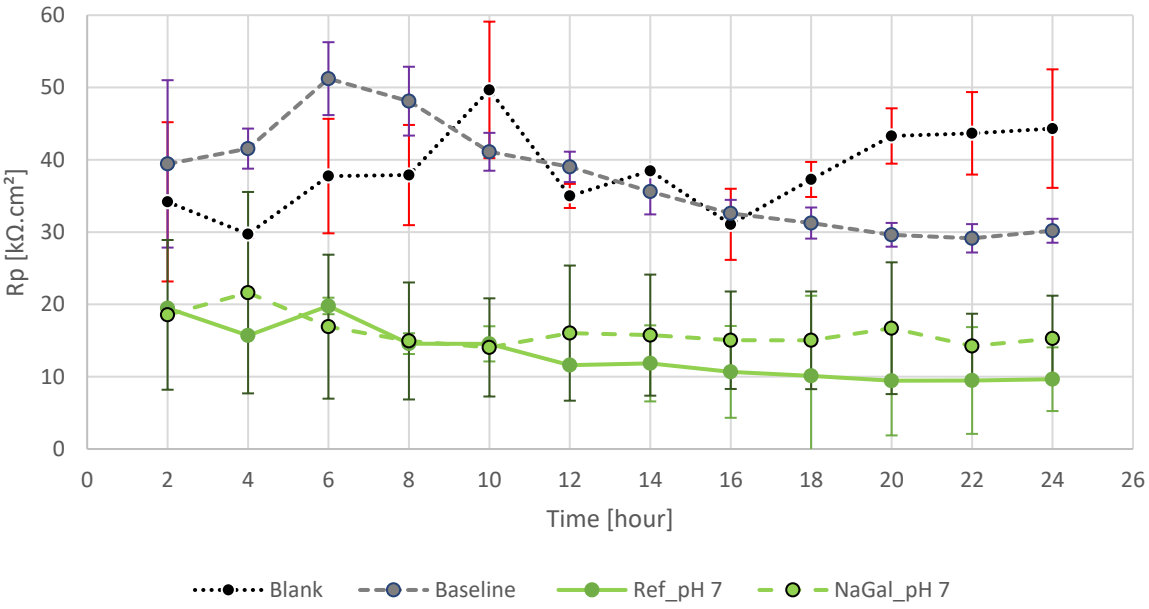

Figure 5.13 Polarization resistance of neutral environment immersion samples in 0.05 M NaCl with S.D.

The hydrated alumina layer caused the Rp of Ref_pH7 to be much lower than Rp of Blank and Baseline. As it was presented in the previous chapter, both Ref_pH7 and NaGal_pH7 surface had increased hydrophilicity relative to the standard samples Although it benefitted the coating adhesion properties, it demoted the corrosion resistance, as shown in Figure 5.13 both samples had lower Rp than the Baseline. The corrosion rate increased because the ions could diffuse easier into the oxide layer. Since Rp did not show an increasing trend during the immersion, it could mean that the NaGal pretreatment did not create a self-healing property like the native oxide Unfortunately, both samples were not reproducible causing the data to overlap. Therefore, few conclusions were made in an individual sample, but no comparison between these two samples was done.

Electrochemical Impedance Spectroscopy

The reproducibility of the samples could not be achieved in pH7 despite the setting adjustment, making it impossible to compare the data with other samples or observe the trend during the immersion. This might have been due to the IMPs on the surface, which were generated during alkaline cleaning, react with the NaGal substance. Because alkaline cleaning randomly increased the IMPs density on the surface, this could lead to random error in the samples and causing them to be unstable. Nevertheless, the overlapping of the data between NaGal_pH7 and Ref_pH7 suggested that the presence of an inhibitor might not have caused any major change in corrosion resistance properties.

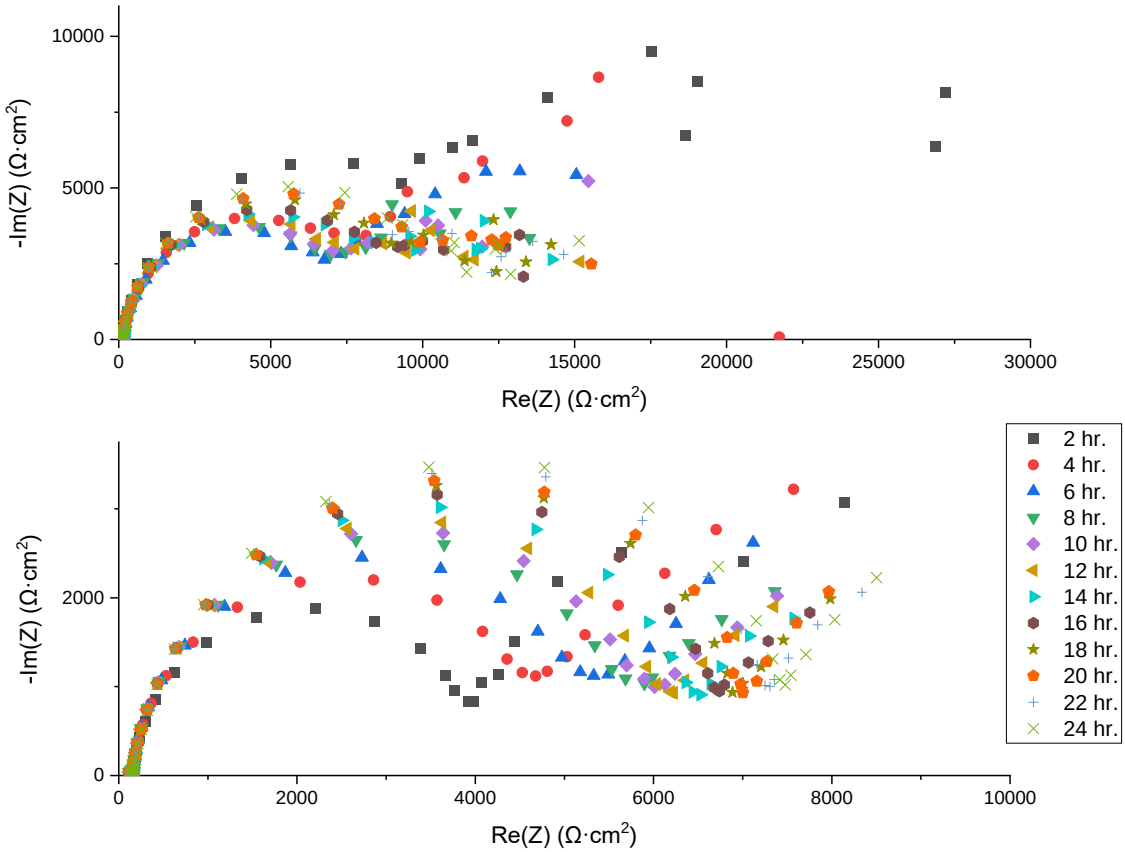

Figure 5.14 Nyquist plot of Ref_pH7 (top) and NaGal_pH7 (bottom) samples in 0.05 M NaCl.

The Nyquist plots for Ref_pH7 and NaGal_pH7 in Figure 5.14 can be practically divided into two parts; the semi-circle part and the linear (semi-infinite) part. The arc represents the charge transfer, which is kinetic control. However, in some electrode, the diffusion can take place and mass transport dominate the reaction instead, this creates a semi-infinite plot.

In order to calculate the Rp, the Warburg element was added to the Randles Cell as demonstrated in Figure 5.15. As described above, the Warburg element represents the linear diffusion part in the Nyquist plot, which is calculated based on the charge transferr parameter and diffusion coefficient.

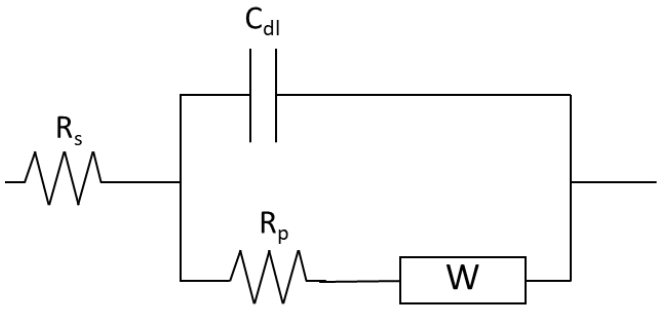

Figure 5.15 Randles cell with Warburg's element equivalent circuit.

The Rp values, which were calculated from the Nyquist plots are presented in Table 5.2. The values were comparable to the Rp calculated from the LPR. Both Reference and NaGal had much lower Rp than the blank. NaGal had Rp lower than the Reference, which was possibly due to the adsorption of NaGal preventing the alloy passivation without an oxide layer growth, the sample was easily exposed to the aggressive environment.

	Time [hour]	**2**	**4**	**6**	**8**	**10**	**12**	**14**	**16**	**18**	**20**	**22**	**24**
Ref_pH7	Rp [kΩ]	9	7	6	7	7	7	8	8	9	9	10	10
NaGal_pH7	Rp [kΩ]	3	4	5	5	5	6	6	6	6	6	7	7

Table 5.2 Polarization resistance of Ref_pH7 and NaGal_pH7 samples from Nyquist plot

Potentiodynamic polarization

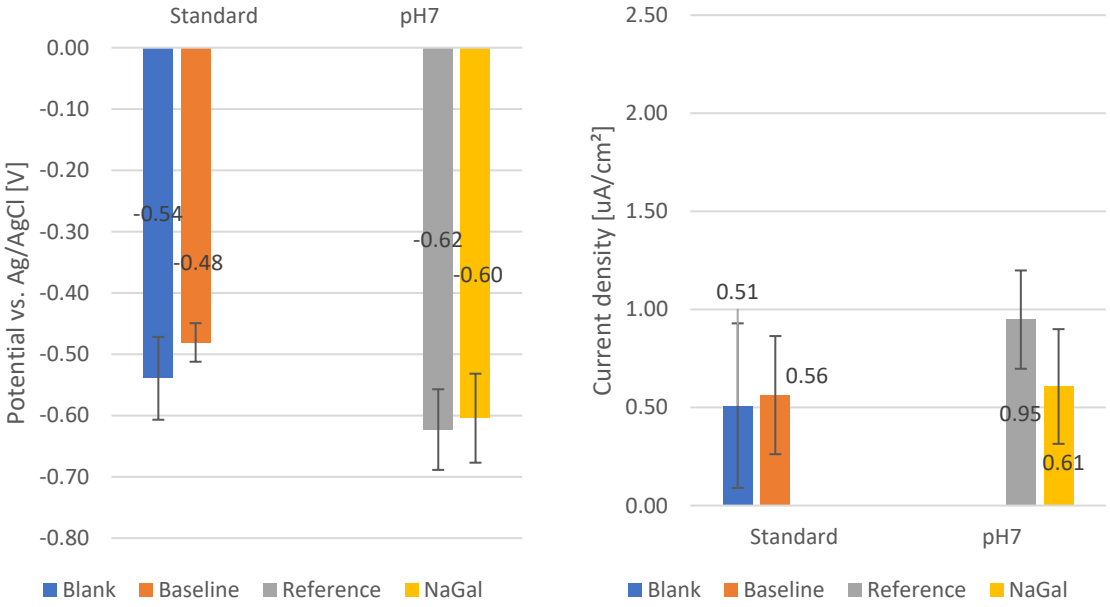

Figure 5.16 Average corrosion potential (left) and corrosion current density (right) of neutral environment immersion samples

The average values of corrosion potential and corrosion current density were calculated from the polarization curve and exhibited in Figure 5.16 with S.D. as error bar. The alkaline cleaning increased the E_{corr} of the sample, but also increased the corrosion rate (from the increased i_{corr}). The previous section showed that Rp of Ref_pH7 and NaGal_pH7 were lower than Rp of the Blank and Baseline, suggesting that the oxide layer formed on the Blank and Baseline gave better corrosion resistance as evidenced that both samples had lower i_{corr}. The possible reason for the increase of the i_{corr} after NaGal pretreatment was possibly caused by the oxide film: in Ref_7, the oxide layer was more hydrophilic, which increased the kinetics of Cl^- ions transfer, hence increasing the corrosion rate of the sample.

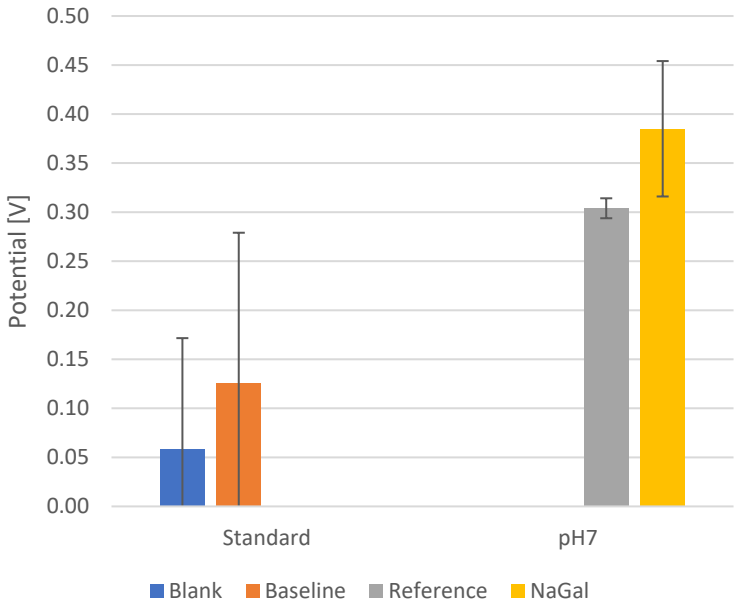

Figure 5.17 Passive potential range of neutral environment immersion samples after 24 hours immersion in 0.05 M NaCl

The passive range was calculated and exhibited in Figure 5.17 with S.D. values as error bars. the standard samples had low ΔE and insufficient reproducibility rate. The variation in passive range in Baseline was presumably due to the random alloying particles distribution on the surface. The literature reports that the dissolution rate of the alloying elements and matrix was not equal in the alkaline cleaning process, the density of some IMPs might have increased after the process and altered the surface properties [81]–[84]. For pH7, NaGal pretreatment remarkably increased the passive potential range of the sample. This suggested that NaGal sample had more resistance in the chloride environment by having a broader passive range [85].

Pitting evaluation

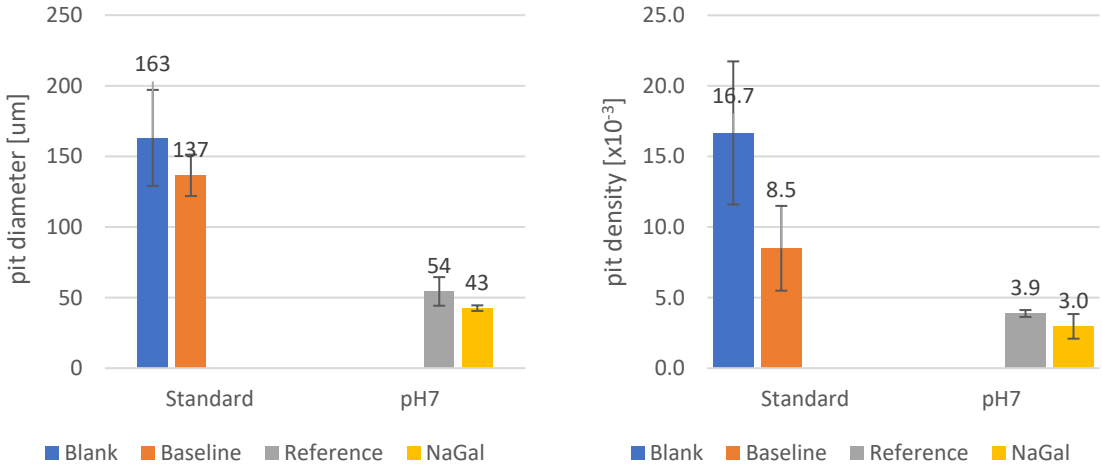

Figure 5.18 Average pit diameters (left) and pit densities (right) after 24 hours immersion in 0.05 M NaCl. The error bars represent the S.D. values.

Despite having a low reproducibility rate caused by IMPs in the Blank and Baseline samples, the pitting evaluation proved that the alkaline cleaning increased the passive range of the Baseline sample because both pit diameters and densities were reduced. However, the stain was only visible on the Baseline sample surface (Figure 5.19).

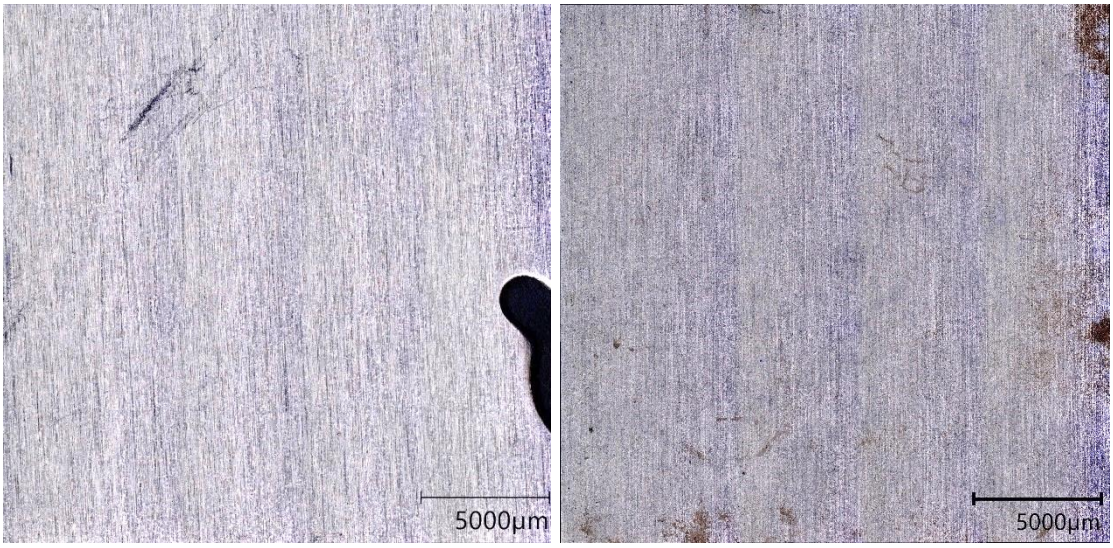

Figure 5.19 Surface images of Blank (left) and Baseline (right).

From the pitting evaluation, it may be concluded that the increase of the ΔE NaGal pretreated samples was owing to their ability to resist pitting corrosion, which was higher than the Baseline, which was merely alkaline cleaned. Nevertheless, the difference between pit diameters and densities between the NaGal_pH7 and Ref_pH7 was minimal that NaGal may not improve the pitting resistance in pH7.

By observing the surface, the corrosion products from the alloying particles were more visible on the Reference (Figure 5.20). As exhibited in Figure 5.9 and Figure 5.12 above, this layer caused by the corrosion products accumulation on the surface, which is called ‘stain’. Although NaGal pretreatment seemed to prevent stains forming on most of the surface areas, corrosion could still be seen on some areas. This might be due to the imperfect film from NaGal adsorption or its desorption with an increase in immersion time. Hence, only some areas were protected from staining.

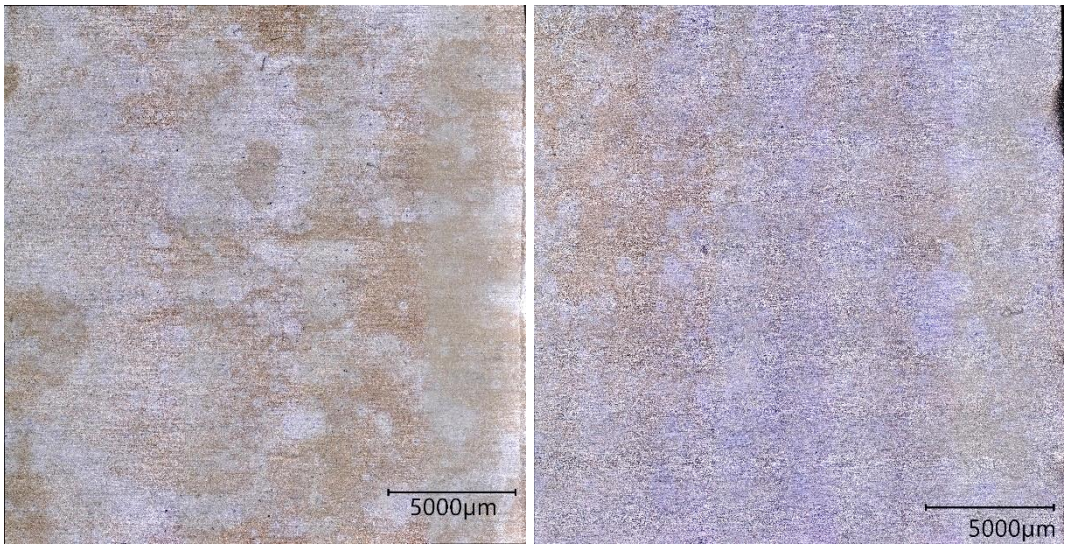

Figure 5.20 Surface images of Ref_pH7 (left) and NaGal_pH7 (right)

Open Circuit Potential

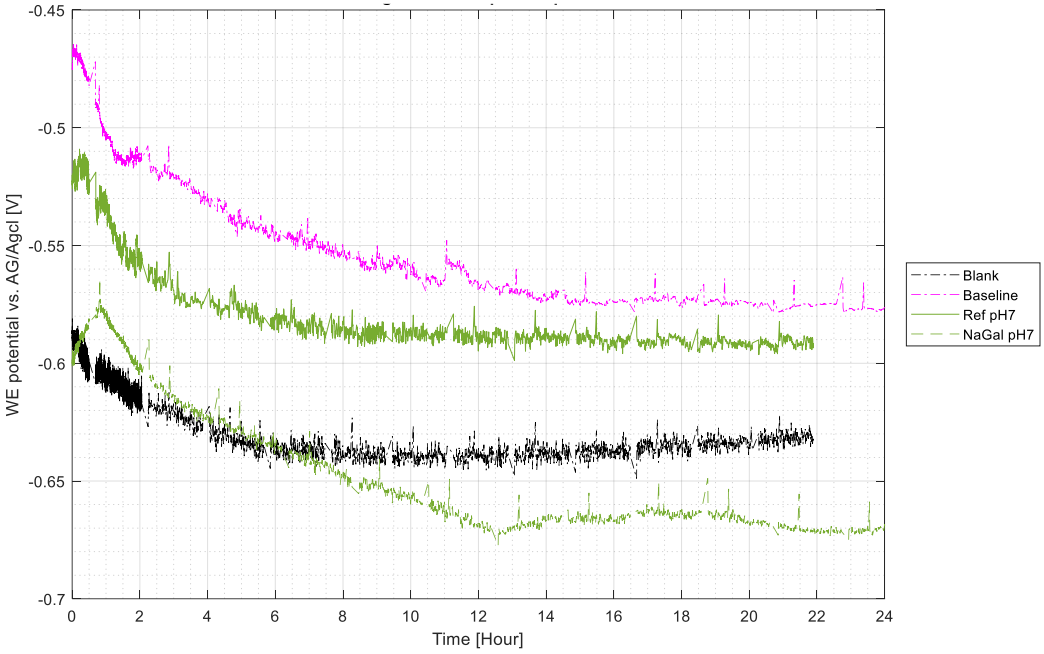

Figure 5.21 Open circuit potential 24 hours monitoring in 0.05 M NaCl.

As shown in the open circuit potential (OCP) plot in Figure 5.21, Blank had fluctuations with a high magnitude, which was likely due to the pitting corrosion that took place on the sample surface. In addition, the high magnitude of fluctuation was probably caused by the cathodic reaction, which was mainly oxygen reduction in pH7 [86]. Although passive layer (oxide/hydroxide) of the aluminium alloy shielded the sample from the chloride environment. The imperfection of oxide film (from IMPs) and micro galvanic corrosion could still occur, which resulted in pitting as the immersion time increased. The Baseline OCP was higher than the Blank owing to the surface modification that caused the density and distribution of the IMPs on the surface to change as the result of aluminium's high dissolution rate compared to the IMPs such as Fe, Mn and Si. The increase of these particles on the surface has substantially increased the potential of the sample. Moreover, the stain that was formed on the Ref_pH7 surface was rich with alloying particles, especially Fe, causing the potential of the Reference to be higher than the NaGal. Since the NaGal layer might deter both stain and alloy's passivation, NaGal_pH7 had a constant drop in potential over a time period.

5.2 Acidic environment immersion

5.2.1 Reference pH3 (Ref_pH3)

Despite the sample being immersed in the pH 3 solution for another hour after the alkaline cleaning, the sample surface was presumed to still have an alumina layer on the surface. This assumption was made based on the Pourbaix diagram of the alloying elements (Figure 5.10) that the alloying particles could not passivate since they corroded in acid.

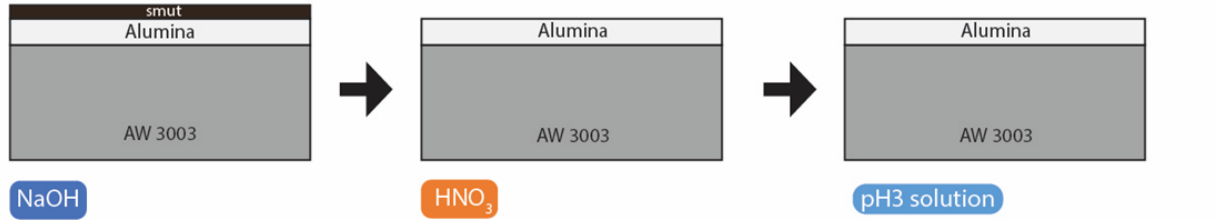

Figure 5.22 Ref_pH3 during the pretreatment

At the beginning of the NaCl immersion, the impedance at 0.01 Hz of Ref_pH3 showed a decreasing trend, suggesting the corrosion (both uniform and localized) had started and decreased the corrosion resistance of the sample. Consequently, the stain redeposited on the surface as evident from LPR and EIS results. The schematics of the development during the NaCl immersion are exhibited in Figure 5.23.

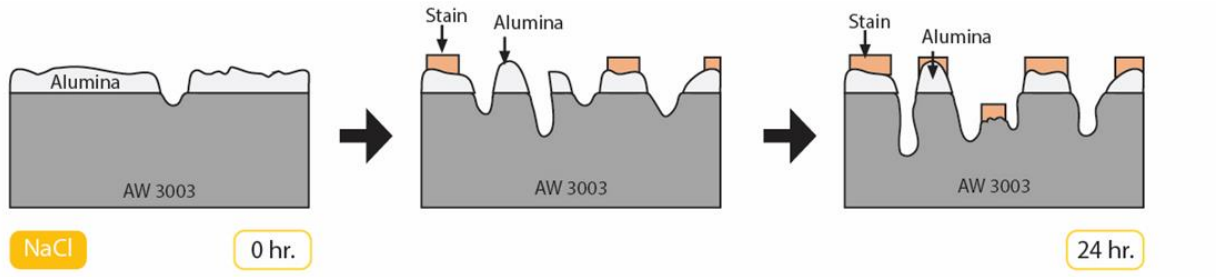

Figure 5.23 Ref_pH3 during the NaCl immersion

5.2.2 Reference pH4 (Ref_pH4)

The layers in the Ref_pH4 sample were also assumed to be similar to Ref_pH3 as exhibited in Figure 5.24. The only difference was that in pH4, the aluminium can still passivate according to the Pourbaix diagram. Therefore, the Alumina layer might have become thicker when compared to the Ref_pH3.

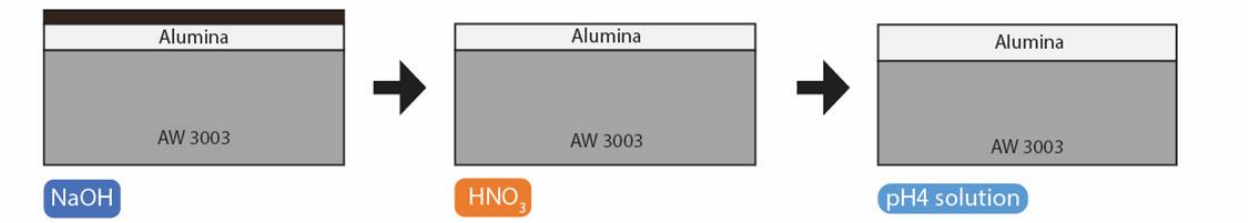

Figure 5.24 Ref_pH4 during the pretreatment

The corrosion progression after NaCl immersion was assumed to be the same as in Ref_pH3, the complex oxides were generated on top of the sample through the IMP passivation. Ref_pH4 started corroding in an early stage of immersion as the stains were formed. Nonetheless, the stain enhanced the corrosion resistance of the sample by blocking or slowing down ion transportation as evidenced by the increase in impedance and polarization resistance.

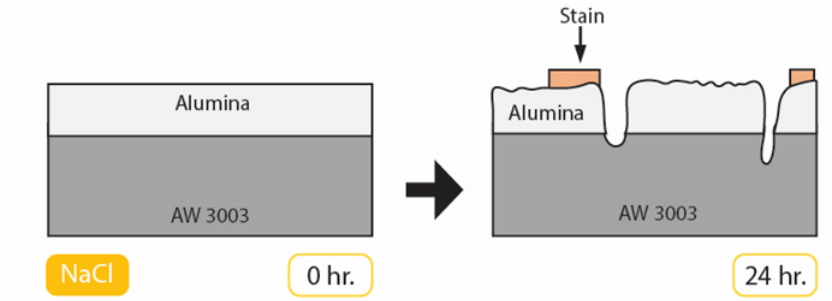

Figure 5.25 Ref_pH4 during NaCl immersion

5.2.3 NaGal_pH3

Similar to the neutral environment, the FTIR provided evidence that NaGal adsorbed on the sample. Hence the structure, which is shown in Figure 5.26, was assumed to be the same as NaGal_pH 7.

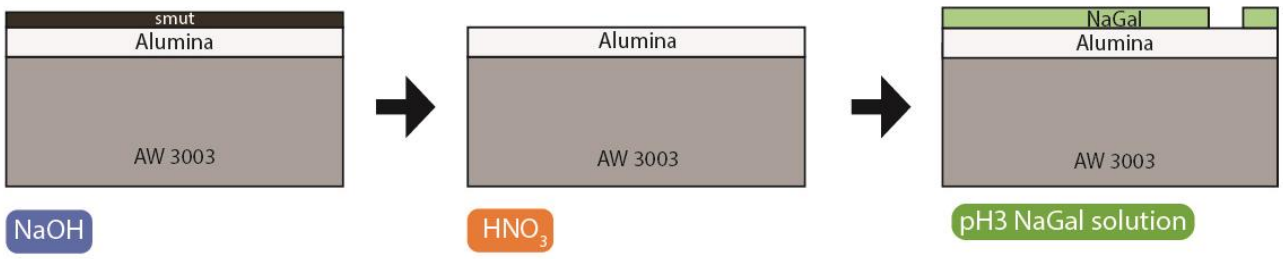

Figure 5.26 NaGal_pH3 during the NaGal pretreatment.

In comparison with the reference sample, the electrochemical behavior of the NaGal sample was stable at the beginning as the sample surface was covered by NaGal. However, NaGal desorbed with increasing immersion time resulting in a decrease of polarization resistance. In the end, some stains could be found, most likely on the areas where no NaGal was adsorbed anymore as illustrated below.

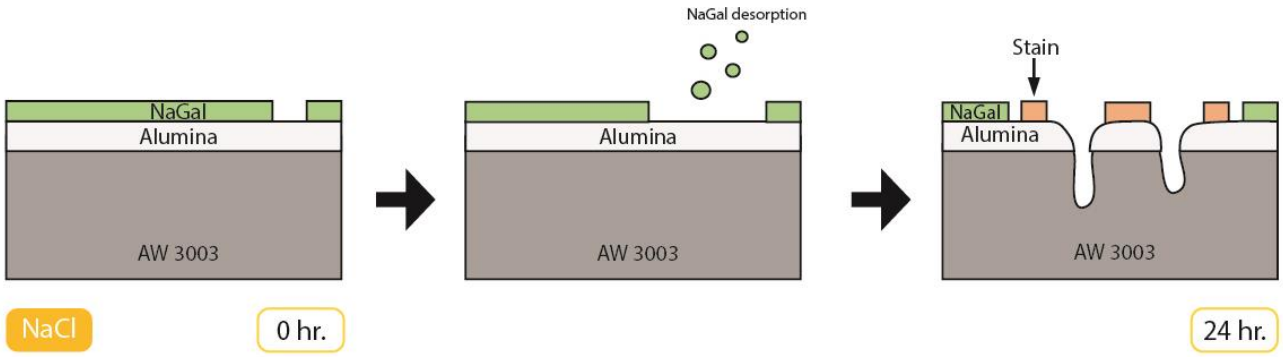

Figure 5.27 NaGal_pH3 during NaCl immersion.

5.2.4 NaGal_pH4

Similar to NaGal_pH3, NaGal was adsorbed on the alumina surface. Although the NaGal layer was assumed to not perfectly cover the surface, the oxide layer, which is identical to the oxide found in NaGal_pH3, was presumed to not be able to grow despite the sample being immersed in pH4. This is because NaGal layer may hinder the oxide growth. The schematic is shown in Figure 5.28 below.

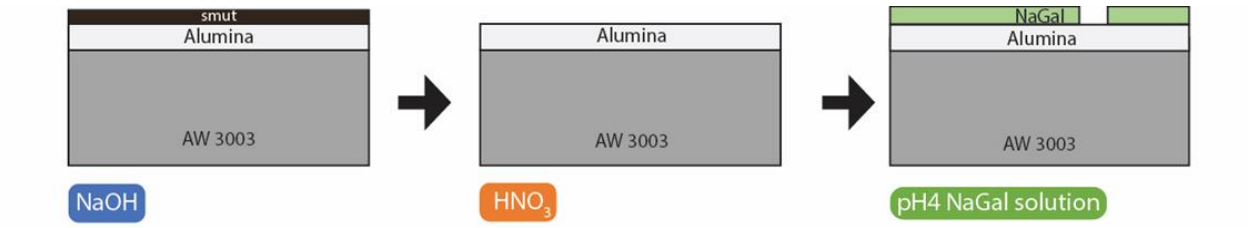

Figure 5.28 NaGal_pH4 during the NaGal pretreatment

As exhibited in previous NaGal samples NaGal was able to prevent the corrosion product redeposition on the sample surface, this phenomenon occurred in pH4 as well. The stain was visible in some confined areas only, presumably, it accumulated after the desorption of NaGal as illustrated in Figure 5.29.

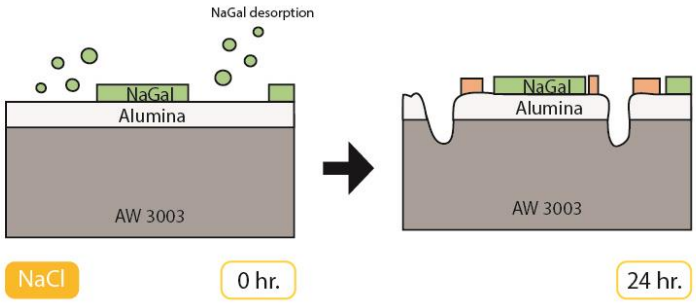

Figure 5.29 NaGal_pH4 during NaCl immersion.

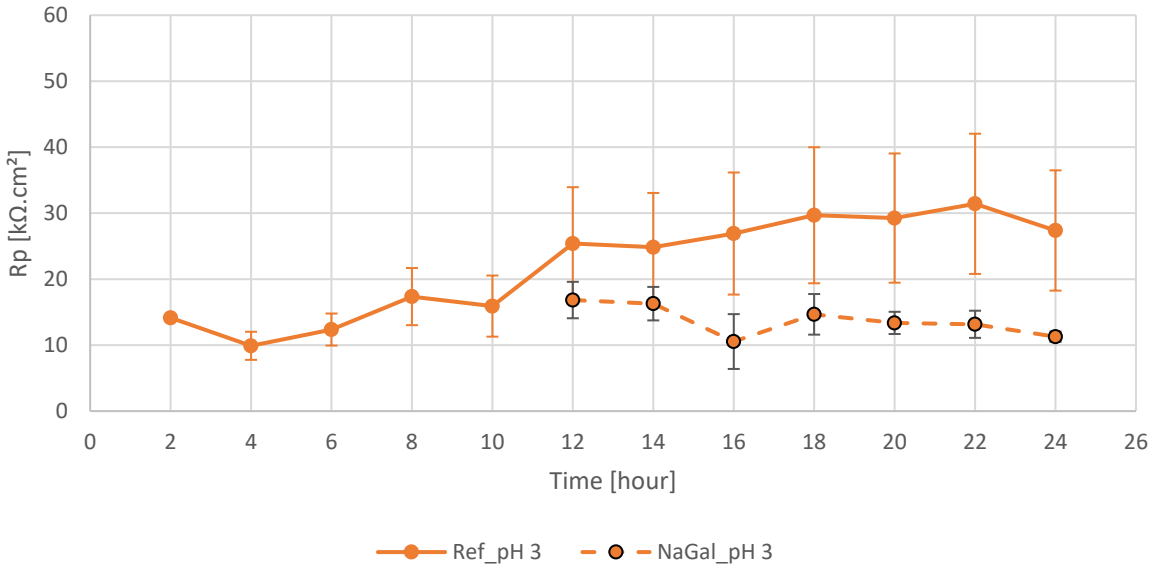

Figure 5.30 Polarization resistance of Ref_pH3 and NaGal_pH3 sample in 0.05 M NaCl.

Figure 5.30 presents the Rps of pH3 samples with S.D. values as error bars. The results from the first 10 hours immersion were neglected from the plot due to the high values of the error bar. The increase of the Rp in Ref_pH3 was related to the stain deposition on the sample surface that acted as a physical barrier blocking the Cl^- ions to adsorb directly to the alloy. In contrast, NaGal prevented most of the stains forming on the surface therefore it was stable without any change throughout the immersion.

The results for pH4 samples were unstable therefore, neither the comparison nor trend during immersion could be drawn from the LPR result. However, this could also mean that NaGal was not very effective in inhibiting the corrosion in pH4.

Potentiodynamic Polarization

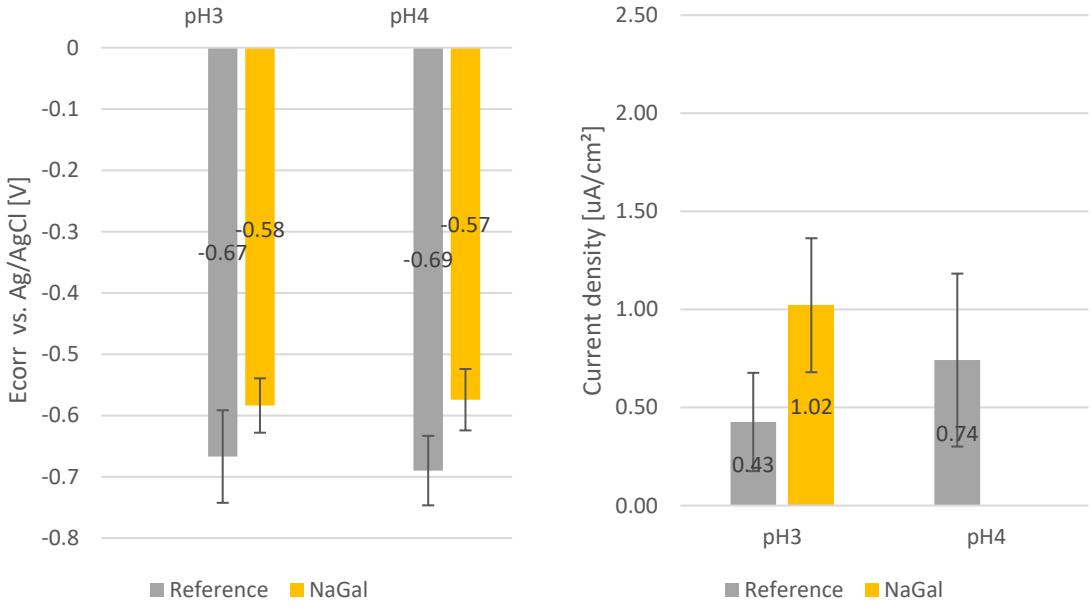

Figure 5.31 Average corrosion potential (left) and corrosion current density (right) of acidic environment immersion samples with S.D. values as error bars

In pH 3, the pretreatment was not effective as the corrosion resistance of the sample did not increase as evidenced in the increase of the i_{corr} in Figure 5.31. NaGal_pH4 had a high S.D., hence it is difficult to make a definitive comparison.

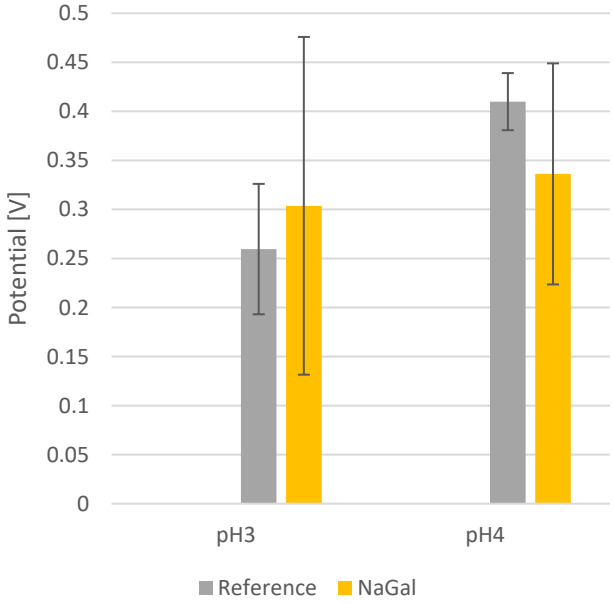

Figure 5.32 Passive potential range of neutral environment immersion samples after 24 hours immersion in 0.05 M NaCl. The error bars represent the S.D. values.

Similarly, in the ΔE plot (Figure 5.32), the S.D. in the NaGal samples were relatively high, compared with the Reference. A comparison between the two samples could not be made. The reason for not being reproducible was likely caused by the adsorption of the NaGal that might not have perfectly covered the entire surface of the alloy causing variations in each sample. Moreover, If the alloying particle was exposed to the NaCl electrolyte, it would passivate, thus causing the corrosion rate to decrease and vice versa. Consequently, each sample might have different electrochemical behavior. Moreover, the metal stain on the surface also induced the pitting corrosion, making the protection range of the samples varied as well.

Pitting evaluation

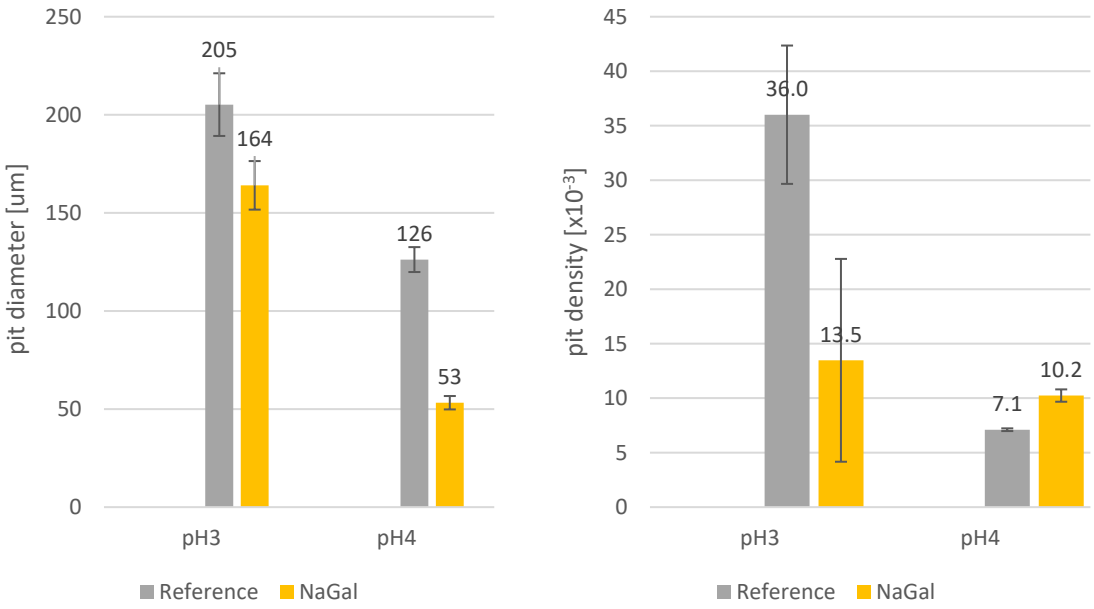

Figure 5.33 Average pit diameters (left) and pit densities (right) of acidic environment immersion samples after 24 hours immersion in 0.05 M NaCl.

Because the corrosion was more severe in pH 3 as it was more acidic environment, hence the pitting in pH 3 samples was more aggressive compared to pH 4 samples. NaGal pretreatment greatly improved the pitting corrosion resistance in pH 3, but moderately in pH 4 since only the pit diameters were decreased, but not the pit density. In Figure 5.34, NaGal_pH3 surface shows less metal stain on the surface, which supports the hypothesis that NaGal prevented the metal stain. A regrettable consequence was that it also increased the corrosion rate.

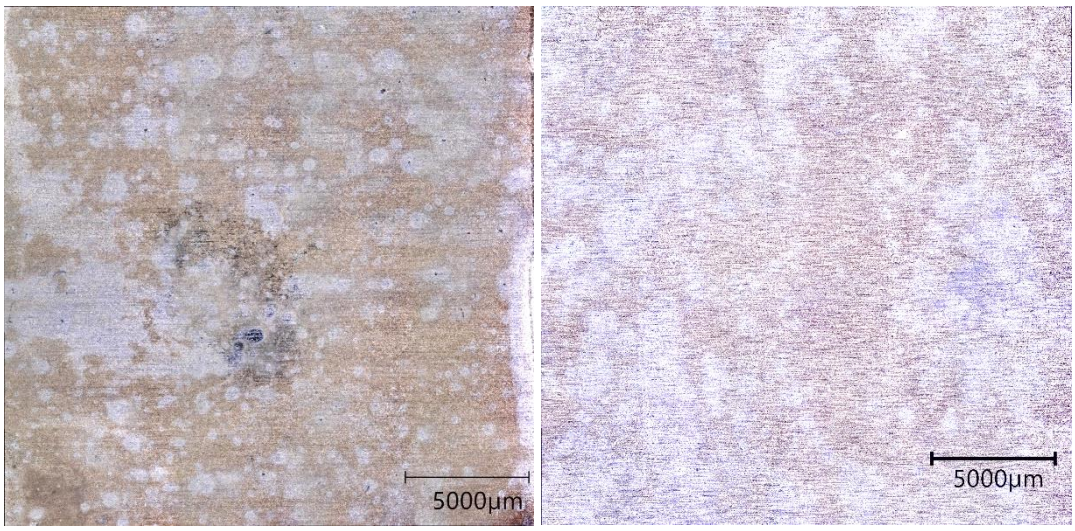

Figure 5.34 Surface images of Ref_pH3 (left) and NaGal_pH3 (right).

The metal stain on Ref_pH4 occurred only on some random areas of the surface (Figure 5.35). This was likely due to the different electrochemical properties of the sample surface. The area that was more cathodic from the influence of the IMPs attracted more ions to redeposit on the surface and created an unwanted stain that degrades the sample's appearance.

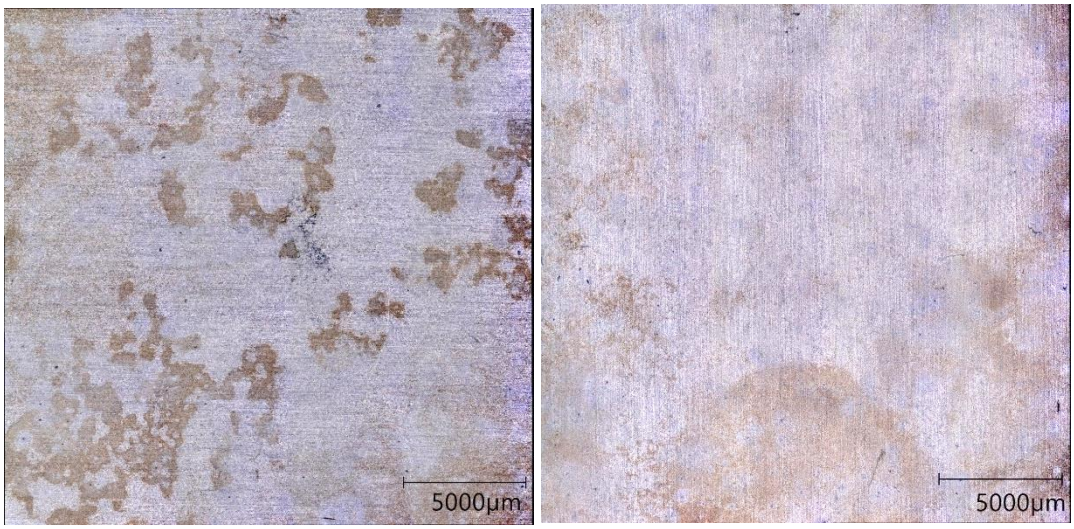

Figure 5.35 Surface images of Ref_pH4 (left) and NaGal_pH4 (right).

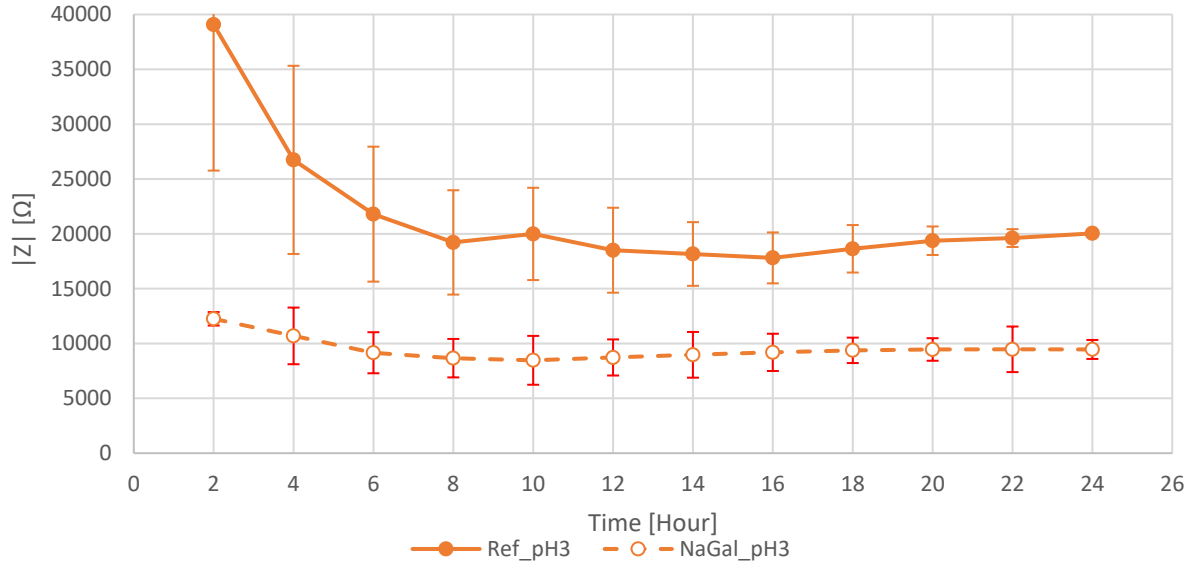

Figure 5.36 Impedance modulus at 0.01 Hz of Ref_pH3 and NaGal_pH3 during 24 hours immersion in
0.05 M NaCl.S.D. values are shown as error bars.

The Ref_pH3 had a higher impedance than NaGal_pH3 due to the metal stain that formed on the surface. Increased impedance modulus did not necessarily result in an increase in the corrosion resistance because the stain induced pitting corrosion as a result of the surface becoming more heterogeneous [87]. Since NaGal_pH3 showed only few stains on the surface, it has less protection against the electrolyte leading to lower impedance modulus.

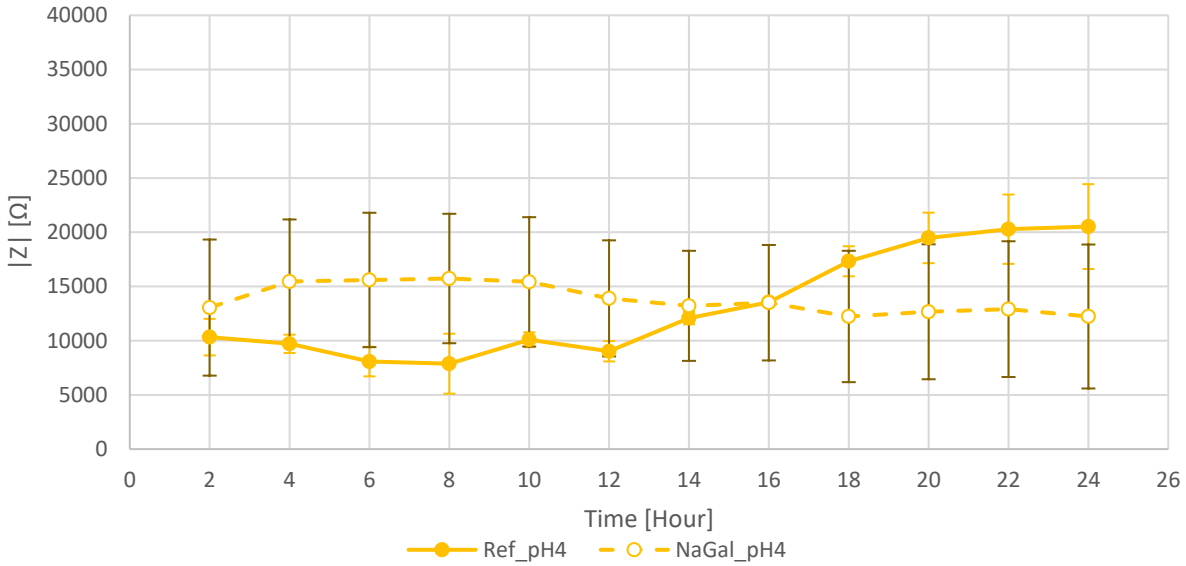

Figure 5.37 Impedance modulus at 0.01 Hz of of Ref_pH4 and NaGal_pH4 during 24 hours immersion in 0.05 M NaCl. S.D. values are shown as error bars.

The increased impedance modulus in the Ref_pH4 may be caused by the growth of the oxide film. As reproducibility was hard to achieve in NaGal_pH4, the observation on the sample was difficult to make. Nevertheless, the differences in Reference and NaGal were not significant, which were similar in Ref_pH7 and NaGal_pH7. This was possibly due to the alloys were already protected by the alumina layer or NaGal might have a low efficiency that its effects could not be clearly seen.

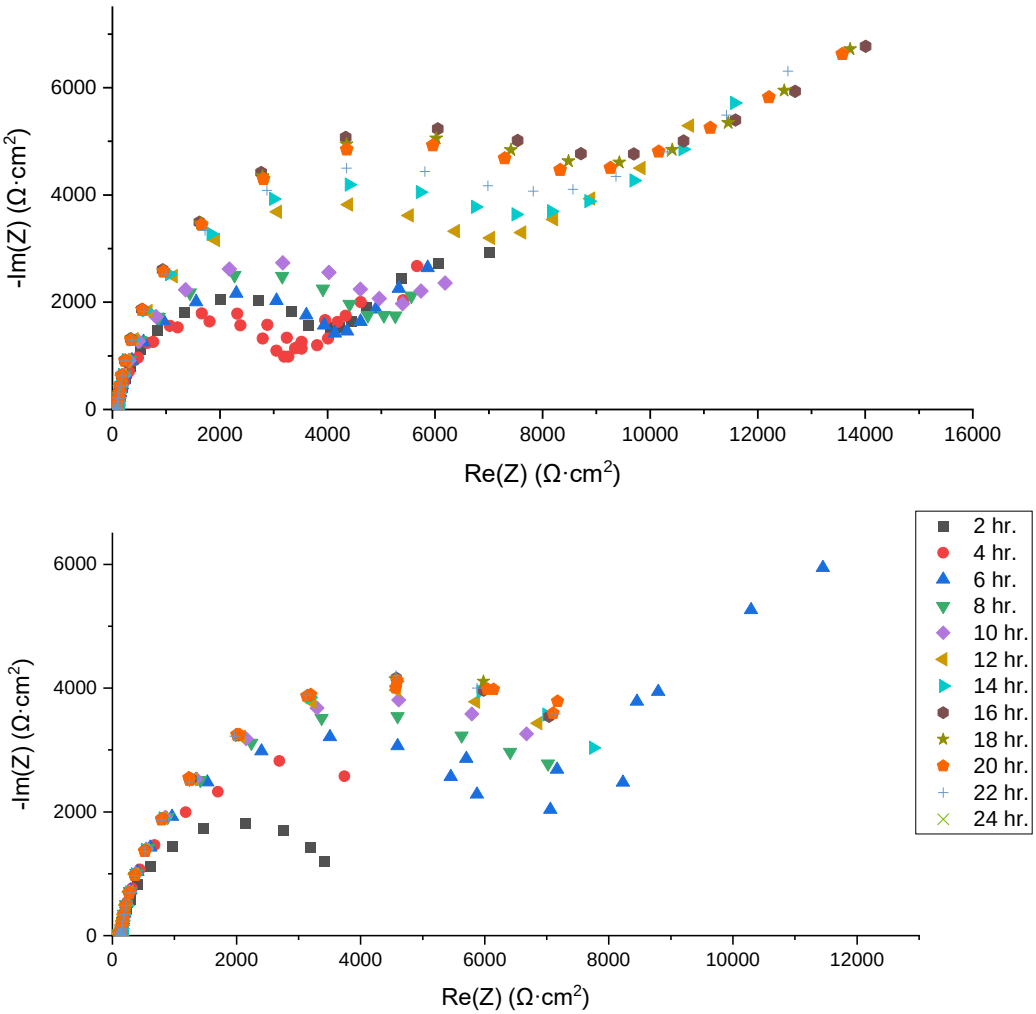

Figure 5.38 Nyquist plot of Ref_pH3 (top) and NaGal_pH3 (bottom) in 0.05 M NaCl.

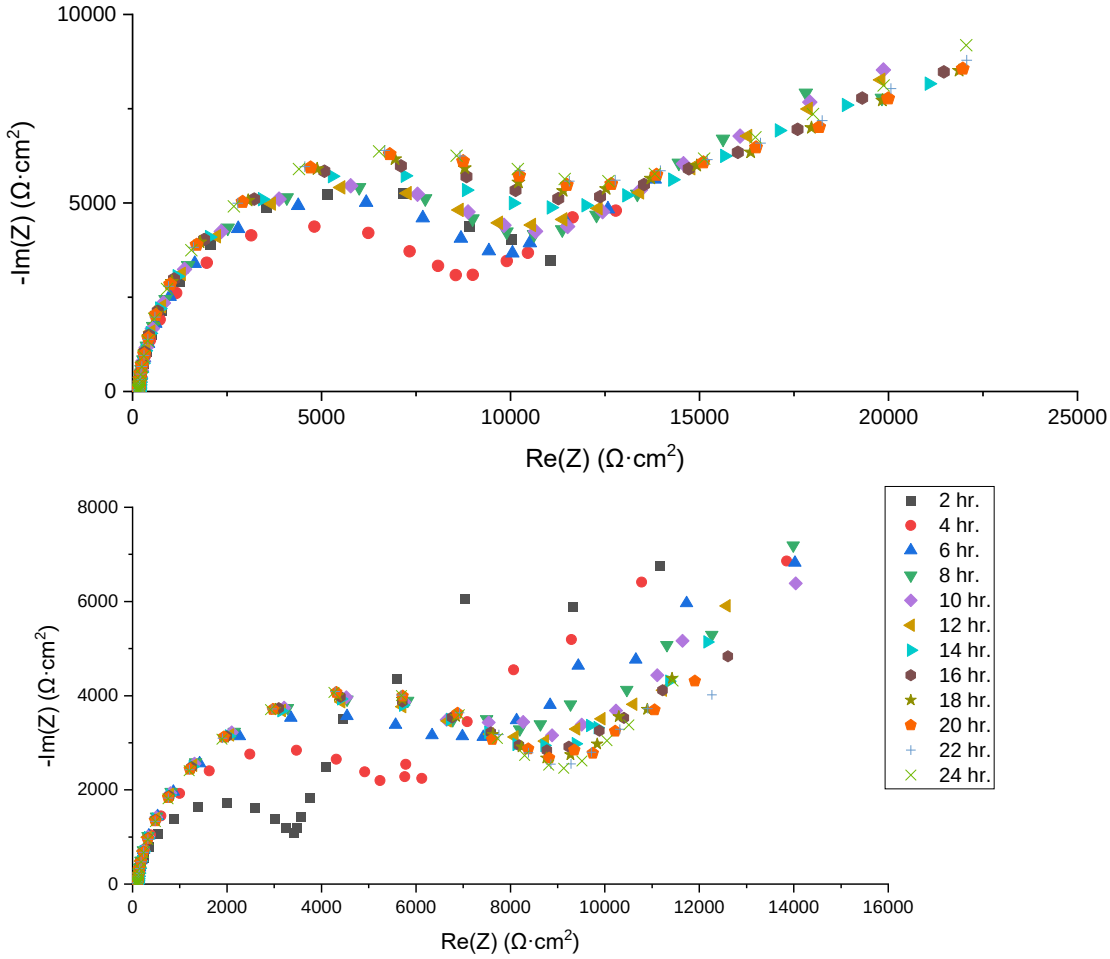

Figure 5.39 Nyquist plot of Ref_pH4 (top) and NaGal_pH4 (bottom) in 0.05 M NaCl.

In Figure 5.38 and Figure 5.39, all samples in both pH 3 and 4 showed a semi-arc shape with a long linear part, which was similar to the typical Warburg's Nyquist plot. Therefore, the equivalent circuit in Figure 5.15 was also used for calculation. The approximated results are shown in Table 5.3.

	Time [hour]	**2**	**4**	**6**	**8**	**10**	**12**	**14**	**16**	**18**	**20**	**22**	**24**
Ref_pH3	Rp [kΩ]	4	3	3	4	4	5	6	7	8	8	8	7
NaGal_pH3	Rp [kΩ]	12	7	6	6	6	6	6	7	7	7	7	7
Ref_pH4	Rp [kΩ]	10	8	9	10	10	10	10	10	10	10	10	10
NaGal_pH4	Rp [kΩ]	3	5	7	7	7	7	7	7	7	7	7	7

Table 5.3 Polarization resistance of acidic environment immersion samples from Nyquist plot

The increase of the Rp in the Ref_pH3 was due to the growth of the alumina layer in a neutral solution. Because of the protection of NaGal layer, the NaGal_pH3 sample had a higher Rp than its reference. This effect decreased with increasing immersion time because NaGal desorbed from the sample surface. This was supported by the polarization curve's outcome which did not show inhibitive behaviour of NaGal. In

Ref_pH4, the stain on the surface acted as a protective layer, increasing its Rp in contrast to the NaGal sample for which NaGal prevented the formation of metal stain.

Open Circuit Potential

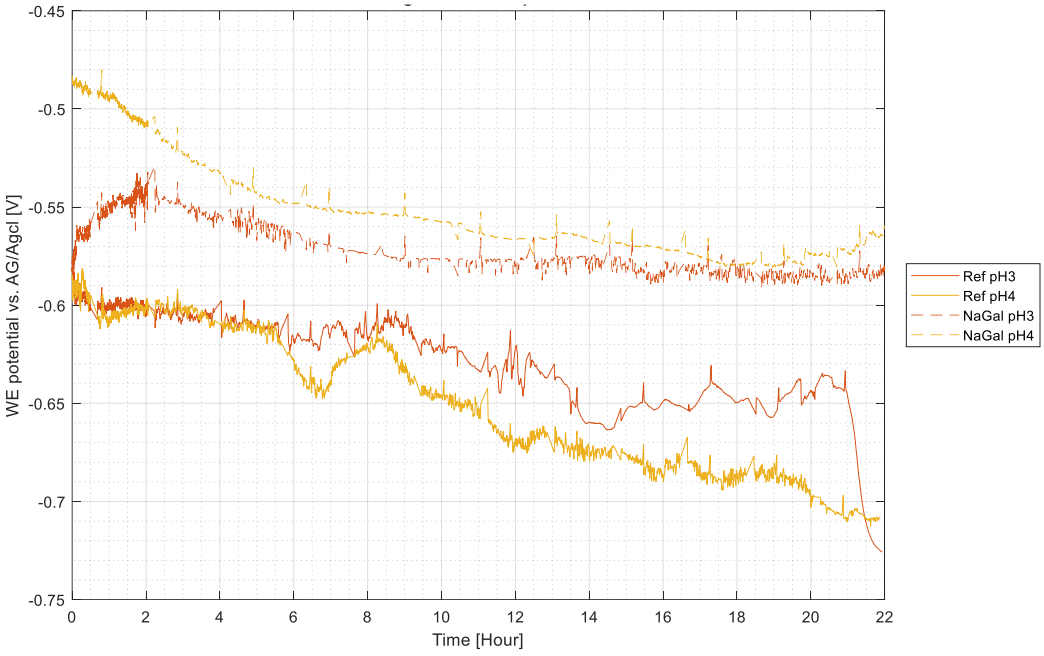

Figure 5.40 Open circuit potential monitoring of acidic immersion samples in 0.05 M NaCl.

In Figure 5.40, the Reference samples in pH3 and 4 had their OCP lower than the NaGal samples. This was due to the pitting corrosion in the samples that was more aggressive than the NaGal samples. Since uniform corrosion was dominated in NaGal samples, it had higher potential.

5.3 Alkaline environment immersion

5.3.1 Reference pH10 (Ref_pH10)

First, the sample was cleaned with NaOH solution. During the cleaning, the smut layer formed on top of the sample, which was later removed in HNO_3. After that the sample was immersed in pH 10 solution as a reference for the pretreatment as exhibited in Figure 5.41. This step created a smut layer on the sample surface, although this smut layer was assumed to not be as thick as the layer formed by alkaline cleaning and it was covered only on confined areas. This smut layer was formed by the passivation of the alloyed particles and the complex compounds formed between the alloying particles and the aluminium that had been dissolved into the solution and re-deposited on the sample surface.

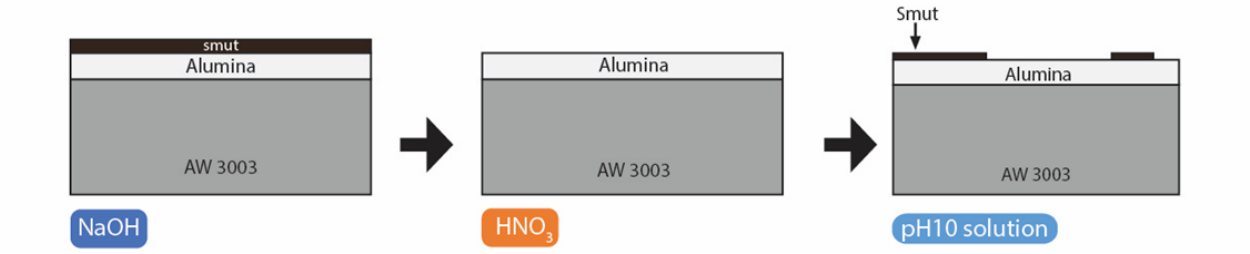

Figure 5.41 Ref_pH10 during the pretreatment

In the figure below, it is shown that the corrosion started immediately at the beginning of the immersion despite smut covering some parts of the surface. Even though the smut layer provided some protection to direct contact with the electrolyte. the layer was not stable and could detach from the surface easily. After the smut layer dissolved into the electrolyte, the surface was fully exposed to the NaCl, resulting in the formation of stains on the surface, which influenced many electrochemical parameters in the process. At the end of the immersion, the surface was fully covered by metal stains.

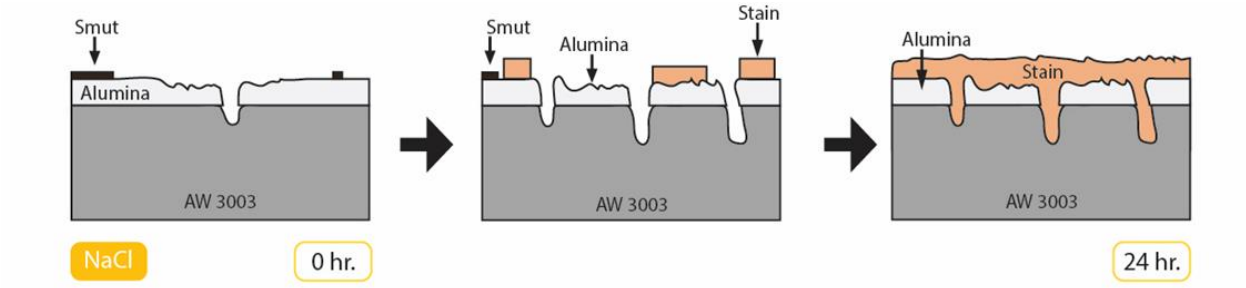

Figure 5.42 Ref_pH10 during NaCl immersion

2.3.3. Reference pH11 (Ref_pH11)

Similar to Ref_pH10, the smut layer formed on the surface when immersed in the pH11 solution. While the smut layer was hardly visible on Ref_pH10, it was clearly visible on Ref_pH11. The development is shown in Figure 5.43.

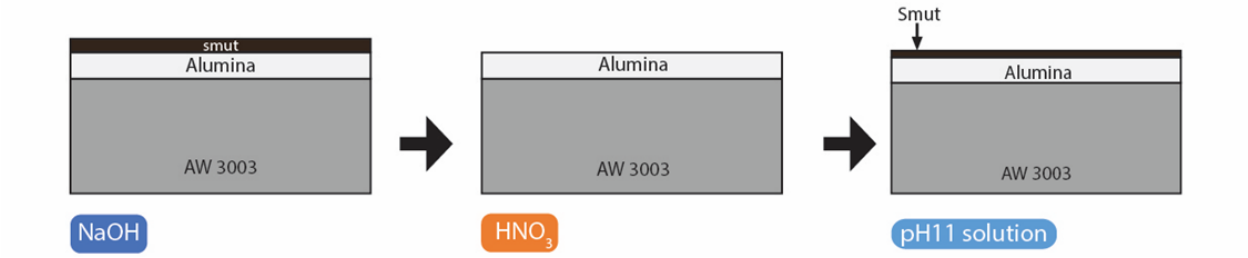

Figure 5.43 Ref_pH11 during the pretreatment

Figure 5.44 showed that at the beginning of immersion in NaCl, the electrochemical parameters of Ref_pH11 were very stable. This suggested that even though the smut layer was loosely attached to the surface it was able to block the contact with the electrolyte and prevented corrosion from starting. Shortly after the smut layer detached from the surface, corrosion occurred as evident by impedance and polarization resistance. Nevertheless, the smut was still forming and re-attached to the sample surface. By the end of the experiment, the sample appeared to have a large number of pits (after ultrasonic cleaning).

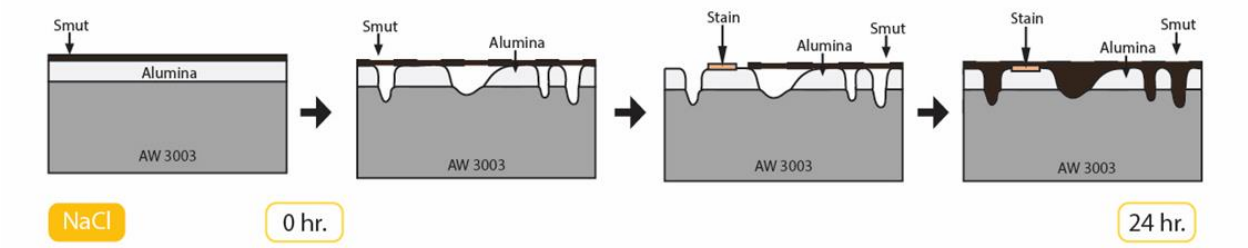

Figure 5.44 Ref_pH11 during the NaCl immersion

2.3.4. NaGal_pH10

After the immersion in NaGal solution with adjusted pH, the surface appearance did not change the color to dark brown but remained shiny. From the previous experiment in different environments, the NaGal samples showed less metal stain layer on the surface, which was considered as the effect of the NaGal treatment that prevented the smut layer to form on the sample surface. Hence, after the alkaline cleaning, the surface layers were considered to be comparable to the previous environment immersion with NaGal adsorbed on the Alumina layer as shown in the figure below.

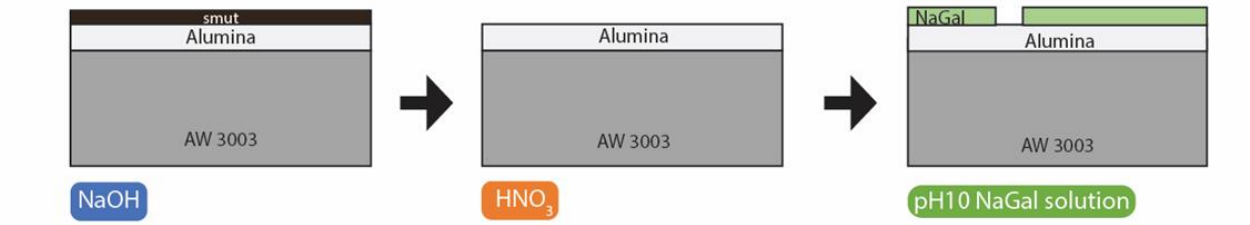

Figure 5.45 NaGal_pH10 during the NaGal pretreatment.

Unlike Ref_pH10 which had a smut layer on top of the surface, NaGal_pH10 was protected by the NaGal layer formed on the sample before it desorbed from the surface, then the corrosion started and caused the stain to redeposit on the surface. However, the stain did not cover the whole surface like Ref_pH10 and nearby areas were heavily damaged by localized corrosion as illustrated in the following figure.

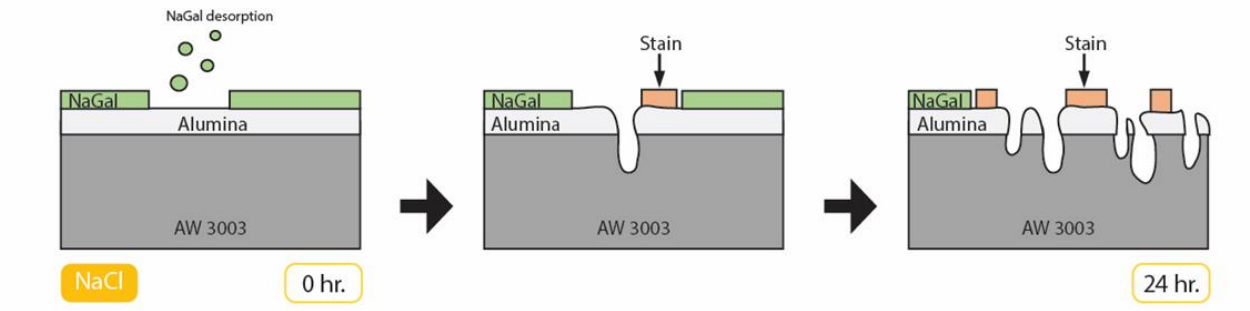

Figure 5.46 NaGal_pH10 during NaCl immersion.

2.3.5. NaGal_pH11

The layer order was assumed to be similar to the NaGal_pH10 as the smut layer was not able to form (Figure 5.47).

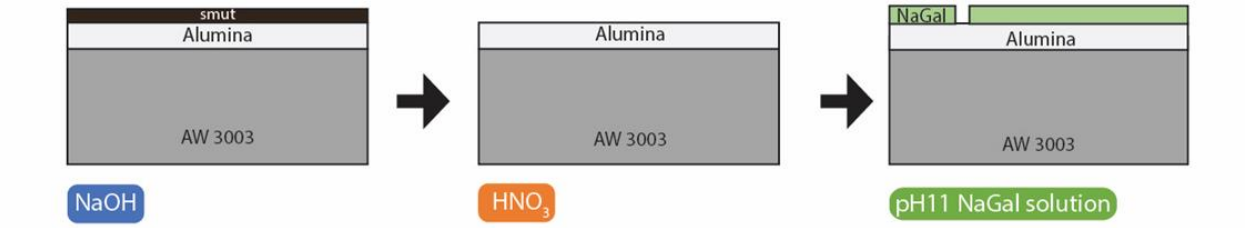

Figure 5.47 NaGal_pH11 during the NaGal pretreatment

Because NaGal was able to prevent smut formation on the surface, the sample only had stain forming. As the stain redeposited on the sample, the impedance and polarization resistance were increasing. At the end of the experiment, NaGal_pH11 showed a similar appearance as NaGal_pH10. The sample's development is shown in Figure 5.48.

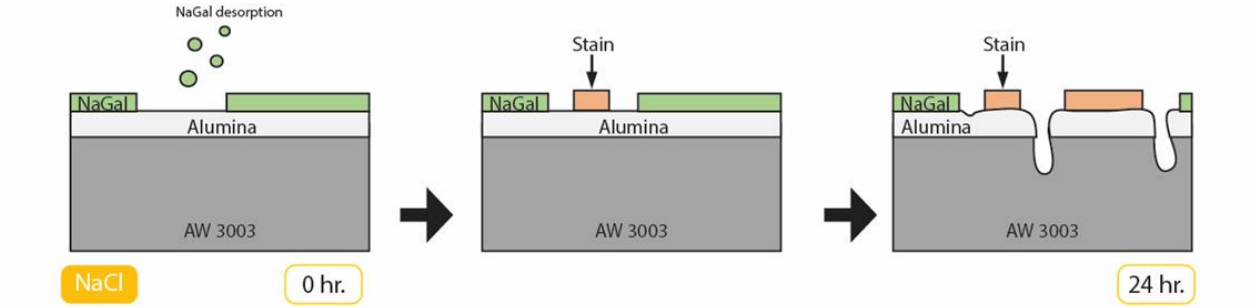

Figure 5.48 NaGal_pH11 during the NaCl immersion.

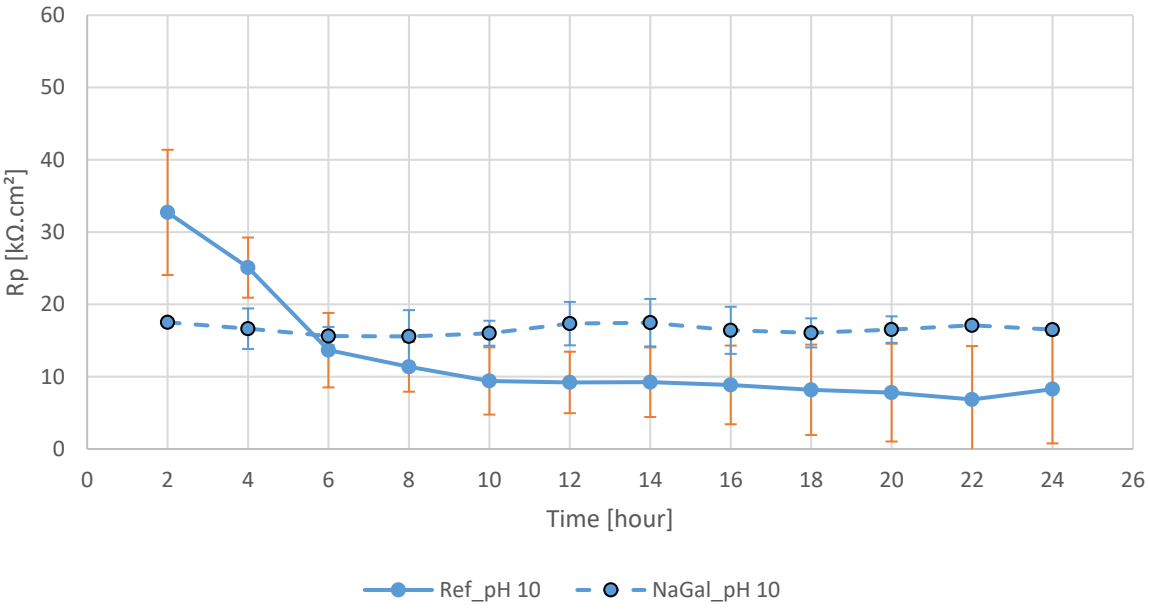

Figure 5.49 Polarization resistance of Ref_pH10 and NaGal_pH10 sample in 0.05 M NaCl

Figure 5.49 shown the Rp of pH10 samples with S.D. values as error bars. The smut on the Reference sample surface caused the surface to become heterogeneous and the electrochemical properties changed depending on the type and density of the alloying particles on that surface area. As shown in the Rp plot from LPR, Ref_pH10 had a lower reproducibility rate than NaGal_pH10. The decrease of the Rp could also indicate that it provided less corrosion resistance than the Alumina layer, not only from its heterogeneous nature that induced pitting. As the smut layer was not formed on the NaGal sample, the Rp progression was stable without any major change.

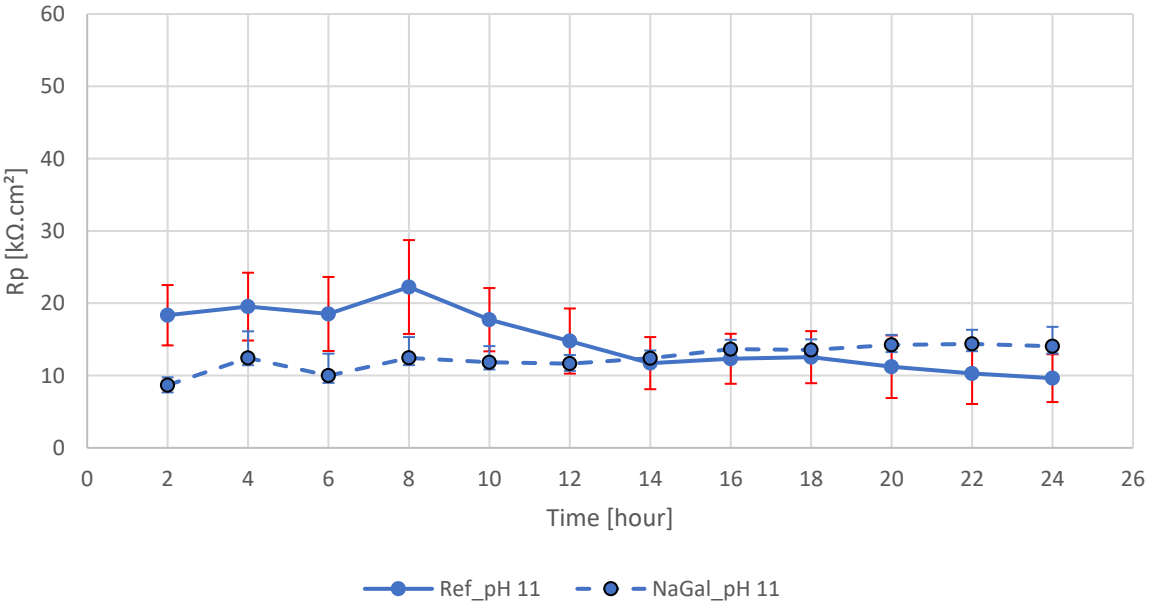

Figure 5.50 Polarization resistance of Ref_pH11 and NaGal_pH11 sample in 0.05 M NaCl.

Figure 5.50 shown the Rp values of pH 11 samples, the error bars represent the S.D. values. As it was exhibited in the surface images that the smut layer in Ref_pH11 covered the sample surface more than Ref_pH10. For this reason, the Rp of Ref_pH11 remained nearly the same and was lower since the smut also hindered the alloying particles to passivate. Similar to pH10, NaGal was stable throughout the immersion. There was no major difference between Reference and NaGal samples.

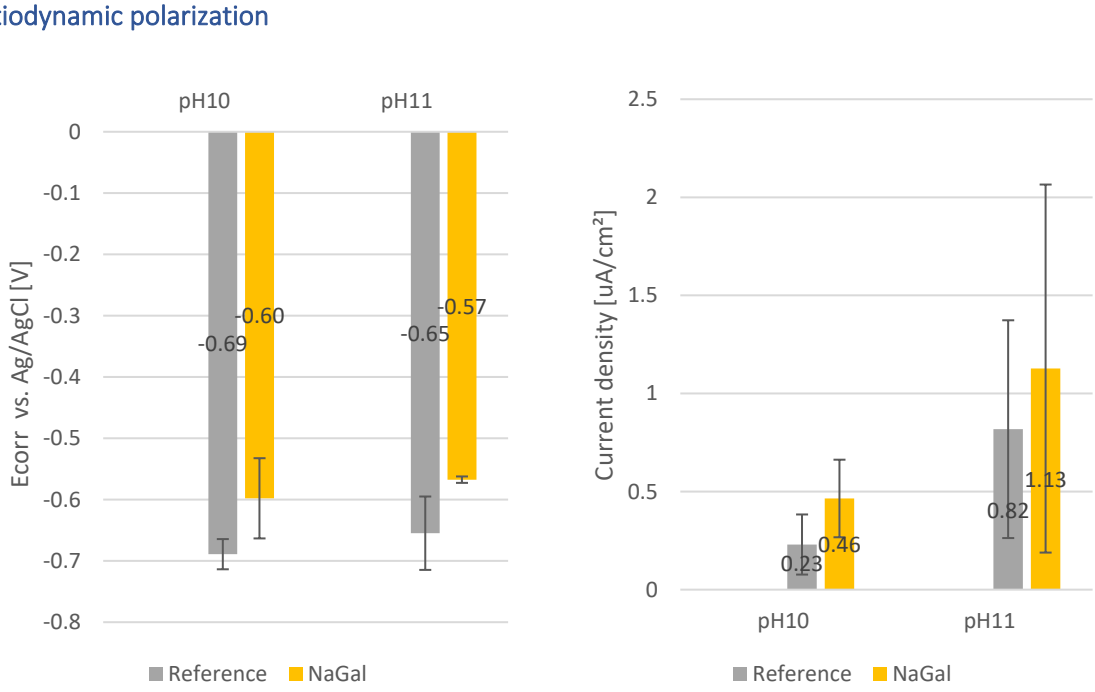

Figure 5.51 Average corrosion potential (left) and corrosion current density (right) of neutral environment immersion samples. The error bars represent the S.D. values

It can be seen from Figure 5.51 that Both NaGal pretreated samples in pH 10 and 11 had i_{corr} significantly increased. The reason for the increase of the i_{corr} could have been the absence of the smut or stain layer that was formed on the Reference but not on the NaGal. It was shown in the i_{corr} graph that the reproducibility rate in pH11 was low, which is possibly related to the different dissolution rates of the IMPs.

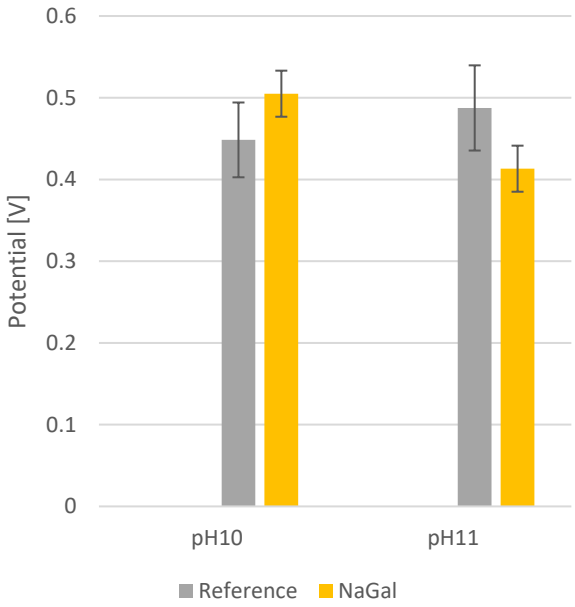

Figure 5.52 Passive potential range of alkaline environment immersion samples after 24 hours immersion in 0.05 M NaCl

Figure 5.52 shown the passive potential range of pH 10 and pH11 sampels with error bars represent S.D. values. In pH 10, NaGal pretreatment slightly improved the passive potential range of the sample, but not in pH11.The passive potential range in the Ref_pH11 was slightly better than NaGal_pH11, this supported the hypothesis that the smut or stain layer that formed on the surface did not increase the corrosion resistance of the sample. However, the plot indicated that the smut layer gave a better passive potential range than NaGal layer. However, it was also possible that the smut layer was thick enough to block the ions transfer between the interface of the alloy and electrolyte.

Pitting evaluation

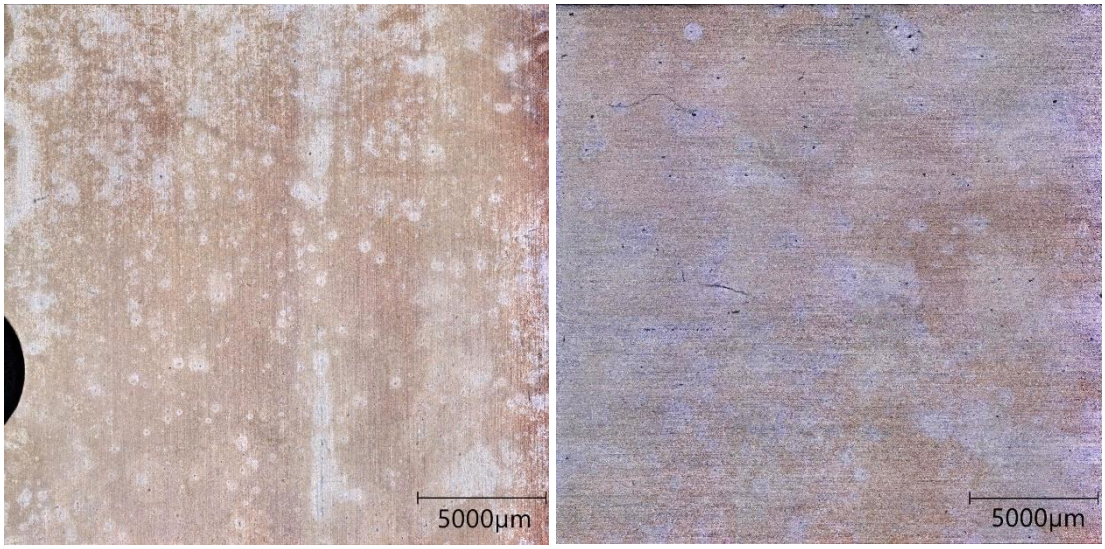

Figure 5.53 Surface images of Ref_pH10 (left) and NaGal_pH10 (right).

The metal stain on the Ref_pH10 appeared to have the thickest layer of all alkaline samples. This made the examination and evaluation difficult, consequently, causing the result of the sample to not be representative. Nonetheless, the stains were formed on all alkaline immersion samples except Ref_pH11 which had the entire surface covered with smut.

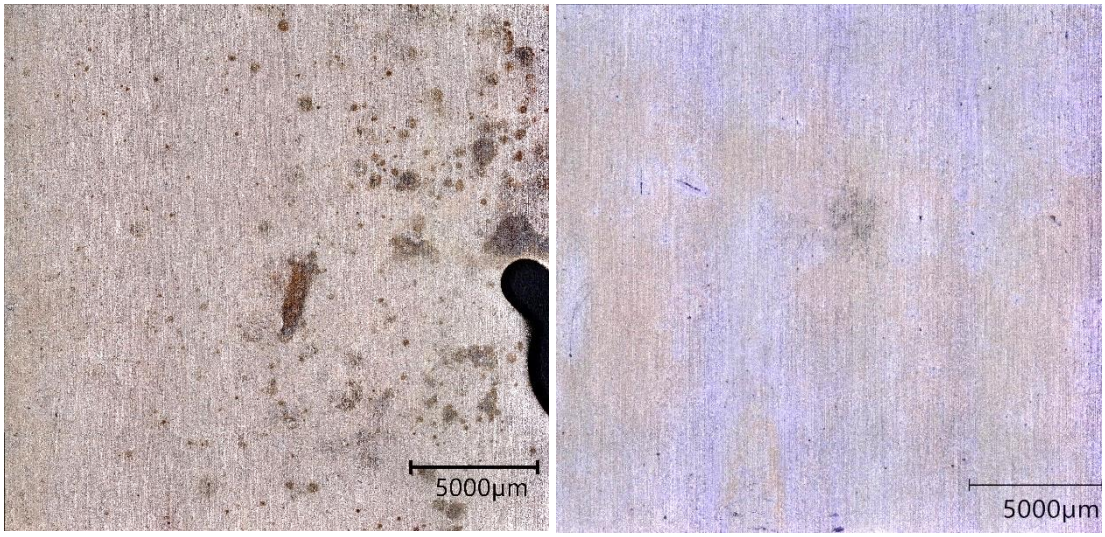

Figure 5.54 Surface images of Ref_pH11 (left) and NaGal_pH11 (right).

Due to the reason mentioned above, the pitting in pH10 appeared to be less in terms of diameter and density (Figure 5.55). The pit diameters and density between NaGal and the reference sample did not show any significant change. In pH11 both samples had low reproducibility rates because of the smut layer in the Reference sample and the different dissolution rates between matrix and alloying particles in NaGal samples. Nevertheless. It was visible on the sample surface that the Ref_pH11 suffered from pitting corrosion more than NaGal_pH11. This was possibly caused by Fe-rich particles on the surface that caused the nearby pit on the matrix to have localized pH increase, hence the pitting corrosion became more aggressive. Because the scope of pit examination in this work did not include depth measurement, the data could have been misled.

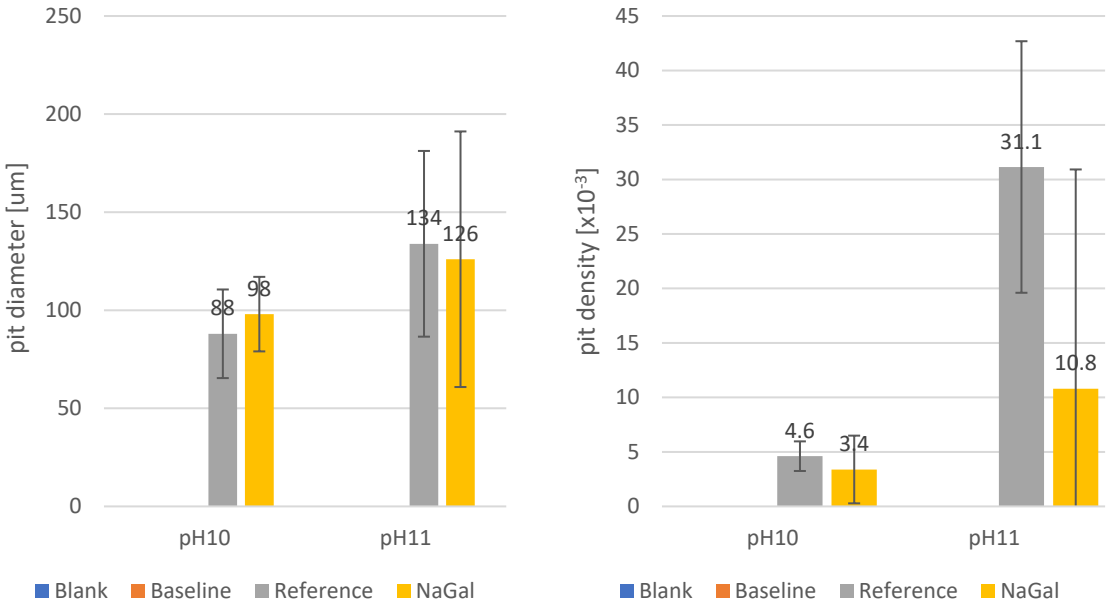

Figure 5.55 average pitting diameters (left) and pitting density (right) after 24 hours immersion in 0.05 M NaCl. The error bars represent the S.D. values.

Electrochemical Impedance Spectroscopy

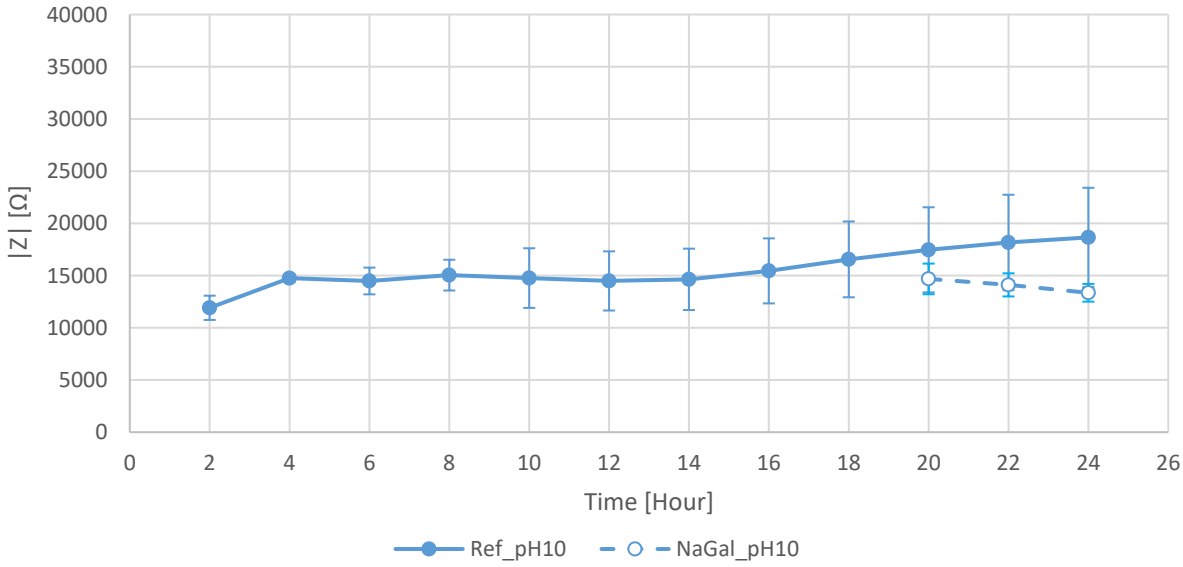

Figure 5.56 Impedance modulus at 0.01 Hz of Ref_pH10 and NaGal_pH10 during 24 hours immersion in 0.05 M NaCl. The S.D. values are presented as error bars.

From the surface examination, the increase of impedance modulus values in Ref_pH10 could have been from the metal stain on the surface. Most of the data on NaGal_pH10 was absent due to the high S.D. that makes solid observation and comparison impossible.

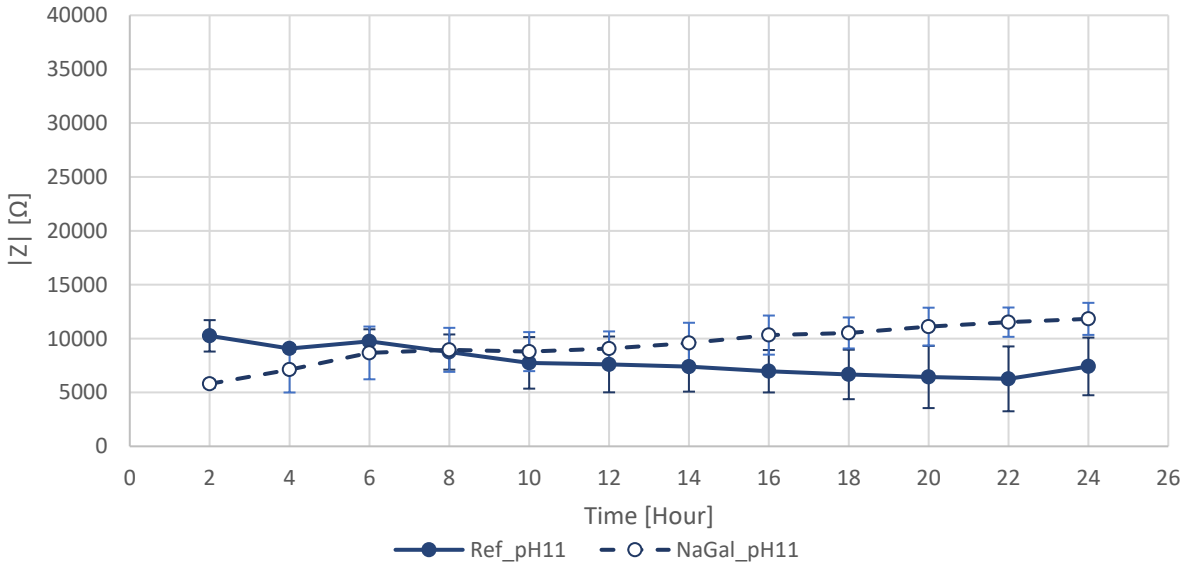

Figure 5.57 Impedance modulus at 0.01 Hz of Ref_pH11 and NaGal_pH11 during 24 hours immersion in 0.05 M NaCl. The S.D. values are presented as error bars.

In pH 11, the impedance modulus between the two samples were quite similar, but NaGal had an increasing trend while the Reference had a decreasing trend. At the end of the experiment, the NaGal had a higher impedance modulus. This supported the hypothesis that the smut layer did not provide a reliable corrosion resistance but acted more like a temporary barrier.

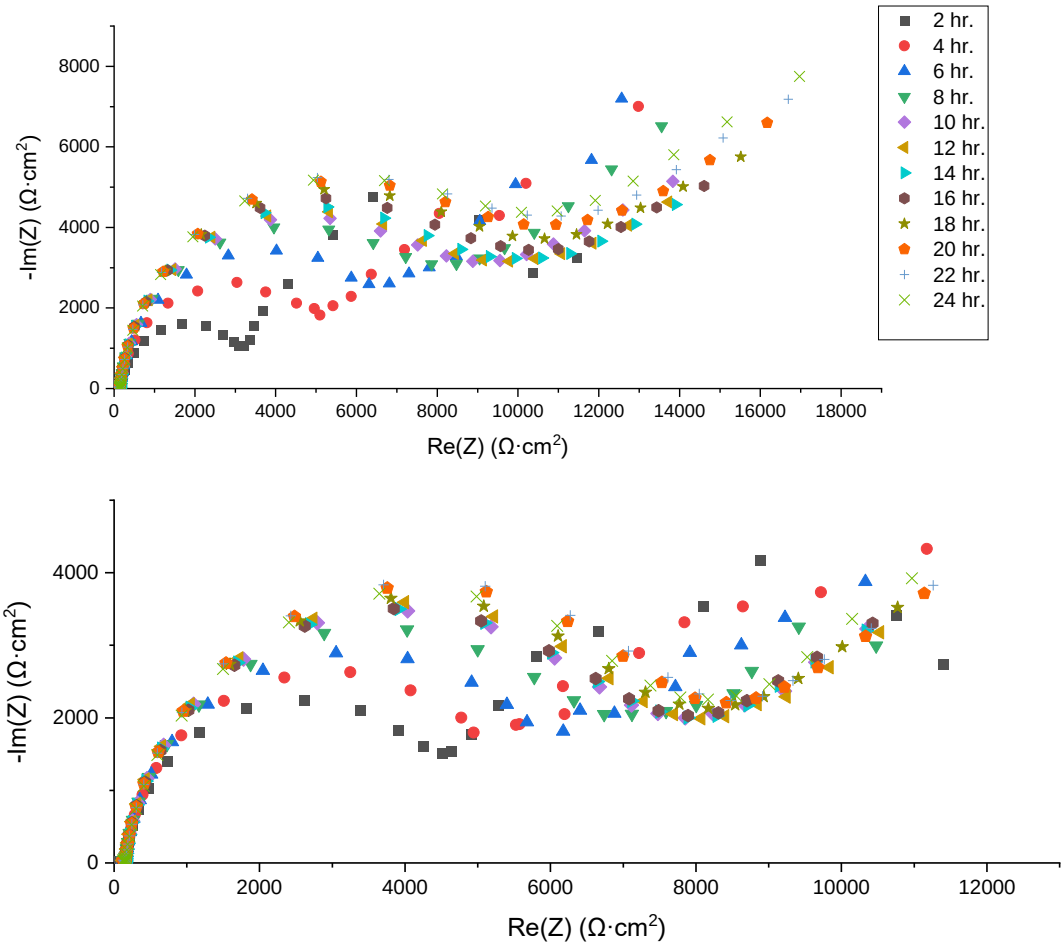

Figure 5.58 Nyquist plot of Ref_pH10 and NaGal_pH10 in 0.05 M NaCl

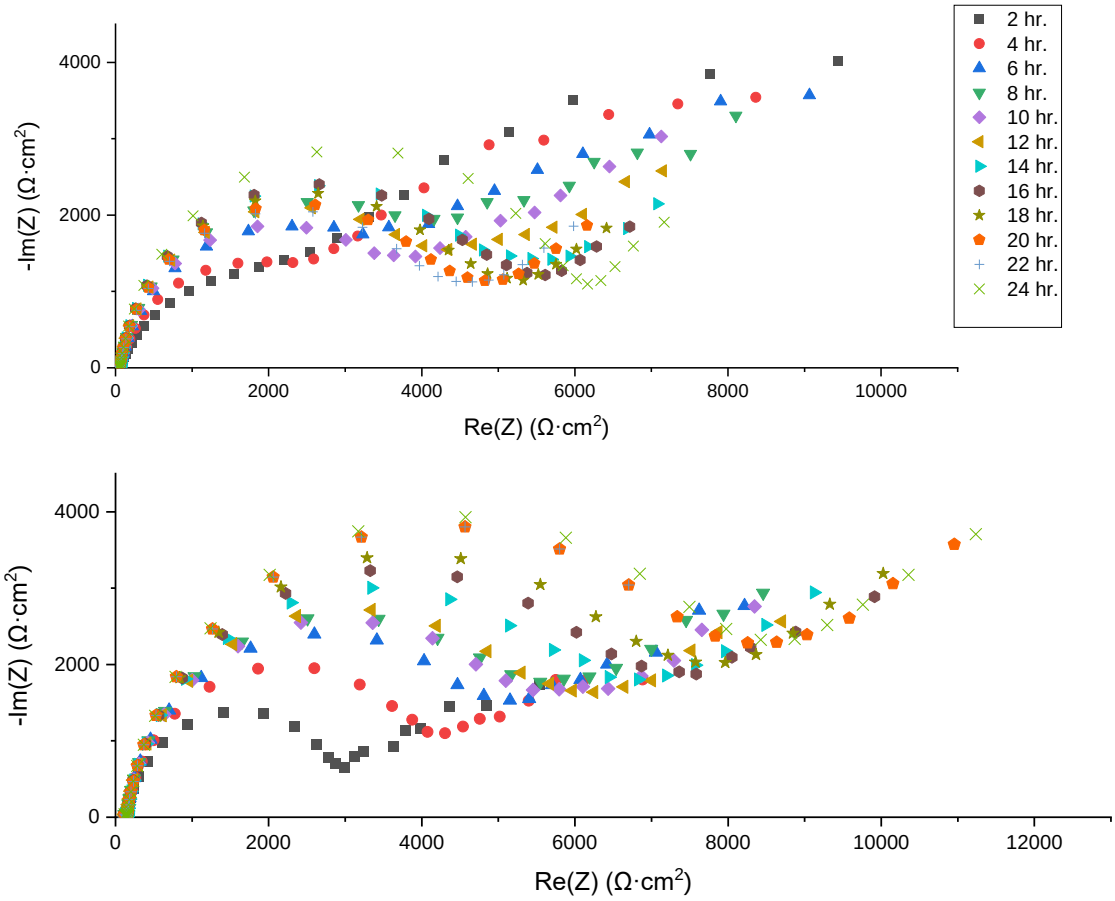

Figure 5.59 Nyquist plot of Ref_pH11 and NaGal_pH11 in 0.05 M NaCl

Similar to previous results, the alkaline immersion samples showed a typical Wurburg impedance plot. Hence, the same equivalent circuit in Figure 5.15 was used to calculate the Rp and presented in Table 5.4.

	Time [hour]	**2**	**4**	**6**	**8**	**10**	**12**	**14**	**16**	**18**	**20**	**22**	**24**
Ref_pH10	Rp [kΩ]	2	4	6	7	8	8	8	9	9	9	9	9
NaGal_pH10	Rp [kΩ]	4	5	5	6	7	7	7	7	7	7	7	7
Ref_pH11	Rp [kΩ]	1	2	3	3	3	4	5	5	4	4	4	2
NaGal_pH11	Rp [kΩ]	3	4	5	5	5	5	6	6	6	7	7	7

Table 5.4 Polarization resistance of alkaline environment immersion samples from Nyquist plot

In pH 10, the Rp calculated from the equivalent circuit exhibited an increased progression over time, which contrasted with the Rp calculated from the LPR. The increase of Rp in Ref_pH10 was related to the effect of the redeposition of metal stains. As presented in the previous section on the polarization curve, the corrosion rate in the NaGal was higher than its reference due to the absence of a stained layer.

In pH 11, both samples had an increasing trend of Rp, although NaGal_pH11 established higher Rp than the Ref_pH11. This might be due to the Ref_pH11's surface being more chemically active than

NaGal_pH11 as presented in the potentiodynamic polarization section. The comparison between the reference and NaGal sample could support the hypothesis that the smut layer on the reference sample did not provide higher corrosion resistance to the sample since it had the lowest Rp.

Open Circuit Potential

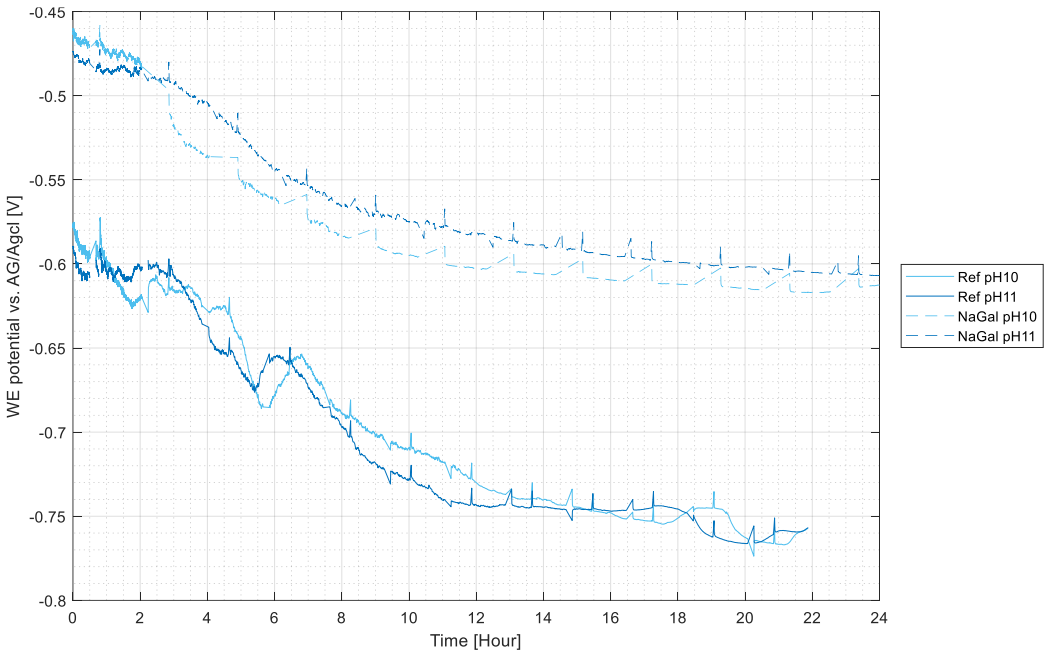

Figure 5.60 Open circuit potential monitoring of alkaline environment immersion samples in 0.05 M NaCl.

In Figure 5.60, it is exhibited that the corrosion was more aggressive in the reference samples than the NaGal samples because, in alkaline solution, the Al could not form any passivation, consequently, there was a significant increase in corrosion rate. Moreover, the dissolution rates of the alloying particles were different from the aluminium matrix since they were nobler. Reference samples also suffered from micro galvanic corrosion between the aluminium matrix and IMPs. While NaGal samples have NaGal layer to block the direct contact with the electrolyte consequently, their OCP appeared to be higher.

6 Conclusions

The main conclusions are divided according to the topics below:

6.1. Coating adhesion properties

- FTIR absorbance spectra showed that NaGal adsorbed via carboxylate ions on aluminium alloy surface in all environments (acid, neutral, and alkaline).
- Although NaGal increased the polar force only in acid immersion samples, adhesion between the coating and aluminium alloy was enhanced in both acidic and alkaline immersion samples.
- The increase of polar force and surface roughness result to stronger coating adhesion.
- In sample with high polar force (samples immersed in pH3 and 11 pretreatment), surface roughness has low influence on coating adhesion property.

6.2. Corrosion resistance properties

- The native oxide that originally formed on the aluminium alloys, which was rich with alumina, created a physical barrier that protects the alloys from the aggressive ions. Although the samples had high polarization resistance and impedance, they were not reproducible, and the film had low resistance to pitting.
- The NaGal pretreatment was not suitable in the neutral pH due to a low reproducibility rate and the electrochemical behaviour between Reference and NaGal samples were considered to be comparable.
- The metal ions dissolved from the alloy into the electrolyte may redeposit on the sample surface again as corrosion products and form an undesired layer such as stain. However, corrosion products only redeposit on the areas that had high chemical reactivity, causing the surface to become heterogeneous, leading to an extremely low reproducibility rate.
- The corrosion products that form the stain layer on the samples' surfaces proved to have corrosion resistance toward uniform corrosion as electrochemical behavior showed lower corrosion rate (from icorr), but pitting evaluation showed that pitting appeared to be more severe
- The smut layers that were found in pH 10 and 11 showed similar electrochemical behavior as the stain layer, but less stable since they attached loosely on the surface.

- NaGal prevented corrosion products such as smut and stain to form on the surface of the alloys in pH 3, 4, 7, 10 and 11. However, the film that was created by NaGal did not fully cover the sample surface as some stain areas were evident on NaGal samples. Nevertheless, there were fewer stain areas when compared with their respective Reference samples.

6.3. Answers to research questions

The answers to the research questions are presented below:

1. **What is the influence of NaGal on the corrosion behavior of AW3003? Does it show an inhibitive effect?**

Unfortunately, NaGal pretreatment did not show any inhibitive effect on the AW3003. The results from electrochemical analyses showed that the samples had their corrosion rate on the uniform corrosion increased, especially in acidic and alkaline environments. It is uncertain without further investigation whether the slight improvement in the neutral environment was due to the NaGal pretreatment or because AW3003 was able to passivate in that environment. However, NaGal pretreatment improved resistance toward pitting corrosion. This is likely because of its ability to prevent corrosion products from forming on the surface, but this would need further research.

2. **Does the NaGal pretreatment improve the organic coating adhesion? If so, how?**

NaGal pretreatment improved the coating adhesion in acidic (pH3) and alkaline (pH11) environments. Due to cohesive failure in the pull-off adhesion test in the Zr sample, an accurate comparison could not be made. Hence, the comparative adhesion strength with the benchmark was not done in this work. The contact measurement showed that NaGal pretreatment greatly enhanced the surface energy, which was owed to the increase of polar force. According to the adsorption theory, the polar force had stronger molecular interaction than the dispersive force. Since the pretreated samples had higher polar force energy than dispersive force, the dispersive force could be disregarded. Therefore, the organic coating was able to bond stronger with the alloy surface that had high polar force. This also applied to the surface roughness, as the results showed that the alkaline cleaning had increased surface roughness, which consequently increased the coating adhesion, but the improvement was minor in acid and alkali. Hence, the main source that promoted coating adhesion in NaGal pretreatment was the increase of the polar force.

The answers to the sub-research questions are presented below:

1.1 What is the NaGal adsorption mechanism on aluminium alloys in different environments (acid, neutral, and alkali)?

For this research question, further investigation on surface analysis and observation over time might be required to answer this question properly. Nevertheless, the results from this work suggest that NaGal was an adsorptive inhibitor-type. Adsorption spectra data from FTIR showed that NaGal was able to adsorb on the AW3003 surface via the chemisorption of the carboxylate ions. However, NaGal was a corrosion accelerator as evidenced by the electrochemical behavior, which showed an increase in corrosion rate in both acidic and alkaline environments. It is still unclear whether it was

due to the prevention of corrosion products redeposited on the surface since the accumulated corrosion products layer (smut/stain) might have contributed to a decrease in the corrosion rate. More electrochemical experiments that focus on the stain area along with surface analysis to learn more on the composition of the stain would be needed to prove this hypothesis. It is noted that the stain composition is influent by the IMPs, which make the stain composition is varied depending on the series of the observed alloy.

1.2 Does pH have an effect on NaGal pretreatment with regard to improvement in coating adhesion?

pH played an important role in the pretreatment because in the low and high pH environments NaGal was able to prevent smut and stain layers, leading to enhancement of the surface quality as those layers typically demote the coating adhesion. While in a neutral environment (pH7), the passivation of AW3003 made the effect of the NaGal pretreatment unclear since less corrosion occurred in that state.

7 Recommendations

Given time limitations, this work presents only a limited scope of the possibilities for the NaGal compound. Further investigation would be able to explore the wider uses of the NaGal compound.

In this work, the NaGal adsorption mechanism was assumed based on the FTIR results and literature study. The high polar force from NaGal samples suggests the chemical adsorption between NaGal and the alloy's surface, further characterization regarding the chemical composition of the sample such as X-ray photoelectron spectroscopy (XPS) would be a good tool to confirm. Moreover, the adsorption mechanism could be fitted with existing adsorption models to explain the mechanism in detail. For example, the Langmuir adsorption model could be used if the monolayer is taken into account.As this work was still in the first stage of the study, many parameters in the pretreatment can be further explored to optimize the condition. For instance, NaGal concentration could be investigated at lower concentration to expect higher efficiency. Furthermore, the immersion time could be studied at a shorter duration because long immersion might not be required if NaGal forms only a monolayer.

In this work, NaGal only showed minor improvement in corrosion resistance in AW3003 when used in pretreatment. This was mainly because it prevented the corrosion products to cover the surface. Due to this ability, it might be a good alternative for acid replacement during the desmutting process because it is non-toxic and much less dangerous compared with the highly concentrated acid that is normally used. It could also be further investigated as an additive to the organic coating to increase corrosion resistance as it might be able to prevent the corrosion reaction products accumulating on the damaged coating area.

The method for applying the organic coating is very crucial for the pull-off adhesion. In order to achieve accurate results, the coating needs to be applied uniformly in one layer. In this thesis, the metal roller was used as a means to apply the coating. The results were not entirely satisfactory and hard to analyze due to the coating layers being too thick and not uniform, causing the measured stress failure to be inaccurate. Therefore, a suitable method that is not complex for applying, requiring less time for preparing, but giving better uniformity on the surface and better control on the thickness,i.e., uniformity, reproducibility, could be further investigated.

NaGal was proved in this work to be a promising adhesion promoter for AW3003. The alloy is often coated with an organic coating as a corrosion protection before use in practice. This will prevent the alloy being directly exposed to the environment. Further investigation on electrochemical properties after the coating such as filiform corrosion, might prove to be more fruitful.

Smut and stain are composed from the corrosion products, which is dissolved from the alloy matrix and IMPs. However, the study on the electrochemical behavior on Mn-based IMPs is still inadequate, further study on micro-galvanic corrosion could lead to a better understanding of smut and stain formation in AW3003.

Bibliography

[1] M. D. Vijayakumar, V. Dhinakaran, T. Sathish, G. Muthu, and P. M. B. ram, "Experimental study of chemical composition of aluminium alloys," *Materials Today: Proceedings*, 2020, doi: 10.1016/j.matpr.2020.07.391.

[2] V. Cicek, "Non-Ferrous Metals and Alloys," in *Corrosion engineering*, 2014, pp. 3–38.

[3] M. Asadikiya, Y. Zhong, and M. Ghorbani, "Corrosion Study of Aluminum Alloy 3303 in Water-Ethylene Glycol Mixture: Effect of Inhibitors and Thermal Shocking," *International Journal of Corrosion*, vol. 2019, 2019, doi: 10.1155/2019/9020489.

[4] J. Devakumar, R. Jaya Santhi, P. Amaladass, and V. Ramesh, "Anticorrosion activities of polymethacrylic acid and grafted/modified polymethacrylic acid on pure aluminium in acid medium," *Materials Today: Proceedings*, 2021, doi: 10.1016/j.matpr.2020.12.537.

[5] K. Nişancioğlu, "Corrosion and protection of aluminum alloys in seawater," in *Corrosion Behaviour and Protection of Copper and Aluminium Alloys in Seawater*, 2007. doi: 10.1533/9781845693084.4.145.

[6] R. Banerjee, S. S. Panja, and M. M. Nandi, "An electrochemical and quantum chemical investigation of some corrosion inhibitors on aluminium alloy in 0.6 M aqueous sodium chloride solution," 2011.

[7] O. Gharbi, S. Thomas, C. Smith, and N. Birbilis, "Chromate replacement: what does the future hold?," *npj Materials Degradation*, vol. 2, no. 1, 2018, doi: 10.1038/s41529-018-0034-5.

[8] R. LAZEROMS, J. BOUWMAN, and S. van den BERG, "WO2020043884 SURFACE TREATMENT COMPOSITIONS, METHOD OF TREATING A SURFACE AND TREATED SURFACE," WO/2020/043884, Mar. 05, 2020 Accessed: Mar. 16, 2022. [Online]. Available: https://patentscope.wipo.int/search/en/detail.jsf?docId=WO2020043884

[9] LAZEROMS ROBERT, BOUWMAN JEROEN, and van den BERG SAM, "EP3844322 SURFACE TREATMENT COMPOSITIONS, METHOD OF TREATING A SURFACE AND TREATED SURFACE," 3844322, Jul. 07, 2021 Accessed: Mar. 16, 2022. [Online]. Available: https://patentscope.wipo.int/search/en/detail.jsf?docId=EP329776254&_cid=P21-KX3CGD-50864-1

[10] J. E. N. VADERS and R. LAZEROMS, "WO2021170635 METHOD FOR REMOVING METAL STAINS FROM A METAL SURFACE," WO/2021/170635, Sep. 02, 2021 Accessed: Mar. 16, 2022. [Online]. Available: https://patentscope.wipo.int/search/en/detail.jsf?docId=WO2021170635&_cid=P21-KX3CGD-50864-1

[11] S. Joshi, W. G. Fahrenholtz, and M. J. OKeefe, "Effect of alkaline cleaning and activation on aluminum alloy 7075-T6," *Applied Surface Science*, vol. 257, no. 6, pp. 1859–1863, Jan. 2011, doi: 10.1016/J.APSUSC.2010.08.126.

[12] E. DELTOMBE and M. POURBAIX, " The Electrochemical Behavior of Aluminum—Potential pH Diagram of the System AI-H 2 O at 25 C ," *CORROSION*, vol. 14, no. 11, 1958, doi: 10.5006/0010-9312-14.11.16.

[13] P. Deepa and R. Padmalatha, "Corrosion behaviour of 6063 aluminium alloy in acidic and in alkaline media," *Arabian Journal of Chemistry*, vol. 10, 2017, doi: 10.1016/j.arabjc.2013.07.059.

[14] I. B. Obot, N. O. Obi-Egbedi, S. A. Umoren, and E. E. Ebenso, "Synergistic and antagonistic effects of anions and ipomoea invulcrata as green corrosion inhibitor for aluminium dissolution in acidic medium," *International Journal of Electrochemical Science*, vol. 5, no. 7, 2010.

[15] J. Zhang, M. Klasky, and B. C. Letellier, "The aluminum chemistry and corrosion in alkaline solutions," *Journal of Nuclear Materials*, vol. 384, no. 2. North-Holland, pp. 175–189, Feb. 15, 2009. doi: 10.1016/j.jnucmat.2008.11.009.

[16] C. Vargel, "The corrosion of aluminium," in *Corrosion of Aluminium*, Elsevier, 2020, pp. 41–61. doi: 10.1016/b978-0-08-099925-8.00008-9.

[17] S. il Pyun and S. M. Moon, "Corrosion mechanism of pure aluminium in aqueous alkaline solution," *Journal of Solid State Electrochemistry*, vol. 4, no. 5, 2000, doi: 10.1007/s100080050203.

[18] K. Xhanari and M. Finšgar, "Organic corrosion inhibitors for aluminum and its alloys in chloride and alkaline solutions: A review," *Arabian Journal of Chemistry*, vol. 12, no. 8. 2019. doi: 10.1016/j.arabjc.2016.08.009.

[19] R. A. Castelli, "The Corrosion Source," in *Nuclear Corrosion Modelling*, Elsevier, 2009, pp. 1–31. doi: 10.1016/b978-1-85617-802-0.00001-3.

[20] C. Vargel, "Influence of alloy composition," in *Corrosion of Aluminium*, Elsevier, 2020, pp. 127–155. doi: 10.1016/b978-0-08-099925-8.00012-0.

[21] C. Vargel, "The oxide film and passivity of aluminium," in *Corrosion of Aluminium*, Elsevier, 2020, pp. 91–111. doi: 10.1016/b978-0-08-099925-8.00010-7.

[22] V. Cicek and et al., "3 Corrosion Types Based on Mechanism," in *Corrosion Chemistry*, John Wiley & Sons, 2011. [Online]. Available: http://ebookcentral.proquest.com/lib/delft/detail.action?docID=818542.

[23] "Understanding the Corrosion Behavior of Aluminum," 1999, doi: 10.1361/caaa1999p025.

[24] I-Wen Huang, "Uniform Corrosion and General Dissolution of Aluminum Alloys 2024-T3, 6061-T6, and 7075-T6," 2016.

[25] E. Mccafferty, *Introduction to Corrosion Science*. Springer, 2009.

[26] V. Cicek, "Types of Corrosion," John Wiley & Sons, 2014, pp. 43–81. Accessed: Apr. 12, 2021. [Online]. Available: https://app.knovel.com/hotlink/pdf/id:kt011I78XD/corrosion-engineering/types-of-corrosion

[27] E. Mccafferty, *Introduction to Corrosion Science*. Springer , 2009.

[28] H. Allachi, F. Chaouket, and K. Draoui, "Protection against corrosion in marine environments of AA6060 aluminium alloy by cerium chlorides," *Journal of Alloys and Compounds*, vol. 491, no. 1–2. 2010. doi: 10.1016/j.jallcom.2009.11.042.

[29] S. Y. Chen, C. Y. Huang, and C. S. Lin, "Microstructure inhomogeneity of the constituent particles of 7075-T6 aluminum alloy after alkaline cleaning and desmutting," *Corrosion Science*, vol. 184, May 2021, doi: 10.1016/j.corsci.2021.109354.

[30] M. H. M. Zaki, Y. Mohd, and N. N. C. Isa, "Surface pre-treatment of aluminium by cleaning, chemical ething and conversion coating," in *AIP Conference Proceedings*, Dec. 2017, vol. 1901. doi: 10.1063/1.5010556.

[31] Z. Jin *et al.*, "The behaviour of iron-containing intermetallic particles in aluminium alloys in alkaline solution," *Corrosion Science*, vol. 179, p. 109134, Feb. 2021, doi: 10.1016/j.corsci.2020.109134.

[32] Z. Jin *et al.*, "Alkaline etching and desmutting of aluminium alloy: The behaviour of Mg2Si particles," *Journal of Alloys and Compounds*, vol. 842, p. 155834, Nov. 2020, doi: 10.1016/j.jallcom.2020.155834.

[33] G. W. Critchlow and D. M. Brewis, "Review of surface pretreatments for aluminium alloys".

[34] Milo˘sev and G. S. Frankel, "Review-Conversion Coatings Based on Zirconium and/or Titanium," *Journal of The Electrochemical Society*, vol. 165, no. 3, pp. 127–144, 2018, doi: 10.1149/2.0371803jes.

[35] P. Santa Coloma, U. Izagirre, Y. Belaustegi, J. B. Jorcin, F. J. Cano, and N. Lapeña, "Chromium-free conversion coatings based on inorganic salts (Zr/Ti/Mn/Mo) for aluminum alloys used in aircraft applications," 2015, Accessed: Mar. 09, 2022. [Online]. Available: http://www.elsevier.com/open-access/userlicense/1.0/

[36] M. Honarvar Nazari *et al.*, "Nanocomposite organic coatings for corrosion protection of metals: A review of recent advances," *Progress in Organic Coatings*, vol. 162, p. 106573, Jan. 2022, doi: 10.1016/J.PORGCOAT.2021.106573.

[37] V. v. Gite, D. Sohn, P. Tatiya, and R. J. Marathe, "Insights of technologies for self-healing organic coatings," *Handbook of Modern Coating Technologies*, pp. 37–65, Jan. 2021, doi: 10.1016/B978-0-444-63237-1.00002-4.

[38] J. H. W. de Wit, D. H. van der Weijde, and G. Ferrari, "Organic Coatings," *Corrosion Mechanisms in Theory and Practice: Third Edition*, pp. 557–579, Jan. 2015, doi: 10.1016/B978-0-444-62722-3.00013-6.

[39] V. Jothi, A. Y. Adesina, A. M. Kumar, N. Al-Aqeeli, and J. S. N. Ram, "Influence of an anodized layer on the adhesion and surface protective performance of organic coatings on AA2024 aerospace Al alloy," *Progress in Organic Coatings*, vol. 138, p. 105396, Jan. 2020, doi: 10.1016/J.PORGCOAT.2019.105396.

[40] M. v. Candal, O. O. Santana, J. J. Sánchez, G. Terife, and A. Gordillo, "Hard/soft combinations based on thermoplastic elastomer and a rigid thermoplastic polymer: Study of the adhesion strength," *High-Performance Elastomeric Materials Reinforced by Nano-Carbons: Multifunctional Properties and Industrial Applications*, pp. 113–131, Jan. 2020, doi: 10.1016/B978-0-12-816198-2.00005-0.

[41] A. de Frutos *et al.*, "Influence of pre-treatments in cerium conversion treatment of AA2024-T3 and 7075-T6 alloys," *Surface and Coatings Technology*, vol. 202, no. 16, pp. 3797–3807, May 2008, doi: 10.1016/J.SURFCOAT.2008.01.027.

[42] B. E. A. Rani and B. B. J. Basu, "Green inhibitors for corrosion protection of metals and alloys: An overview," *International Journal of Corrosion*, vol. 2012, 2012, doi: 10.1155/2012/380217.

[43] C. B. Verma, P. Singh, I. Bahadur, E. E. Ebenso, and M. A. Quraishi, "Electrochemical, thermodynamic, surface and theoretical investigation of 2-aminobenzene-1,3-dicarbonitriles as green corrosion inhibitor for aluminum in 0.5 M NaOH," *Journal of Molecular Liquids*, vol. 209, 2015, doi: 10.1016/j.molliq.2015.06.039.

[44] Q. Liu *et al.*, "A novel green reinforcement corrosion inhibitor extracted from waste Platanus acerifolia leaves," *Construction and Building Materials*, vol. 260, 2020, doi: 10.1016/j.conbuildmat.2020.119695.

[45] J. v. Nardeli, C. S. Fugivara, M. Taryba, E. R. P. Pinto, M. F. Montemor, and A. v. Benedetti, "Tannin: A natural corrosion inhibitor for aluminum alloys," *Progress in Organic Coatings*, vol. 135, 2019, doi: 10.1016/j.porgcoat.2019.05.035.

[46] E. Mccafferty, *Introduction to Corrosion Science*. 2010.

[47] C. Verma, J. Haque, M. A. Quraishi, and E. E. Ebenso, "Aqueous phase environmental friendly organic corrosion inhibitors derived from one step multicomponent reactions: A review," *Journal of Molecular Liquids*, vol. 275. Elsevier B.V., pp. 18–40, Feb. 01, 2019. doi: 10.1016/j.molliq.2018.11.040.

[48] "PubChem Compound Summary for CID 33037, Glucaric acid," *National Center for Biotechnology Information*, 2022. https://pubchem-ncbi-nlm-nih-gov.tudelft.idm.oclc.org/compound/Glucaric-acid (accessed Mar. 18, 2022).

[49] "PubChem Compound Summary for CID 3037582, Galactaric acid," *National Center for Biotechnology Information*, 2022. https://pubchem-ncbi-nlm-nih-gov.tudelft.idm.oclc.org/compound/Galactaric-acid (accessed Apr. 05, 2022).

[50] A. Yurt, G. Bereket, and C. Ogretir, "Quantum chemical studies on inhibition effect of amino acids and hydroxy carboxylic acids on pitting corrosion of aluminium alloy 7075 in NaCl solution," *Journal of Molecular Structure: THEOCHEM*, vol. 725, no. 1–3, pp. 215–221, Jul. 2005, doi: 10.1016/j.theochem.2005.01.048.

[51] British Standards Institution, "BS EN 573-3:2013 Aluminium and aluminium alloys - chemical composition and form of wrought products. Chemical composition and form of products (Withdrawn)," BS EN 573-3:2013, 2013 Accessed: Mar. 08, 2022. [Online]. Available: https://www.thenbs.com/PublicationIndex/documents/details?Pub=BSI&DocID=305144

[52] R. S. Hebbar, A. M. Isloor, and A. F. Ismail, "Contact Angle Measurements," in *Membrane Characterization*, Elsevier Inc., 2017, pp. 219–255. doi: 10.1016/B978-0-444-63776-5.00012-7.

[53] G. Giridhar, R. K. N. R. Manepalli, and G. Apparao, "Contact Angle Measurement Techniques for Nanomaterials," in *Thermal and Rheological Measurement Techniques for Nanomaterials Characterization*, vol. 3, Elsevier, 2017, pp. 173–195. doi: 10.1016/B978-0-323-46139-9.00008-6.

[54] L. Robinet, S. Heu-Thao, M. Radepont, and C. Bonnot-Diconne, "Non-invasive analysis of gilt leather gold varnish and protective layer by infrared reflection-absorption spectroscopy," *Vib Spectrosc*, vol. 110, p. 103133, Sep. 2020, doi: 10.1016/j.vibspec.2020.103133.

[55] M. Jbeily, C. Schwieger, and J. Kressler, "Mixed Langmuir monolayers of perfluorostearic acid and stearic acid studied by epifluorescence microscopy using fluorinated rhodamines and infrared reflection absorption spectroscopy (IRRAS)," *Colloids and Surfaces A: Physicochemical and Engineering Aspects*, vol. 529, pp. 274–285, Sep. 2017, doi: 10.1016/j.colsurfa.2017.06.004.

[56] ASTM Compass, "Standard Test Method for Pull-Off Strength of Coatings Using Portable Adhesion Testers," 2021 doi: 10.1520/D4541-17.

[57] X. Li, S. Deng, and X. Xie, "Experimental and theoretical study on corrosion inhibition of oxime compounds for aluminium in HCl solution," *Corrosion Science*, vol. 81, 2014, doi: 10.1016/j.corsci.2013.12.021.

[58] S. Brossia, "The use of probes for detecting corrosion in underground pipelines," in *Underground Pipeline Corrosion: Detection, Analysis and Prevention*, Elsevier Ltd., 2014, pp. 286–303. doi: 10.1533/9780857099266.2.286.

[59] M. Meeusen *et al.*, "A Complementary Electrochemical Approach for Time-Resolved Evaluation of Corrosion Inhibitor Performance," *Journal of The Electrochemical Society*, vol. 166, no. 11, pp. C3220–C3232, 2019, doi: 10.1149/2.0271911jes.

[60] P. Taheri *et al.*, "On the importance of time-resolved electrochemical evaluation in corrosion inhibitor-screening studies," *npj Materials Degradation*, vol. 4, no. 1, 2020, doi: 10.1038/s41529-020-0116-z.

[61] J. G. Speight, "Corrosion Monitoring and Control-LPR," in *Oil and Gas Corrosion Prevention - From Surface Facilities to Refineries*, 2014, pp. 114–115. Accessed: Mar. 24, 2021. [Online]. Available: https://app.knovel.com/hotlink/pdf/id:kt00U8RUE3/oil-gas-corrosion-prevention/linear-polarization-resistance

[62] C. Valero and A. Igual, "Electrochemical Aspects in Biomedical Alloy Characterization: Electrochemical Impedance Spectrosopy," in *Biomedical Engineering, Trends in Materials Science*, 2011. doi: 10.5772/13039.

[63] B. N. Popov, "Basics of Corrosion Measurements," in *Corrosion Engineering*, Elsevier, 2015, pp. 181–237. doi: 10.1016/b978-0-444-62722-3.00005-7.

[64] E. S. M. Sherif, "Effects of 3-amino-1,2,4-triazole-5-thiol on the inhibition of pure aluminum corrosion in aerated stagnant 3.5wt.% NaCl solution as a corrosion inhibitor," *International Journal of Electrochemical Science*, vol. 7, no. 6, 2012.

[65] M.-G. Olivier and M. Poelm, "Use of Electrochemical Impedance Spectroscopy (EIS) for the Evaluation of Electrocoatings Performances," in *Recent Researches in Corrosion Evaluation and Protection*, 2012. doi: 10.5772/33844.

[66] A. D. Bas, E. Ghali, and Y. Choi, "A review on electrochemical dissolution and passivation of gold during cyanidation in presence of sulphides and oxides," *Hydrometallurgy*, vol. 172, pp. 30–44, Sep. 2017, doi: 10.1016/j.hydromet.2017.06.021.

[67] D. K. Yadav, B. Maiti, and M. A. Quraishi, "Electrochemical and quantum chemical studies of 3,4-dihydropyrimidin-2(1H)-ones as corrosion inhibitors for mild steel in hydrochloric acid solution," *Corrosion Science*, vol. 52, no. 11, pp. 3586–3598, Nov. 2010, doi: 10.1016/j.corsci.2010.06.030.

[68] K. F. Khaled and N. Hackerman, "Investigation of the inhibitive effect of ortho-substituted anilines on corrosion of iron in 1 M HCl solutions," *Electrochimica Acta*, vol. 48, no. 19, pp. 2715–2723, Aug. 2003, doi: 10.1016/S0013-4686(03)00318-9.

[69] D. D. Macdonald, "Theory of the Transpassive State."

[70] ASTM Compass, "Standard Guide for Examination and Evaluation of Pitting Corrosion," 2021 doi: 10.1520/G0046-21.

[71] National Center for Biotechnology Information, "PubChem Compound Summary for CID 139057208, Sodium galactarate," 2022. https://pubchem-ncbi-nlm-nih-gov.tudelft.idm.oclc.org/compound/Sodium-galactarate (accessed Feb. 05, 2022).

[72] B. Smith, "The Infrared Spectra of Polymers V: Epoxies," *Spectroscopy*, pp. 17–19, [Online]. Available: https://www.spectroscopyonline.com/view/the-infrared-spectra-of-polymers-v-epoxies

[73] K. D. Dobson and A. James McQuillan, "In situ infrared spectroscopic analysis of the adsorption of aliphatic carboxylic acids to from aqueous solutions," 1999.

[74] K. Djebaili, Z. Mekhalif, A. Boumaza, and A. Djelloul, "EDX, and XRD Analysis of Al 2 O 3 Scales Grown on PM2000 Alloy," *Research Article XPS*, 2015, doi: 10.1155/2015/868109.

[75] O. D. Agboola and N. U. Benson, "Physisorption and Chemisorption Mechanisms Influencing Micro (Nano) Plastics-Organic Chemical Contaminants Interactions: A Review," *Frontiers in Environmental Science*, vol. 9, p. 167, May 2021, doi: 10.3389/FENVS.2021.678574/BIBTEX.

[76] S. Kwon, M. Fan, H. F. M. DaCosta, A. G. Russell, K. A. Berchtold, and M. K. Dubey, "CO2 Sorption," *Coal Gasification and Its Applications*, pp. 293–339, Jan. 2011, doi: 10.1016/B978-0-8155-2049-8.10010-5.

[77] SUSANNA LAURÉN, "Contact angle What is it and how do you measure it," *BIOLIN SCIENTIFIC*.

[78] S. G. Croll, "Surface roughness profile and its effect on coating adhesion and corrosion protection: A review," *Progress in Organic Coatings*, vol. 148, p. 105847, Nov. 2020, doi: 10.1016/J.PORGCOAT.2020.105847.

[79] W. S. Kim, I. H. Yun, J. J. Lee, and H. T. Jung, "Evaluation of mechanical interlock effect on adhesion strength of polymer–metal interfaces using micro-patterned surface topography," *International Journal of Adhesion and Adhesives*, vol. 30, no. 6, pp. 408–417, Sep. 2010, doi: 10.1016/J.IJADHADH.2010.05.004.

[80] "How Does Adhesion Work: Bonding & Assembly Education | 3M." https://www.3m.com/3M/en_US/bonding-and-assembly-us/resources/how-does-adhesion-work/ (accessed Apr. 04, 2022).

[81] S. Liao, B. Yu, B. Zhang, P. Zhou, T. Zhang, and F. Wang, "Chemically depleting the noble impurities from AZ91-T4 magnesium alloy: A new and efficient pretreatment method to improve the corrosion resistance of phosphate conversion coatings," *Corrosion Science*, vol. 191, p. 109725, Oct. 2021, doi: 10.1016/J.CORSCI.2021.109725.

[82] E. v. Koroleva, G. E. Thompson, G. Hollrigl, and M. Bloeck, "Surface morphological changes of aluminium alloys in alkaline solution:: effect of second phase material," *Corrosion Science*, vol. 41, no. 8, pp. 1475–1495, Aug. 1999, doi: 10.1016/S0010-938X(98)00188-7.

[83] Z. Jin *et al.*, "Alkaline etching and desmutting of aluminium alloy: The behaviour of Mg2Si particles," *Journal of Alloys and Compounds*, vol. 842, p. 155834, Nov. 2020, doi: 10.1016/j.jallcom.2020.155834.

[84] Z. Jin *et al.*, "The behaviour of iron-containing intermetallic particles in aluminium alloys in alkaline solution," *Corrosion Science*, vol. 179, p. 109134, Feb. 2021, doi: 10.1016/J.CORSCI.2020.109134.

[85] G. Šekularac, J. Kovač, and I. Milošev, "Prolonged protection, by zirconium conversion coatings, of AlSi7Mg0.3 aluminium alloy in chloride solution," *Corrosion Science*, vol. 169, p. 108615, Jun. 2020, doi: 10.1016/J.CORSCI.2020.108615.

[86] A. Davoodi, J. Pan, C. Leygraf, and S. Norgren, "Multianalytical and In Situ Studies of Localized Corrosion of EN AW-3003 Alloy—Influence of Intermetallic Particles," *Journal of The Electrochemical Society*, vol. 155, no. 4, p. C138, 2008, doi: 10.1149/1.2834454.

[87] A. Davoodi, J. Pan, C. Leygraf, and S. Norgren, "Integrated AFM and SECM for in situ studies of localized corrosion of Al alloys," *Electrochimica Acta*, vol. 52, no. 27, pp. 7697–7705, Oct. 2007, doi: 10.1016/J.ELECTACTA.2006.12.073.

Appendix A: Contact angle measurement

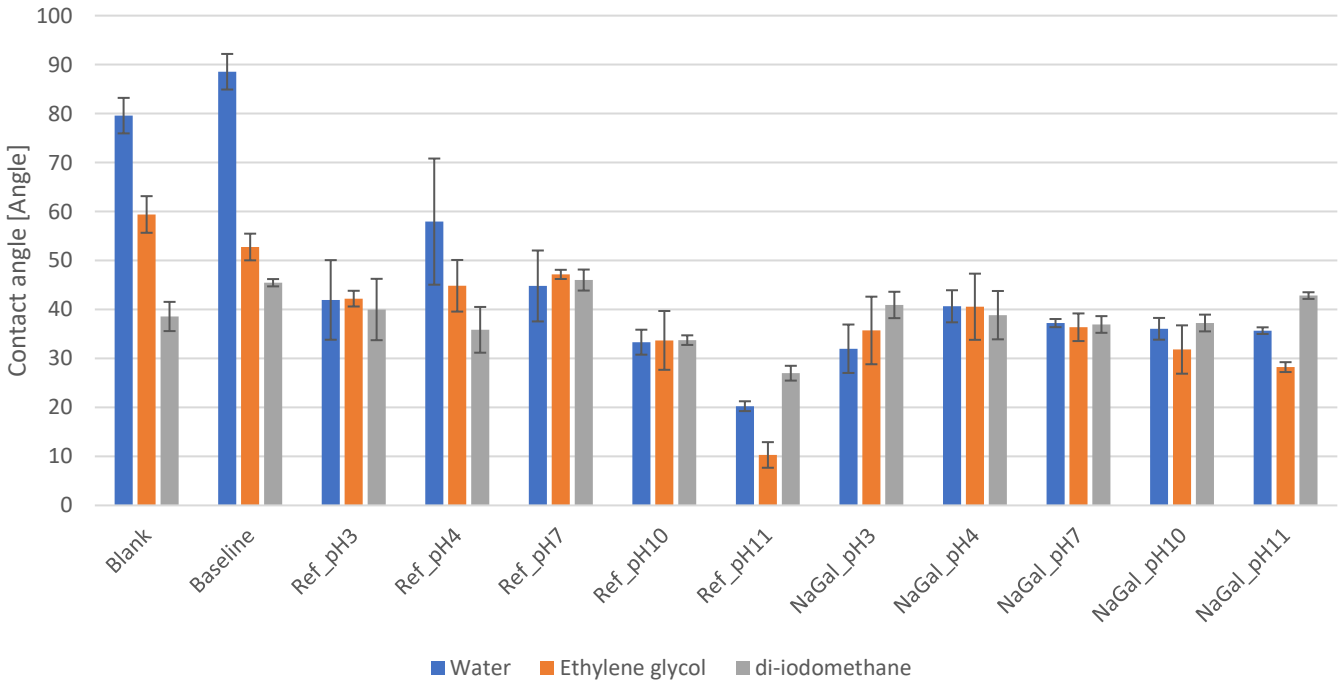

The S.D. values are presented in error bars.

Appendix B: R_p calculated from equivalent circuits

Time [hour]	2	4	6	8	10	12	14	16	18	20	22	24
	Rp [Ω]											
Blank	23770	46313	52422	55413	44700	48431	49336	48131	43283	36749	30798	25807
Baseline	4878	5273	5989	6479	6776	7022	7302	7617	7950	8260	8451	8610
NaGal_pH3	11529	7151	6363	6167	6055	6212	6388	6580	6723	6760	6780	6741
NaGal_pH4	2493	4421	5857	6538	6719	6758	6853	6977	7101	7194	7259	7215
NaGal_pH7	3292	3961	4554	5028	5230	5422	5721	5962	6160	6223	6444	6581
NaGal_pH10	3901	4650	5281	6038	6520	6754	6554	6531	6776	7017	7089	6778
NaGal_pH11	2584	3725	4422	4843	4842	5086	5579	6036	6330	6668	6937	7113
Ref_pH3	3756	2947	3245	3586	4173	4533	6180	6809	8382	8139	7942	7260
Ref_pH4	9615	7948	8821	9403	9480	9454	10182	10561	10841	11048	11178	11067
Ref_pH7	8469	6802	6055	6650	6949	7360	7945	8175	8791	9098	9495	9622
Ref_pH10	2397	4256	5683	7001	7724	8107	8321	8600	8859	9041	9120	8879
Ref_pH11	1091	1922	2970	3697	3252	3788	4452	4525	4297	4014	3858	5343